UNIVERSITY OF CALIFORNIA SAN DIEGO

A multiparametric MRI protocol for PDFF, ADC, T_1 and T_2: applications in the NAFLD and NASH disease spectrum evaluated using multiple mouse models

A thesis submitted in partial satisfaction of the requirements for the degree Master of Science

in

Biology

by

Gabrielle Blizard

Committee in charge:

Professor Patrick McConville, Chair
Professor Michael David, Co-Chair
Professor Brenda Bloodgood

2020

The Thesis of Gabrielle Blizard is approved, and it is acceptable in quality and form for publication on microfilm and electronically:

_____

_____

Co-chair

_____

Chair

University of California San Diego

2020

DEDICATION

To my cats, Louis and Mouse, for keeping me company during the many weeks I spent locked away writing this.

TABLE OF CONTENTS

LIST OF FIGURES

LIST OF TABLES

ACKNOWLEDGEMENTS

I would like to thank Dr. Patrick McConville for seeing potential in me as a young undergraduate and grooming me into a prudent scientist. I am grateful for you mentoring me through this project and always being available and willing to help me through all of the challenges that came with it. You taught me so much about what it means to be a scientist and the three most important rules of imaging that I will never forget: positioning, positioning, and positioning.

I would also like to thank Deanne Lister for rescuing me countless times when the MRI 'wasn't working'. I would like to recognize the invaluable assistance that you provided and the effort that went into creating and testing the MRI protocols for my experiments. I could always go to you with any problems I was having or ask your opinion on my observations and I always appreciated your great advice.

Lastly, I would like to thank Edward Cabral for always being willing to assist with my experiments when needed and for helping keep me sane during some long days in the 'dungeon'.

ABSTRACT OF THE THESIS

A multiparametric MRI protocol for PDFF, ADC, T_1 and T_2: applications in the NAFLD and NASH disease spectrum evaluated using multiple mouse models

by

Gabrielle Blizard

Master of Science in Biology

University of California San Diego, 2020

Professor Patrick McConville, Chair
Professor Michael David, Co-Chair

Purpose – Nonalcoholic fatty liver disease (NAFLD) and its subtype, Nonalcoholic steatohepatitis (NASH), are highly prevalent diseases which are characterized by diagnostic limitations and unmet therapeutic need. The disease spectrum in the liver includes hepatic steatosis, inflammation, and fibrosis. In this study we investigate a multiparametric MRI protocol across multiple research standard mouse models of NAFLD and NASH in order to provide biomarkers which can noninvasively and objectively quantify disease progression or regression longitudinally

Methods – Male C57BL/6 mice were subjected to diet- and chemical-based induction of NAFLD and NASH for 12 weeks and imaged at specified time points throughout the disease time course. At each timepoint, a sequence of MRI protocols were acquired at 11.7T which enabled the quantification of MRI-PDFF, ADC, T_1, and T_2 in the liver.

Results – Liver PDFF was found to increase in all experimental diet groups versus control mice on a standard diet over the 12 week time course. In contrast, liver ADC decreased in all experimental diet groups. Liver T_1 relaxation time was found to decrease and liver T_2 relaxation time increased in all experimental groups.

Conclusions – We conclude that PDFF and T_1 relaxation time are accurate and robust biomarkers in the quantification of hepatic steatosis. Additionally, ADC may be a viable biomarker in the detection of liver fibrosis while T_2 relaxation time has indications in liver inflammation. Our multiparametric MRI protocol has implications in diagnosis, clinical trial stratification, and therapeutic advance.

INTRODUCTION

Nonalcoholic Fatty Liver Disease (NAFLD) and Nonalcoholic Steatohepatitis (NASH)

Background

Nonalcoholic fatty liver disease (NAFLD) is a disease which is characterized by hepatic steatosis, or fat accumulation in the liver, in the absence of other causes such as alcohol consumption [1, 2]. The American Association for the Study of Liver Diseases (AASLD) considers fat accumulation above 5 to 10% by weight in the liver to be sufficient for diagnosis of NAFLD [3]. While fatty liver itself is often reversible and benign, NAFLD can progress to a more severe subtype known as nonalcoholic steatohepatitis (NASH) which is further accompanied by liver inflammation with or without liver fibrosis (scarring) [1, 4]. Fibrosis often occurs within and surrounding inflamed tissue and is characterized by the overaccumulation of fibrous connective tissues such as collagen [5]. The presence of fibrosis in the liver is associated with higher rates of morbidity and mortality [3]. In extreme cases in which fibrosis becomes severe enough to impair normal liver function, liver cirrhosis will occur [6]. Liver cirrhosis is associated with a greater risk of developing hepatocellular carcinoma (HCC), or liver cancer [1, 6]. An estimated 30% of patients with NAFLD will develop NASH, and of those patients, 20% will eventually develop fibrosis [6]. Understanding and accurately identifying NASH is paramount in diagnosis, prognosis, and therapeutic advances in this disease [7].

Epidemiology: Prevalence and Population

There is an array of comorbidities that are associated with NAFLD, and a bidirectional association has been observed between NAFLD and Metabolic Syndrome (MetS) [8]. MetS encompasses a range of lifestyle type diseases including obesity, hyperlipidemia, and type II diabetes [2]. Incidence of NAFLD increases notably in individuals with these conditions: patients with obesity are 80 to 90% more likely to have NAFLD, 60% more likely if they have hyperlipidemia, and 30 to 50% more likely if they have diabetes [9]. Along with increasing rates of obesity and diabetes, NAFLD is becoming increasingly prevalent globally [1]. A meta-analysis conducted in 2017 estimated NAFLD occurrence as high as one billion globally [2]. NAFLD is currently the leading cause of chronic liver disease worldwide and is projected to soon become the leading indication for liver transplantation [2, 9].

The prevalence of NAFLD has been most well-characterized in Caucasian cohorts in the United States [10]. Rates in the United States are an estimated 24% with Europe following close behind at 23% [10]. However, a recent review warned against characterizing NAFLD as an affliction restricted to affluent Western societies [10]. Rates of NAFLD are reported to be highest in the Middle East (32%) followed by South America (31%) and Asia (27%) with the lowest rates being observed in Africa at 14% [10]. There is mounting evidence which suggests that ethnic background may be an independent risk factor both in developing the disease and severity of progression [10].

Disease Management and Current Treatments

At present, lifestyle modifications are the primary interventions in the treatment and management of NAFLD and NASH [7]. Lifestyle modifications include both diet and exercise; it has been shown that body weight loss of ≥10% is correlated with significant improvement in NAFLD and NASH including fibrosis [7]. Lifestyle changes have proven to be more efficacious than current drugs in phase III trials, however, lifestyle modifications which are substantial and sustained are challenging to accomplish and highly variable in individuals [11]. Furthermore, clinical trials which investigate the effects of lifestyle modulation on disease progression or regression tend to last between 3 and 12 months and lack long-term data [11].

Drugs that treat comorbidities such as type II diabetes and hyperlipidemia have proven beneficial in reducing NAFLD and NASH [12]. In patients with type II diabetes, the anti-diabetic pioglitazone can be used [12]. Pioglitazone can improve hepatic steatosis, inflammation, and fibrosis [12]. However, pioglitazone has been shown to have negative effects including edema and increases in body weight [13]. NAFLD or NASH patients with hyperlipidemia can be treated with statins, a class of lipid lowering drugs [12]. Vitamin E has also been indicated for the treatment of hepatic steatosis and inflammation due to its antioxidant characteristics [14]. However, long term use of vitamin E is not recommended due to concern of induced bladder cancer or hemorrhagic stroke [14].

Therapeutics in Development

There are currently no NAFLD-specific therapies approved by the US Food and Drug Administration (FDA), but promising therapies appear to be on the horizon [7]. A significant limitation with therapeutics in development is the fact that subpopulations within the NASH spectrum are still not well characterized and therefore do not permit proper stratification in clinical trials [13].

Therapies which have reached phase 3 trials include elafibranor, cenicriviroc, obeticholic acid, aramchol, resmetirom, MSDC-0602K and selonsertib [7, 12, 13]. Elafibranor has shown promise in reducing hepatic steatosis, inflammation and fibrosis through activation of the peroxisome proliferator-activated receptors (PPARs) PPARα and PPARδ [12]. Its phase 3 trial is targeted for completion in December 2021 (NCT02704403) [12]. Cenicriviroc specifically targets liver fibrosis through inhibition of the chemokine receptor CCR2/5 [12]. The phase 3 trial which is currently underway for cenicriviroc has a study completion date targeted for October 2028 (NCT03028740) [12]. Obeticholic acid agonizes the farnesoid X receptor (FXR) throughout the entire body and is indicated in the reduction of liver inflammation (NCT02548351) [12, 13]. However, there are currently no quantitative biomarkers which have been established to predict NASH patient response to FXR agonist drugs and response has only been reported in < 25% of patients in which it has been tested [13]. Additionally, FXR agonists have been shown to increase low density lipoprotein (LDL) cholesterol while decreasing high density lipoprotein (HDL) cholesterol [13]. Armachol inhibits steroyl-CoA desaturase-1 (SCD-1)

in the liver and was shown to improve fibrosis-stage in a phase 2b trial and is currently being investigated in a phase 3/4 trial (NCT04104321) [13]. Resmetirom is a thyroid hormone receptor beta (TRβ) agonist with proven efficacy in reducing hepatic steatosis as well as NASH resolution in a phase 2b trial and is currently being investigated in a phase 3 trial (NCT03900429) [13]. MSDC-0602K is a mitochondria pyruvate carrier (MPC) inhibitor which had indication in glycemic control and improvement in NAFLD activity score in a phase 2b trial [13] MSDC-0602K will soon be investigated in a phase 3 trial (NCT03970031) [13]. Lastly, selonsertib is an inhibitor of an apoptosis-regulating kinase (ASK1) [12]. Selonsertib was found to reduce hepatic steatosis and fibrosis as well as body weight in both a preclinical NASH model and a phase 2 clinical study [12]. However, selonsertib did not demonstrate adequate efficacy as a monotherapy drug in its phase 3 (NCT03053050 and NCT03053063) study and is now being investigated as a potential combination therapy drug (NCT02781584) [13]. Additional information regarding therapeutics in active and completed phase 2 trials can be found in Table 1.

The diversity of targets and related NASH physiologies being examined for therapeutic potential, coupled with the lack of a single approved disease modifying therapy today underlies a major need for improved translational and quantitative biomarkers to increase the efficiency and predictive potential of preclinical and clinical trials. Ideally future translational biomarkers will be tailored for specific disease subtypes and also specific therapeutic targets, as a one size fits all

biomarker is unachievable in such a diverse disease with multiple downstream hallmarks and indications.

Table 1. Therapeutics with indications in NAFLD or NASH. Information was adapted from a recent comprehensive review by Dufour *et al.* of the current therapeutic landscape in NAFLD and NASH [13]. This table does not include all compounds currently in phase 2 trials.

Drug	Target / Mechanism	Phase / Trial Number
Saroglitazar	PPAR-α agonist PPAR-γ agonist	Phase 2 NCT03061721
Lanifibranor	pan-PPAR agonist	Phase 2b NCT03008070
MSDC-0602K	PPAR-γ agonist	Phase 2 NCT02784444
Tropifexor	FXR agonist	Phase 2 NCT02855164
Cilofexor	FXR agonist	Phase 2 NCT03449446
EDP-305	FXR agonist	Phase 2 NCT03421431
EYP 001	FXR agonist	Phase 2 NCT03812029
Nidufexor	FXR agonist	Phase 2 NCT02913105
PF-05221304	Acetyl-CoA carboxylase (ACC) inhibitor	Phase 2 NCT03248882
PF-06865919	Ketohexokinase (KHK) inhibitor	Phase 2 NCT03256526
VK2809	TRβ agonist	Phase 2b NCT04173065
Pegbelfermin	Fibroblast growth factor 21 (FGF21) analogue	Phase 2b NCT03486899 NCT03486912

Table 1. Therapeutics with indications in NAFLD or NASH, continued.

Drug	Target / Mechanism	Phase / Trial Number
Semaglutide	Glucagon-like peptide-1 (GLP-1) agonist	Phase 2b NCT02970942
Tirzepatide	Glucose-dependent insulinotropic polypeptide and GLP-1 agonist	Phase 2b NCT04166773

Current Clinical Diagnostic Paradigm

Liver Biopsy and Limitations

Liver biopsy and subsequent histopathology remains the gold standard in clinical diagnosis of NAFLD and NASH; it is used to confirm or exclude diagnosis, determine the presence of other liver diseases, and to conclude prognosis [9]. However, liver biopsy is an invasive procedure and can be dangerous to the patient, especially if they have other comorbidities [9]. In fact, the AASLD has listed morbid obesity as a contraindication for liver biopsy [15]. Potential complications include pain, bleeding, and even death [15].

A further limitation of liver biopsy is the subjective nature associated with it and the inherently limited sampling size of biopsy; a biopsy represents only 1/50,000th of the liver [16]. Also, there have been no histopathologic biomarkers shown to consistently indicate the severity of NASH [7,16]. A recent study of 91 bariatric surgical patients revealed histological variability in samples which were biopsied from different lobes of the liver [17]. While there was significant agreement between pathologists on the presence of NAFLD or NASH in the liver samples, there was substantial disagreement on the presence of fibrosis [17]. A preclinical

NAFLD/NASH study mirrored this finding in which five sections of diseased mouse liver were sampled and blindly scored for fibrosis by two independent pathologists [18]. The difference between the two observers' scores was found to be statistically significant both intra- and interlobularly suggesting both that fibrosis was distributed heterogeneously throughout the liver and that observer scoring was subjective [18]. Since increasing evidence has elucidated fibrosis as the single most robust histological predictor of mortality [1], subjectivity and spatial heterogeneity could result in life-threatening underestimation of disease stage in using biopsy and pathology [16].

The presentation of NAFLD and NASH varies markedly across populations and so diagnostic discrepancies which arise from heterogeneity of disease presentation and subjectivity become increasingly concerning when ethnic variability is taken into account [3,9]. When comparing the histological features of NAFLD across ethnic populations, it was found that those of African descent tend to exhibit a lesser extent of steatosis and inflammation while those of East Asian descent show more severe hepatic inflammation [10]. Those of Hispanic ethnicity elicit the most severe NAFLD phenotype and those of Caucasian and South Asian descent display a similar histopathological profile [10]. Due to such variability, predicting which patients will exhibit disease progression is one of the biggest issues facing clinicians [6].

The level of risk associated with liver biopsy has brought into question its practicality as a screening tool [9]. Nevertheless, early diagnosis of NASH has important implications in disease management as patients can implement lifestyle changes, treat underlying syndromes, or participate in clinical trials with promising therapies [2]. The limitations of histopathology along with the major disease diversity in patients that present with NAFLD and NASH, again points to

a need for quantitative biomarkers, especially those that are customized to specific aspects of NAFLD and NASH. Better understood and more versatile non-invasive biomarkers will directly improve the ability to diagnose, complete accurate prognosis and to translate and determine efficacy of treatments.

Serum Biomarkers: Alanine Transaminase (ALT)

NAFLD is typically asymptomatic and so liver biopsy and subsequent diagnosis often occurs as the result of initial abnormal blood findings [19]. Elevated levels of the liver enzyme alanine transaminase (ALT) can be an indicator of liver disease, however, an estimated 80% of patients with NAFLD have levels of ALT within the normal range [19]. Of those with elevated ALT levels, it is known that this level decreases during the progression of fibrosis to cirrhosis [19]. Therefore, ALT levels do not correlate with the severity of NAFLD or the progression of NASH and are not reliable as a diagnostic biomarker [19]. Clinical reliance on this biomarker has caused significant underdiagnosis of NAFLD and NASH [19].]. Generally, blood-based biomarkers have not been successful in addressing unmet needs in NAFLD and NASH, but are one of the avenues for future developments in this regard and remain a subject of current research.

Noninvasive Imaging Biomarkers: Computed Tomography (CT) and Ultrasound (US)

There is an urgent need for the standardization of noninvasive, highly sensitive, translational and quantitative tools for diagnosis and longitudinal evaluation of NAFLD and NASH [16]. Translational imaging modalities have emerged as potential noninvasive tools for determining the presence of diffuse liver disease [20].

Computed tomography (CT) can be used to assess hepatic steatosis through detectable differences in the X-ray absorbing properties of fat and water [16]. Fat has less of an effect on X-rays as compared to water and so fatty livers would have a lower attenuation as compared with a normal liver [16]. While CT is useful in diagnosing moderate to severe steatosis, it is limited in its ability to detect mild steatosis [16, 20]. Additionally, the nature of CT makes it unsuitable for longitudinal evaluation due to the risk of ionizing radiation [16].

Ultrasound (US) is currently the most widely used noninvasive imaging method for diagnosing hepatic steatosis by detecting the degree of attenuation of the sound wave, or echogenicity [3, 16]. Whereas normal liver tissue only marginally attenuates ultrasound waves, fatty tissue has a much more pronounced effect on sound wave scatter and attenuation and appears bright [16, 20]. However, ultrasound is heavily operator dependent, qualitative in nature, and can only detect steatosis when fat content exceeds 33% in the liver [3, 20]. Using ultrasound in a study of 161 clinical patients, the diagnosis of hepatic steatosis differed significantly between two observers' in 21.7% of cases [20]. Furthermore, the simplistic four-point scoring system which is used for grading hepatic steatosis has been criticized as impervious to detecting small changes in longitudinal evaluation or following therapeutic intervention [20]. Additionally, the presence of fibrosis or other underlying liver disease has also been suggested to increase echogenicity and may therefore confound diagnosis [20].

New ultrasound methods which have been developed to enable objectivity in the evaluation of NAFLD and NASH include FibroScan [16]. FibroScan measures transient

elastography, a parameter that quantifies the velocity in which an elastic shear wave can propagate throughout the liver [21]. The speed with which the wave transits the liver is proportional to the stiffness of the tissue, or the liver stiffness measurement (LSM) [21]. Collagen accumulation in the liver as a result of fibrosis confers rigidity; in the assessment of liver fibrosis, increases in LSM have been associated with severity of fibrosis [20, 22]. However, the usefulness of this parameter in NAFLD patients is contested as some studies have shown that steatosis increases liver stiffness and other studies do not [21]. More recently the controlled attenuation parameter (CAP) has been developed for evaluation of hepatic steatosis which quantifies transient elastography at the same time as sound wave attenuation [21]. Nevertheless, CAP has not demonstrated precise discrimination between steatosis grades [21]. Additionally, CAP has shown deficiency in the presence of covariates including obesity, NAFLD, and diabetes [16, 21].

Noninvasive Imaging Biomarkers: Magnetic Resonance Imaging (MRI) and Elastography (MRE)

Magnetic resonance imaging (MRI) is a uniquely versatile translational imaging modality that does not incorporate any ionizing radiation. One of the major advantages of MRI, compared with other imaging modalities is the broad array of contrast types and related biomarkers that can be obtained from a single imaging session in a living subject. Conventional MRI detects signal from hydrogen nuclei or protons, which in living subjects originate primarily from water and secondarily, labile protons of fat (eg. those in methyl groups) [20]. Underlying this is the

excellent, relatively high resolution anatomical and structural images that MRI has become known for, and that enhance diagnosis and longitudinal monitoring across many major diseases. Additionally, MRI facilitates highly efficient multiplexing of individual scan-based exams and associated biomarkers making a conventional MRI exam one of the most comprehensive imaging exams that can be done in major hospitals and clinics today.

In NASH, magnetic resonance elastography (MRE) can be used to assess liver stiffness associated with fibrosis[21]. Similar to ultrasound-based elastography, MRE involves the mechanical generation of elastic shear waves [21]. A gradient echo pulse sequence is then used to generate MRE stiffness maps in which LSM is a measure of the mean stiffness per pixel [21, 22]. MRE has demonstrated accuracy and precision in the assessment of hepatic fibrosis independent of patient populations and disease severity [22]. Additionally, inter-observer agreement was achieved [22]. Performing MRE, however, requires additional software and hardware modifications beyond standard MRI leading to limitations of cost and availability of MRE [21].

While CT and US measure hepatic steatosis indirectly, through X-ray attenuation and echogenicity/elastography, respectively, magnetic resonance imaging (MRI) uniquely allows for more direct quantification of fat by measuring the proton density fat fraction (PDFF) in tissues [20]. PDFF is the number of protons which are bound to triglycerides as a fraction of the total number of protons which are bound to triglycerides and water [16]. PDFF is expressed as a percentage between 0-100% and can be used as a biomarker to reflect hepatic steatosis [16].

Whereas histological analysis is inherently subjective in nature, PDFF can be quantified via MR images through computational analysis, which has proven to be highly accurate (correlation reportedly >0.9 with histologically quantified fat) and reproducible [12, 20]. MRI also has relatively high sensitivity for fat detection (approaching 100%) and is capable of detecting liver fat content greater than or equal to 5.56% [7]. MRI poses no risk to the patient and can be used both as a screening tool and longitudinally to assess steatosis progression or regression [20]. However, MRI-PDFF has no indication in inflammation or fibrosis [16]. Furthermore, the degree of steatosis in the liver does not appear to predict disease progression in NASH, and the degree of progression of steatosis should not be used as an indicator for disease severity [1, 23].

Apparent diffusion coefficient (ADC) is another quantitative biomarker measurable by MRI, which has applications in liver fibrosis and can be quantified using diffusion-weighted imaging (DWI) [24]. DWI reflects structural characteristics of tissues by quantifying the degree in which water molecules can freely diffuse through tissues, or the ADC value [24]. The presence of increased hydrophobic cellular structures, such as collagen, attenuates the diffusion of water molecules through tissues, thus decreasing the effective rate of diffusion, and the ADC [24] . A decrease in ADC may therefore be associated with an increasing presence of fibrosis in the liver, and ADC may serve as a biomarker for NASH [24]. Of note, inconsistencies in image acquisition and analysis have led to poor reproducibility in this biomarker, and further standardization is required [24].

The longitudinal relaxation time (T_1) and transverse relaxation time (T_2) are intrinsic MRI parameters which reflect the interaction between tissues and an applied magnetic field [25]. More specifically, T_1 measures the rate in which fat and water protons in a tissue relax back into a state of equilibrium following magnetic perturbation and is sensitive to higher frequency rotational motion of the nuclei (eg. water or labile fat protons) being detected [25]. T_2 is a parameter that measures the time in which the transverse magnetization exponentially decays to equilibrium and is more sensitive to lower frequency rotational motion of nuclei [25]. As such, structural characteristics of tissues which affect water and fat rotational motion, influence both T_1 and T_2 relaxation times [26]. Discerning between the signals produced by both fat and water allow for the investigation of morphological changes in tissues [27]. The T_1 relaxation time of fat protons is shorter than the T_1 relaxation time of water protons [27]. As such, the effective liver T_1 relaxation time (comprised of T_1 from both water and fat) has been demonstrated to shorten as a result of chronic fat accumulation and therefore may be an additional biomarker to identify hepatic steatosis [25]. Because fibrosis and scarring only comprise a relatively small volume of the liver, it does not significantly affect T_1 or T_2 relaxation times [26]. Inflammation and edema in tissues, which also affects water and fat proton rotational motion, has been reported to lengthen relaxation times [26]. Therefore, liver T_1 and T_2 relaxation time may serve as viable biomarkers in the detection, quantification and monitoring of NAFLD and NASH.

MRI therefore presents a non-invasive and translational modality that may enable measurement of several complementary aspects of NAFLD and NASH through multiple quantitative biomarkers that could be measured in a single, efficient imaging session.

Translational Research: Preclinical Models

The exact pathogenesis of NAFLD remains to be elucidated; it has been suggested that the progression of NAFLD to NASH and subsequently to HCC is not always linear [7]. For example, it is possible for a NASH patient to develop liver cancer in the absence of fibrosis [6]. This gap in knowledge has plagued the translational value of research in the field as researchers struggle to develop preclinical models which mimic the varied human pathogenesis and presentation of NAFLD and NASH [14, 29].

Mouse Models

An ideal preclinical model would closely replicate the human phenotype by inducing obesity, hepatic steatosis, inflammation, and fibrosis [14]. Murine models are the most broadly used preclinical models in this field of research [29]. The C57BL/6 strain of mice are most commonly used due to their predisposition towards developing NAFLD and its associated syndromes including obesity and type II diabetes [29]. Dietary and/or chemical modulations can be used to induce phenotypical features of NAFLD and the composition of such influences both the time frame of development as well as the severity of NAFLD progression [29].

A variety of high fat and/or sugar- based diets have become the standard for mouse models of NASH. The methionine and choline deficient diet (MCD) based model is one of the best characterized models [29]. The MCD diet contains approximately 40% sucrose and 10% fat while being completely deficient in methionine and choline [29, 30]. Because they are essential nutrients in hepatic functioning, the deficiency in methionine and choline causes impaired β-oxidation and very low-density lipoprotein (VLDL) secretion in the liver [30]. These events result in oxidative stress and increased lipid deposition in the liver which ultimately induce features of NASH including steatosis, inflammation, and fibrosis [30]. The MCD diet, however, has been demonstrated to cause weight loss [31]. Although the mechanism in which this model induces NASH is not clinically relevant, this model is sufficient for the study of intrahepatic events related to this disease [29, 31].

A more recently used model which negates the weight loss issues in the MCD model in the choline deficient L-amino acid defined diet (CDAA) [30]. The CDAA diet elicits similar features of NASH as the MCD diet due to the shared deficiency in choline [30]. The addition of L-amino acids supplements the lacking proteins in the diet [30]. The choline sufficient L-amino acid defined diet (CSAA) serves as a control for the CDAA diet. The Western diet (WD) contains high levels of fat, cholesterol, and sugar [31]. The WD brings about features similar to the MCD diet including steatosis, inflammation, and fibrosis while also promoting weight gain [31]. Carbon tetrachloride (CCl_4) is a chemical which, upon repeated administration, enhances

the effects of the WD by inducing hepatic oxidative stress and therefore exacerbating the development of fibrosis [29].

Unfortunately, therapies that have proven efficacious in these preclinical models have repeatedly failed in clinical settings [29]. ASP9831, a phosphodiesterase-4 inhibitor, was shown to lessen both liver inflammation and fibrosis in an MCD diet model, however, upon translation to the clinic, no evidence for efficacy was observed [29]. Other drugs which have mirrored this phenomenon include the antioxidant resveratrol and the hypolipidemic drug ezetimibe [29]. A clinical study which enrolled obese patients with NAFLD showed no decrease in hepatic steatosis compared to baseline following eight-week administration of reveratrol [32]. Similarly, a meta-analysis of clinical studies employing ezetimibe showed that although the drug significantly reduced hepatic steatosis, hepatic inflammation and fibrosis were unchanged in NAFLD and NASH patients [33].

Several factors are thought to contribute to the consistent translational failure in this area of research [14]. First, preclinical models can never fully replicate the heterogenous physiological environment which is seen in the human population [14]. Confounding this phenomenon is the inherent nature of scientific experiments in which variability, or heterogeneity, between subjects is controlled for [14]. Secondly, while a number of mouse models have been developed to mimic the human disease, each model is limited in its ability to elicit the entire disease spectrum with relevant pathogenesis both on the molecular level and its associated syndromes [14, 29]. Additionally, these results underpin limitations with IHC and

gross assessment of body weight as indicators of efficacy, and the need for more specific and quantitative biomarkers to better predict potential treatments based on work in preclinical models. Tailored and well understood biomarkers that are sensitive to different aspects of NAFLD and NASH (such as steatosis, inflammation and fibrosis) and that can be measured in the same subject or patient will improve the ability to successfully translate therapies and predict clinical outcomes.

Therefore, in preclinical NAFLD and NASH research, it is of exceeding importance to select the model as well as biomarkers which are most relevant to the targeted pathological component of the disease in order to preserve clinical relevance, and to test therapeutic interventions across multiple models [29, 34].

Table 2. Table representing the different NAFLD and NASH mouse models used in this study and their associated phenotypes. *Expected based on diet composition, reference not available.

Diet / Chemical	Diet Composition	Liver Histology	Metabolic Features	
			Obesity	Various
MCD	~40% sucrose ~15% fat Methionine deficient Choline deficient [Appx A]	Steatosis, Inflammation, Fibrosis, NASH [31]	-- [31]	Weight loss, Increase in AST and ALT levels [29]
CDAA	~40% sucrose ~15% fat Choline deficient [Appx A]	Steatosis, Inflammation, Fibrosis, NASH [29]	Not Expected [29]	Body weight gain, Insulin resistance, Increase in AST and ALT levels [29]
CSAA	~40% sucrose ~15% fat Choline sufficient [Appx A]	Steatosis, Inflammation, Fibrosis, NASH *	Not Expected [29]	Body weight gain, Increase in AST and ALT levels *

Table 2. Table representing the different NAFLD and NASH mouse models used in this study and their associated phenotypes, continued.

Diet / Chemical	Diet Composition	Liver Histology	Metabolic Features	
			Obesity	Various
WD	50% sucrose 5% fat [Appx A]	Steatosis, Inflammation, Fibrosis, NASH [31]	Yes [31]	Insulin resistance [29]
CCl_4	N/A	Steatosis, Inflammation, Dose-dependent Fibrosis [29]	-- [29]	Increased AST and ALT levels [29]

A Noninvasive and Comprehensive Approach: MRI and Multiple Mouse Models

While certain MRI biomarkers have shown promise in NASH, they are largely non-standardized, and to date have not been used in parallel in a controlled setting across NASH disease models. In this study we sought to test and implement a multi-parametric MRI protocol enabling the quantification of liver PDFF, ADC, T_1 and T_2 longitudinally at specific time points over the course of disease induction, and in parallel measure body weight. We originally sought to use liver histopathology for correlative data, but unfortunately closures in our IHC providers prevented such work. We then sought to test the ability of the MRI protocol to provide biomarkers of aspects of NASH including hepatic steatosis, inflammation and fibrosis.

Secondarily we aimed to characterize several industry and academic research standard NAFLD/NASH mouse models in the context of our experimental MRI protocol. By employing a broad spectrum of mouse models, our research aimed to incorporate the variability of disease presentation as seen in the clinical population, as well as test the breadth of applicability of the experimental MRI biomarkers in accurately detecting and following the progression of both NAFLD and NASH. This represents the first comprehensive comparison of multiple MRI biomarkers in multiple NAFLD/NASH models. This work will help advance our knowledge of MRI biomarkers for future use in elucidating disease biology and therapeutic testing in both mouse models of NASH and in clinical translation.

MATERIALS AND METHODS

Study Design

Fat Phantom

A fat phantom was designed in order to permit evaluation of the fat/water content dependence of MRI parameters including PDFF, T_1 and T_2. Soy oil was mixed with agarose at the following concentrations: 5%, 10%, 15%, 20%, 25%, 30%, 40%, 50%, and 100%. The soy oil and agarose solution was transferred into 5 mm glass NMR tubes and allowed to solidify. The eight tubes containing the various concentrations of soy oil were arranged in a 50 mL conical tube containing saline.

Animal Experiments

All experimental work was performed under an approved Institutional Animal Care and Use Committee (IACUC) protocol. Male, 7-8 weeks old C57BL/6 mice were purchased from Envigo (Placentia, CA). Mice were allowed to acclimatize for at least 48 hours before experimentation and were provided diet and water ad libitum. All mice were subjected to a standard 12-hour light/12-hour dark cycle. Body weight was taken twice weekly for all mice over the 12-week time course.

Mouse Models of NAFLD and NASH

Mice were provided either a standard diet or an experimental diet ad libitum, with or without carbon tetrachloride (CCl_4) for 4, 9, or 12 weeks. In each study, mice were stratified into 6 groups: 1 control group and 5 experimental groups. Mice in the control group remained on the standard diet for the duration of observation. The five experimental groups included mice on the

methionine and choline deficient diet (MCD), the choline deficient diet (CDAA), the choline sufficient diet (CSAA), the western diet (WD), and the western diet with weekly administration of carbon tetrachloride (WD + CCl_4) (see Appendix A for more detailed diet information). Mice that received CCl_4 were dosed once each week (QW) by body weight at a volume of 0.1 mL/g. CCl_4 was diluted in mineral oil at a ratio of 1:9 and administered via oral gavage throughout the 12-week time course. MCD-fed mice displayed marked weight loss which did not permit observation past week 9 in study 1. Due to the observed trend, MCD-fed mice were only observed until week 4 in the studies 2 and 3.

In study 2, a dietary intervention was introduced following the 12-week disease time course in which the experimental diet was removed from all groups (excluding MCD due to early body weight loss) and mice were placed back on standard diet.

Imaging Experiments

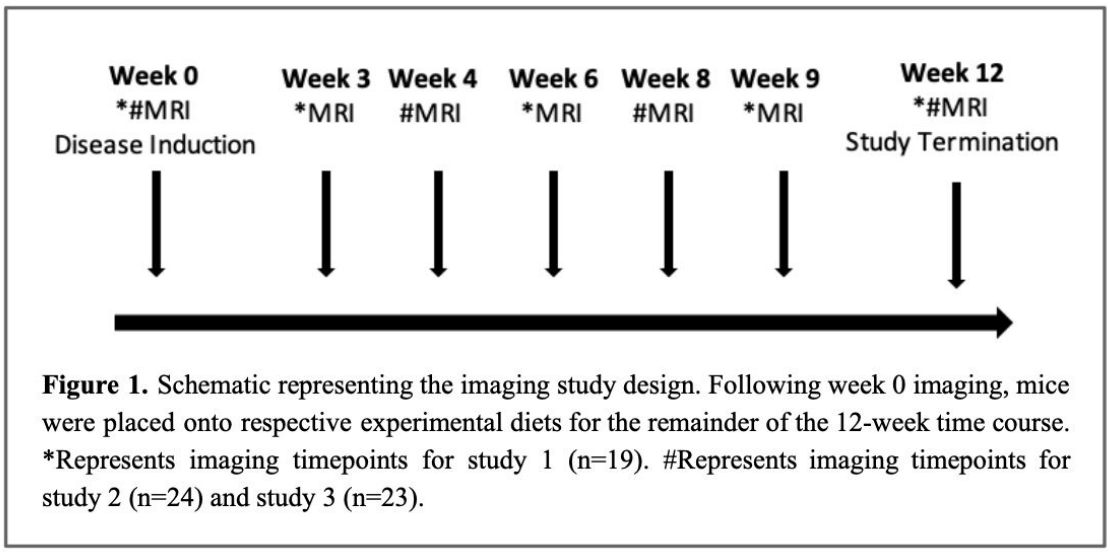

Figure 1. Schematic representing the imaging study design. Following week 0 imaging, mice were placed onto respective experimental diets for the remainder of the 12-week time course. *Represents imaging timepoints for study 1 (n=19). #Represents imaging timepoints for study 2 (n=24) and study 3 (n=23).

Animal Handling and Preparation for Imaging

Mice underwent imaging at week 0, 3, 6, 9, and 12 weeks post diet- and chemical-based disease induction in study 1. After elucidating trends in our NAFLD and NASH models in the context of our multiparametric MRI protocol and body weight time course in study 1, mice were imaged at 0, 4, 8, and 12 weeks in study 2 and 3 which was considered to be a sufficient time course for the observation of major trends in these models. In study 2, mice were additionally imaged at week 14.5 and 16.5 (week 2.5 and 4.5 post-intervention).

Mice were anesthetized using 2% isoflurane and 98% oxygen using an induction box which was placed under a heat lamp in order to maintain the mouse body temperature at 33℃. Animals were then transferred to a mouse bed in the MRI bore with a nose cone which maintained isoflurane flow rate at 0.8 L/min throughout the duration of scanning. Mice were positioned supine with the liver positioned in the center of a Bruker 38-mm transmit/receive quadrature radio frequency (RF) coil. The amount of isoflurane administered was adjusted throughout the scan session to maintain respiration at approximately 40 breaths/min. Using a Small Animal Monitoring and Gating System (SA Instruments, Inc. Model 1025), mice were heated at 33℃ throughout the course of scanning using a temperature sensor which was inserted into the rectum and a warm air blower. A respirator pad with a pressure sensor was taped just beneath the rib cage on the abdomen of the mice to monitor the respiration rate as well as to respiratory gate the scans. Body temperature as well as respiration were monitored using the PC-SAM32 software provided by SA Instruments to ensure mice remained at physiological conditions.

Images were acquired on a 11.7 Tesla (T) Bruker BioSpec Avance III preclinical MRI system with a tuned and matched 38-mm RF coil. A series of imaging protocols which lasted approximately 75 minutes was used for the fat phantom and the mice. Scans were acquired and reconstructed using Bruker ParaVision 6.0. For each sample or live subject, a localizer scout scan was performed first to ensure proper positioning within the isocenter of the magnet. Shimming was performed after acquisition of a B_0 map (using 2 averages and a repetition time (TR) of 10 ms) with subsequent use of the MAPSHIM automated shimming routine including higher order shims. A slice packet containing 7 contiguous transaxial slices of 1.5mm thickness was then planned using the scout scan to ensure full coverage of the liver. Slice packet geometry and positioning was constant throughout the scanning session.

Proton Density Fat Fraction

Animals underwent four sequential T_2* map multiple gradient-echo (MGE) scans with staggered starting echo times (TE) of 1.304 ms, 1.769 ms, 2.234 ms, and 2.699 ms, and a total of 8 echoes per scan with 1.86 ms echo spacing. Image size was maintained at 128x192 while field of view was adjusted to each mouse accordingly; typically 24x36mm or 30x40mm. The images were acquired with 6 averages, TR was fixed at 300 ms, and flip angle was 45°. The nominal scan time for each MGE was 4m19s, however the actual scan time was increased due to respiratory gating.

Apparent Diffusion Coefficient

A diffusion weighted (DWI) spin echo scan was used to quantify the water ADC and incorporated B values of 0, 300 (2 averages) and 600 (2 averages). Slice packet geometry and positioning was maintained as above for the MGE. The image size was 128x96 across the same field of view as used for the MGE . TE was 17.524ms and TR was 1000ms. The nominal scan time was 12m0s, however the actual scan time was increased due to respiratory gating.

T_1 and T_2

Mice underwent a combined T_1 and T_2 mapping RARE spin-echo scan. Slice packet geometry and positioning was maintained as above. The image matrix size used was 128x96. The T_1/T_2 images were acquired with 2 averages and a RARE factor of 2. For T_2, TE for the first echo was 6.50 ms, the echo spacing was 6.50 ms, and a total of 5 echoes were used. Eight TR values were used for T_1: 5500 ms, 3000 ms, 1500 ms, 1000 ms, 1000 ms, 550 ms, 550 ms, 550 ms. The T_1/T_2 map scan time was 21m50s400ms and the scan was not gated.

Image Analysis

Images were transferred from ParaVision 6.0 onto an analysis computer using the FTP client FileZilla. All images were imported into the image analysis tool VivoQuant (Invicro, Boston, MA). Using VivoQuant, a region of interest (ROI) was drawn in the reconstructed images over the entire liver for each mouse with this ROI applied to each scan type.

Proton Density Fat Fraction

All 4 MGE scans were loaded as Bruker MR files into VivoQuant. Proton density fat fraction was quantified by fitting to a standard multi-interference multi-echo model that included six lipid resonances and included temperature (recorded during each scan) as a variable. The ROI was drawn to include the entire liver and exclude other anatomical features such as lungs, stomach, intestines, kidneys and major vessels, and mean liver PDFF calculated over this ROI.

Apparent Diffusion Coefficient

The diffusion scan was imported into VivoQuant as a DICOM file. A map for the apparent diffusion coefficient (ADC) was generated in VivoQuant by fitting to a Stejskal-Tanner diffusion model [35]. Mean ADC was then quantified over the entire liver using the same ROI that was drawn for the MGE scans.

T_1 Relaxation

A T_1 relaxation map was generated using ParaVision by fitting the variable TR data to a single exponential recovery model and imported into VivoQuant as a DICOM file. ROIs were drawn to encompass the entire liver using the T_1 maps. Mean liver T_1 relaxation time was then quantified over each ROI.

T_2 Relaxation

A T_2 relaxation map was generated using ParaVision by fitting the variable TE data to a single exponential decay model and imported into VivoQuant as a DICOM file. ROIs were

drawn to encompass the entire liver using the T_2 maps. Mean liver T_2 relaxation time was then quantified over each ROI.

Statistical Analysis

Using the SPSS Statistics (version 26) software package, a mixed ANOVA was conducted for each of the three studies and for each biomarker within each study in order to compare all groups and determine the effects of both time and diet on the MRI parameters PDFF, ADC, T_1 relaxation time, and T_2 relaxation time. Due to differential timing associated with the MCD diet group, a secondary mixed ANOVA was conducted for each study and each biomarker in order to compare the MCD group to all other experimental groups using only the time points for which the MCD group was studied. A post-hoc Tukey HSD test was used in order to determine which groups were statistically different from the control group and each other. For biomarker correlations, a correlation coefficient (R^2) was calculated using a simple linear regression in GraphPad Prism 8.

RESULTS

Body Weight

Body weight was recorded at each imaging time point across the three studies for each of the NAFLD/NASH models and the control mice on the standard diet (Fig. 2). Mice on the standard diet exhibited marginal increases in body weight over the 12-week time course consistent with age. Mice on the standard diet had a combined average weight of 24.7 ± 0.8 g at baseline and 30.4 ± 1.2 g at week 12 (Fig. 2D). MCD-fed mice displayed marked weight loss in each study, consistent with published data on this model, which did not permit observation past week 9 in study 1. In study 1, MCD-fed mice had a mean body weight of 19.7 ± 1.7 g at week 3 (Fig. 2A) representing a -27% decrease versus control (Fig. 3). Due to the observed trend, MCD-fed mice were only observed until week 4 in the subsequent studies and combined data. CDAA-fed and CSAA-fed mice showed very similar trends in body weight in each of the three studies. At week 12, CDAA-fed mice had a combined mean body weight of 37.1 ± 1.2 g (Fig. 2D) which represents a +22% increase versus control (Fig. 3). CSAA-fed mice showed a +25% increase in body weight versus control (Fig. 3) with a combined mean body weight of 38.0 ± 1.0 g (Fig. 2D). WD-fed mice showed large increases in body weight, generally similar to that observed in the CDAA and CSAA groups, and greater than mice on the WD + CCl_4 regimen. At week 12, mice on the WD had a combined mean body weight of 40.8 ± 1.2 g while mice on the WD + CCl_4 regimen had a combined mean body weight of 35.1 ± 1.1 g (Fig. 2D). At week 12, WD-fed mice showed a +34% increase versus control while mice on the WD + CCl_4 regimen showed a +15% increase versus control (Fig. 3).

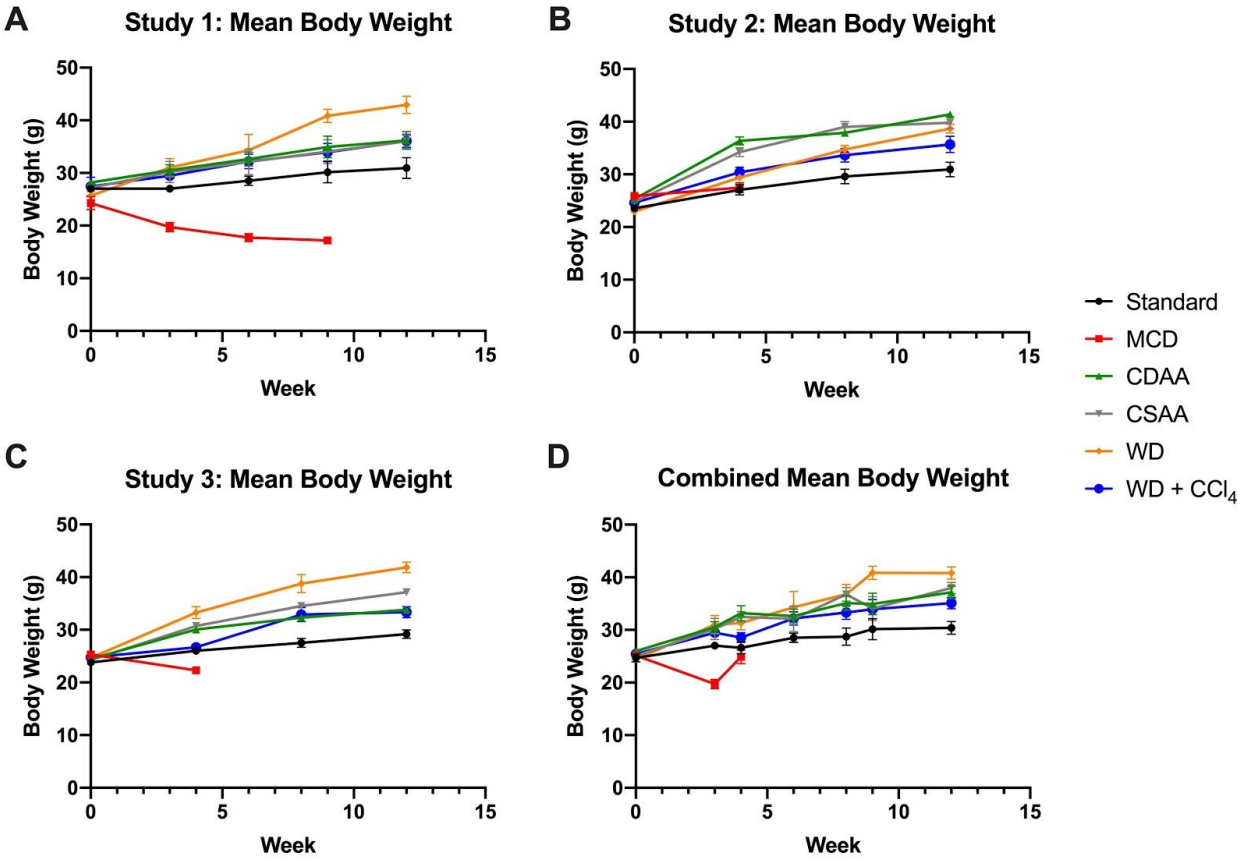

Figure 2. Graphs showing the mean body weight with standard error vs time by group. Standard error bars which are not shown are shorter than the symbol at each data point. **A.** Study 1: Standard (n=3), MCD (n=4), CDAA (n=4), CSAA (n=2), WD (n=3), WD + CCl_4 (n=3); **B.** Study 2: Standard (n=4), MCD (n=4), CDAA (n=4), CSAA (n=4), WD (n=4), WD + CCl_4 (n=4); **C.** Study 3: Standard (n=3), MCD (n=4), CDAA (n=4), CSAA (n=4), WD (n=4), WD + CCl_4 (n=4); **D.** Combined mean across the three studies: Standard (n=10), MCD (n=12), CDAA (n=12), CSAA (n=10), WD (n=11), WD + CCl_4 (n=11).

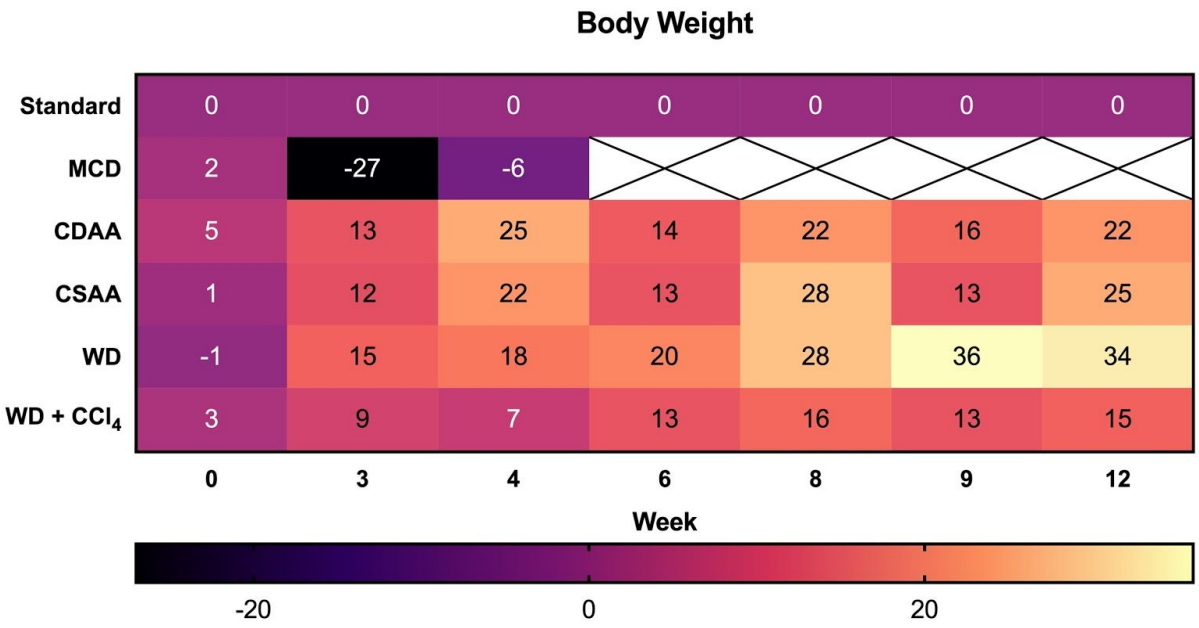

Figure 3. Heat Map representing the percent difference in combined mean body weight between experimental diet groups and mice on the standard diet at each timepoint over the three studies. Group labels are to the left of the heat map and week labels are at the bottom. Color bar indicates percent differences ranging from -27 to +36.

Proton Density Fat Fraction

in vitro

A calibration experiment was performed to evaluate the accuracy of the MRI-PDFF against our fat phantom with tubes containing varying concentrations of oil. The calculated PDFF values across the various concentrations of oil in the phantom exhibited strong correlation with the actual percentage of fat (by volume) in each vial ($R^2 = 0.97$) (Fig. 4B). At lower oil percentages, PDFF was quantified to be 7% in the reference vial containing 5% fat and 10% in the reference vial containing 10% fat (Fig. 4). At fat percentages which would be consistent with hepatic steatosis, PDFF was calculated to be 19% in the 20% reference vial, 28% in the 30% reference vial, and 40% in the 40% reference vial (Fig. 4).

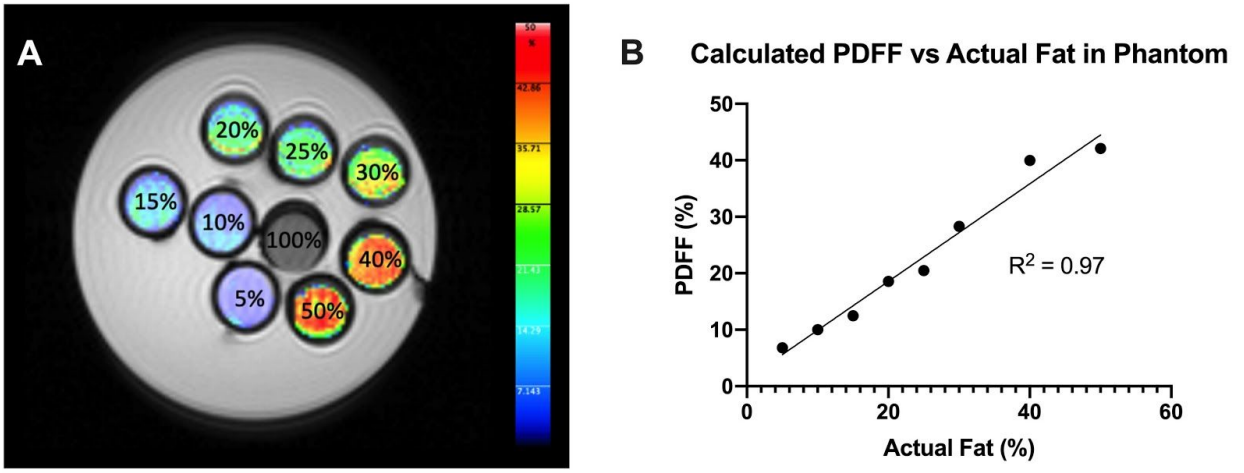

Figure 4. Calibration of MRI-PDFF parameter showing strong correlation between MRI quantified PDFF and oil content in fat phantom. **A.** Color map of single transversal slice through fat phantom representing PDFF values from 0% (blue) to 50% (red). Actual oil percentage in each tube is shown. The 100% tube was excluded from analysis as PDFF *in vivo* never reached that large of a percentage. **B.** Correlation between measured MRI-PDFF versus actual oil percentage in the various tubes in the fat phantom.

in vivo

Extending this platform *in vivo*, liver PDFF was quantified in all mice at each of the imaging time points in order to evaluate the induction and severity of hepatic steatosis across various mouse models of NAFLD and NASH. The individual gradient echo images in the MGE protocol used were generally of high quality and showed relatively uniform liver contrast. Fitted PDFF maps showed relatively uniform PDFF with evidence of some small heterogeneity and the data was generally well fitted to the PDFF equation (Fig. 5). PDFF was found to increase in all experimental groups in each of the three studies over the 12-week time course consistent with the expected development of NAFLD and underlying fatty liver.

In study 1, all NAFLD/NASH models (including diet- and chemical-based models) showed significantly increasing PDFF over time. In contrast, mice on the standard diet exhibited

marginal fluctuations throughout each of the studies. Both time and diet were found to have a significant effect on liver PDFF (Appendix B). A significant difference was found between all experimental groups (MCD, $p < 0.001$; CDAA, $p < 0.001$; CSAA, $p = 0.007$; WD, $p = 0.002$; WD + CCl_4, $p = 0.001$) and mice on the standard diet (Appendix B). Mice on the standard diet exhibited relatively consistent PDFF values over the time course studied, with a mean liver PDFF of 8 ± 5% at baseline and 10 ± 3% at week 12 (Fig. 6A). Mice on the WD exhibited the highest mean liver PDFF of 41 ± 8% at week 12 (Fig. 6A). Of the experimental groups, mice on the WD + CCl_4 regimen exhibited the lowest increase by week 12 with a mean liver PDFF of 24 ± 6%.

In study 2, a similar increase in PDFF was found across all the diseased groups, with relatively consistent PDFF observed across the 12 week period in mice on the standard diet. Both time and diet were again found to have a significant effect on liver PDFF with CDAA-fed ($p < 0.001$) and CSAA-fed ($p = 0.009$) mice exhibiting significant differences in liver PDFF as compared to mice on the standard diet (Appendix B). Mice on the standard diet exhibited a mean liver PDFF of 10 ± 4% at baseline and 15 ± 1% at week 12 (Fig. 6B). CDAA-fed mice exhibited the highest mean liver PDFF followed by CSAA-fed mice at week 12. Mice on the CDAA diet had a mean liver PDFF of 47 ± 2% and mice on the CSAA diet had a mean liver PDFF of 40 ± 4% at week 12 (Fig. 6B). Of the experimental groups, mice on the WD + CCl_4 regimen exhibited the lowest increase by week 12 with a mean liver PDFF of 25 ± 5% (Fig. 6B).

In study 3, the PDFF results were consistent with those in study 2. Both time and diet had a significant effect on liver PDFF (Appendix B). CDAA-fed ($p = 0.001$) and CSAA-fed ($p = 0.038$) mice exhibited increases in liver PDFF which were found to be statistically different from liver PDFF of mice on the standard diet (Appendix B). While mice on the standard diet exhibited a mean liver PDFF of 11 ± 4% at week 12, CDAA-fed mice had a mean liver PDFF of 36 ± 2% and CSAA-fed mice had a mean liver PDFF of 26 ± 8% (Fig. 6C). Of the experimental groups, mice on the WD + CCl_4 regimen exhibited the lowest liver PDFF increase by week 12 with a mean liver PDFF of 16 ± 4% (Fig. 6C).

Due to the consistency of the data across the 3 studies, the data was also combined (averaged across all mice on all studies). After combining the data, mice on the standard diet exhibited a combined mean liver PDFF of 12 ± 2% (Fig 6D). CDAA-fed mice exhibited the largest overall increase in mean liver PDFF by week 12. Combined mean liver PDFF of CDAA-fed mice was 41 ± 2% at week 12 (Fig. 6D). This represents a +237% increase as compared to the combined mean liver PDFF of mice on the standard diet at week 12 (Fig. 7). MCD-fed mice exhibited a precipitous increase by week 4 with a combined mean liver PDFF of 29 ± 2% (Fig. 6D) representing a +209% increase as compared to the combined mean liver PDFF of mice on the standard diet at week 4 (Fig. 7). Mice on the CSAA diet exhibited the third largest increase in combined mean liver PDFF by week 12 at 33 ± 4%, followed by WD-fed mice at 29 ± 4% and WD + CCl_4 mice at 22 ± 2% (Fig. 6D). Together, these represent +171,

+141, and +86% differences between these groups and combined mean liver PDFF of mice on the standard diet, respectively (Fig. 7).

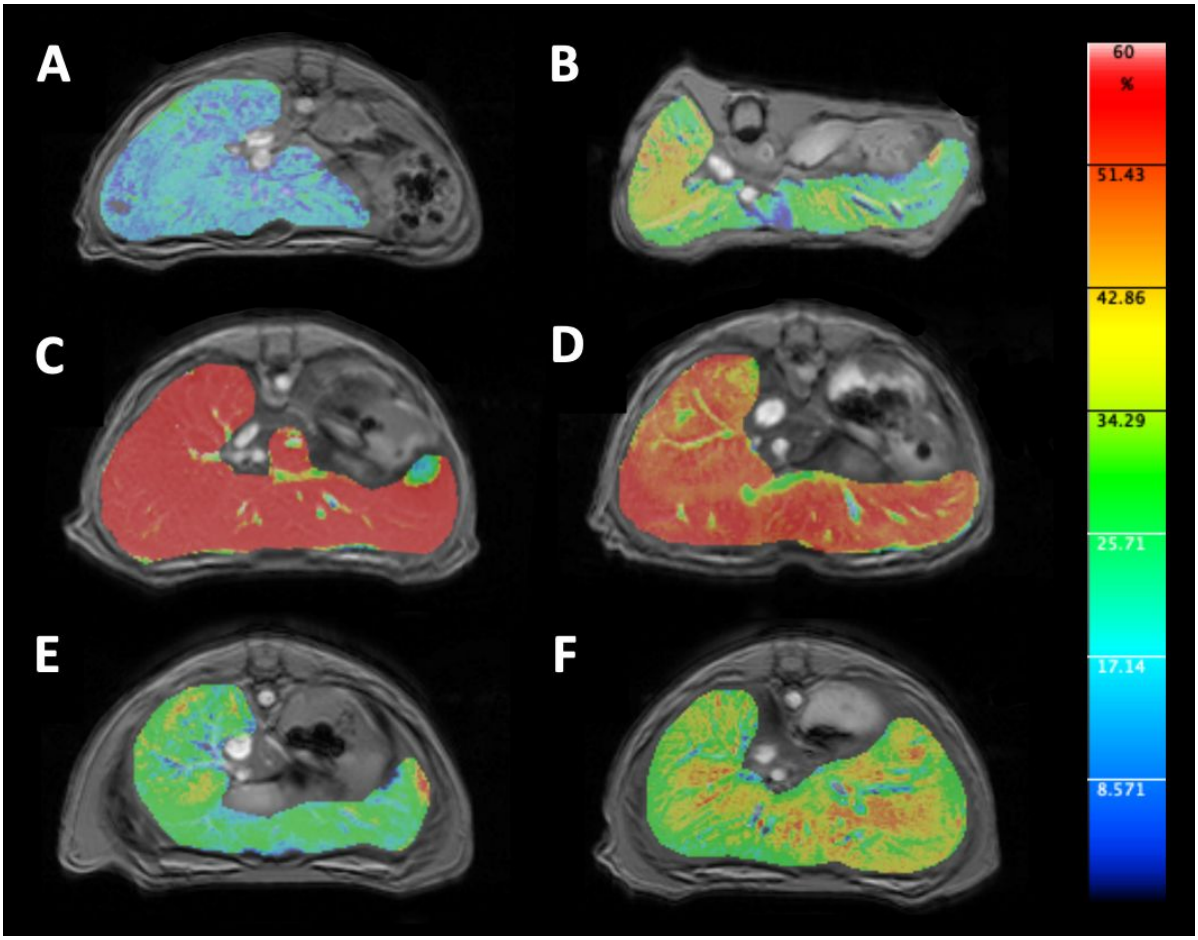

Figure 5. Color maps of a single transversal slice (out of 7) visualizing liver PDFF map of a representative animal from each group in study 2 at week 4 or 12, overlaid on a grey scale anatomical scan. Color bar represents PDFF values from 0% (blue) to 60% (red). **A.** Standard diet, 16% at week 12; **B.** MCD diet, 29% at week 4; **C.** CDAA diet, 52% at week 12; **D.** CSAA diet, 47% at week 12; **E.** WD, 24% at week 12; **F.** WD + CCl_4regimen, 30% at week 12.

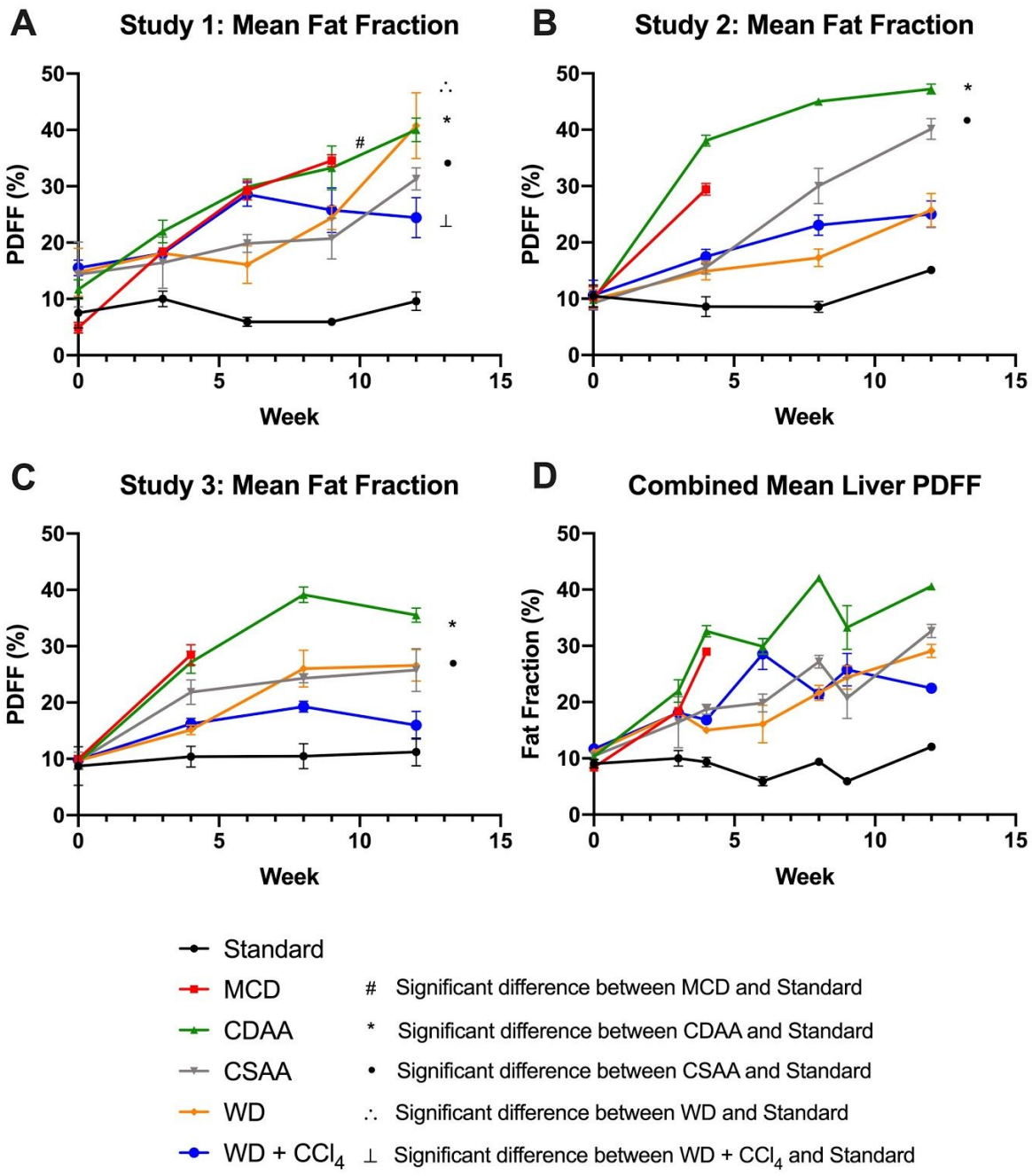

Figure 6. Graphs showing the mean liver PDFF with standard error vs time by group. Standard error bars which are not shown are shorter than the symbol at each data point. **A.** Study 1: Standard (n=3), MCD (n=4), CDAA (n=4), CSAA (n=2), WD (n=3), WD + CCl_4 (n=3); **B.** Study 2: Standard (n=4), MCD (n=4), CDAA (n=4), CSAA (n=4), WD (n=4), WD + CCl_4 (n=4); **C.** Study 3: Standard (n=3), MCD (n=4), CDAA (n=4), CSAA (n=4), WD (n=4), WD + CCl_4 (n=4); **D.** Combined mean across the three studies: Standard (n=10), MCD (n=12), CDAA (n=12), CSAA (n=10), WD (n=11), WD + CCl_4 (n=11).

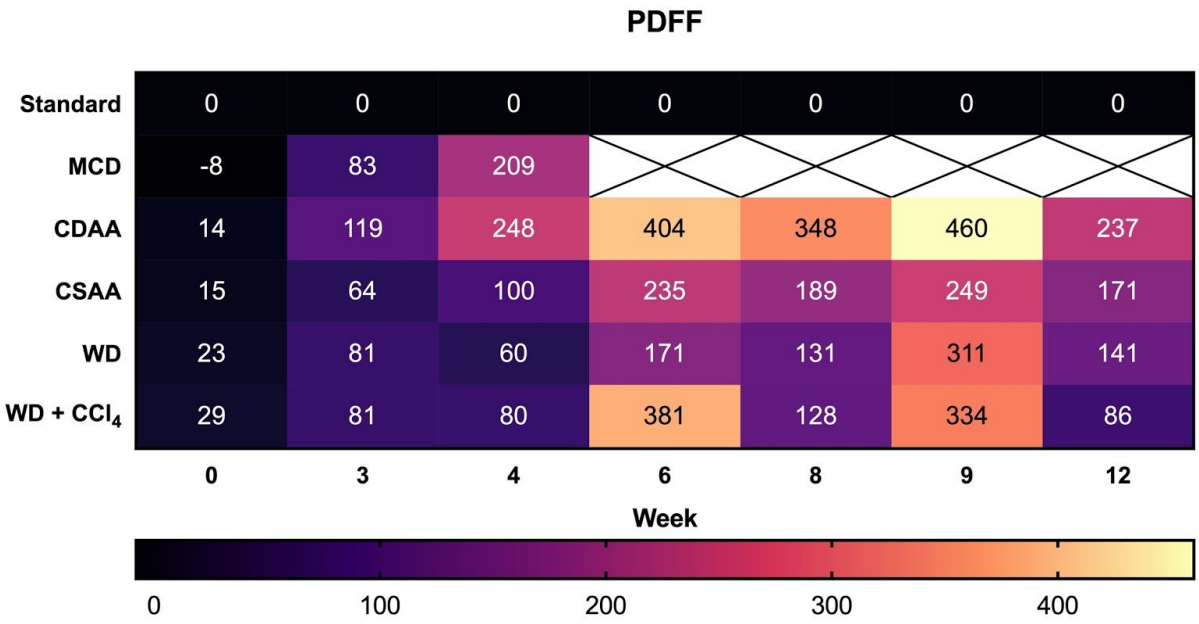

Figure 7. Heat Map representing the percent difference in combined liver PDFF between experimental diet groups and mice on the standard diet at each timepoint over the three studies. Group labels are to the left of the heat map and week labels are at the bottom. Color bar indicates percent differences ranging from -8 to +460.

Apparent Diffusion Coefficient

The apparent diffusion coefficient (ADC) of pure water at 25°C has been previously determined to be 2.24 x 10^{-3} mm^2/s and 2.84 x 10^{-3} mm^2/s at 35°C [36]. Baseline mean liver ADC values at 33°C ranged between 1.39 x 10^{-3} mm^2/s and 1.98 x 10^{-3} mm^2/s. When attenuation due to tissue structure is taken into account, these values exhibit good agreement with the previously determined diffusion coefficient of pure water and also typical values measured in tissues.

Apparent Diffusion Coefficient (ADC) was quantified in all mice over the entire diet- and chemical-based disease induction period in order to quantify the diffusion of water throughout the liver tissue. The individual spin echo images in the DWI protocol used were generally of high quality and showed relatively uniform liver contrast. Fitted ADC maps show relatively uniform ADC signal with evidence of some small heterogeneity and the data was generally well

fitted to the Stejskal-Tanner equation (Fig. 8). Liver ADC was found to decrease across all disease groups in each study over the 12-week time course, but by comparison was generally relatively constant for the mice on the standard diet over this period.

In study 1, both time and diet were found to have significant effects on liver ADC (Appendix B). All experimental groups (MCD, $p = 0.005$; CDAA, $p = 0.040$; CSAA, $p = 0.039$; WD, $p = 0.007$; WD + CCl_4, $p = 0.035$) were found to be significantly different from mice on the standard diet (Appendix B). Mice on the standard diet exhibited relatively constant mean liver ADC values over the first 6 weeks before a moderate decrease of -16% was observed after 12-weeks, relative to baseline for this group (Fig. 9A). Liver ADC in mice on the standard diet was quantified to be $1.9 \times 10^{-3} \pm 0.2 \times 10^{-3}$ mm^2/s at baseline and $1.6 \times 10^{-3} \pm 0.2 \times 10^{-3}$ mm^2/s at week 12 (Fig. 9A). At week 12, mice on the WD exhibited the lowest mean liver ADC of $0.8 \times 10^{-3} \pm 0.0 \times 10^{-3}$ mm^2/s followed closely by mice on the CSAA diet with a mean liver ADC of $0.8 \times 10^{-3} \pm 0.0 \times 10^{-3}$ mm^2/s (Fig. 9A). Of the experimental groups, mice on the WD + CCl_4 regimen exhibited the smallest decrease by week 12 with a mean liver ADC of $1.0 \times 10^{-3} \pm 0.3$ mm^2/s (Fig. 9A).

In study 2, the mixed ANOVA which excluded MCD-fed mice due to differing disease time courses, revealed both time and diet were found to have significant effects on liver ADC (Appendix B). In this analysis, all included experimental groups (CDAA, $p < 0.001$; CSAA, $p = 0.002$; WD, $p = 0.013$; and WD + CCl_4, $p = 0.010$) were found to be statistically different from mice on the standard diet (Appendix B). Mice on the standard diet had a mean liver ADC of $1.5 \times 10^{-3} \pm 0.1 \times 10^{-3}$ mm^2/s at baseline and $1.7 \times 10^{-3} \pm 0.1 \times 10^{-3}$ mm^2/s at week 12 (Fig. 9B). Mice on the WD again exhibited the lowest liver ADC value of $0.6 \times 10^{-3} \pm 0.1 \times 10^{-3}$ mm^2/s at week

12 followed by mice on the CDAA diet at $0.7 \times 10^{-3} \pm 0.1 \times 10^{-3}$ mm^2/s (Fig. 9B). Mice on the WD + CCl_4 regimen exhibited the smallest decrease by week 12 with a mean liver ADC of $1.2 \times 10^{-3} \pm 0.3$ mm^2/s (Fig. 9B). The mixed ANOVA performed including data from MCD-fed mice and all other groups up to week 4 only, did not show significant effects of either time or diet on liver ADC by week 4 (Appendix B). Furthermore, liver ADC of MCD-fed mice was not found to be statistically different from mice on the standard diet or any other experimental groups (Appendix B).

In study 3, the mixed ANOVA performed on data excluding MCD-fed mice revealed that time and diet both had significant effects on liver ADC while the mixed ANOVA including MCD-fed and all other groups up to week 4 revealed a significant effect of time but not diet on liver ADC (Appendix B). Liver ADC of CDAA-fed ($p = 0.024$) mice was found to be statistically different as compared to mice on the standard diet (Appendix B). Control mice exhibited a mean liver ADC value of $1.6 \times 10^{-3} \pm 0.2 \times 10^{-3}$ mm^2/s at week 12 while CDAA-fed mice exhibited a mean liver ADC value of $1.0 \times 10^{-3} \pm 0.1 \times 10^{-3}$ mm^2/s at week 12 (Fig. 9C). Mice on the WD + CCl_4 regimen exhibited the smallest decrease by week 12 with a mean liver ADC of $1.3 \times 10^{-3} \pm 0.1$ mm^2/s (Fig. 9C). Liver ADC of mice in the MCD, CSAA, WD, and WD + CCl_4, was not found to be significantly different as compared to mice on the standard diet (Appendix B).

When liver ADC data was combined across each of the three studies, mice on the standard diet had a combined mean liver ADC of $1.7 \times 10^{-3} \pm 0.4 \times 10^{-3}$ mm^2/s at week 12 (Fig. 9D). WD-fed mice exhibited the greatest decrease by week 12 with a combined mean liver ADC of $0.9 \times 10^{-3} \pm 0.1 \times 10^{-3}$ mm^2/s which represents a -48% difference versus combined mean liver

ADC of mice on the standard diet at week 12 (Fig. 9D, 10). CDAA-fed and CSAA-fed mice exhibited similar decreases in combined mean liver ADC across the three studies. At week 12, both CDAA-fed and CSAA-fed mice had a combined mean liver ADC of $0.9 \times 10^{-3} \pm 0.1 \times 10^{-3}$ mm^2/s (Fig. 9D). This represents a -46% difference and -45% difference versus combined mean liver ADC of mice on the standard diet at week 12 for both CDAA-fed and CSAA-fed mice, respectively (Fig. 10). Mice on the WD + CCl_4 regimen showed the least decrease in combined mean liver ADC by week 12. Mice on the WD + CCl_4 regimen exhibited a combined mean liver ADC of 1.2×10^{-3} $mm^2/s \pm 0.1 \times 10^{-3}$ which represents a -30% difference versus mean liver ADC of mice on the standard diet at week 12 (Fig. 9D, 10). MCD-fed exhibited a precipitous decrease in combined mean liver ADC by week 4 with a mean value of $1.2 \times 10^{-3} \pm 0.1 \times 10^{-3}$ mm^2/s which represents a -30% change versus control mice on the standard diet (Fig. 9D, 10).

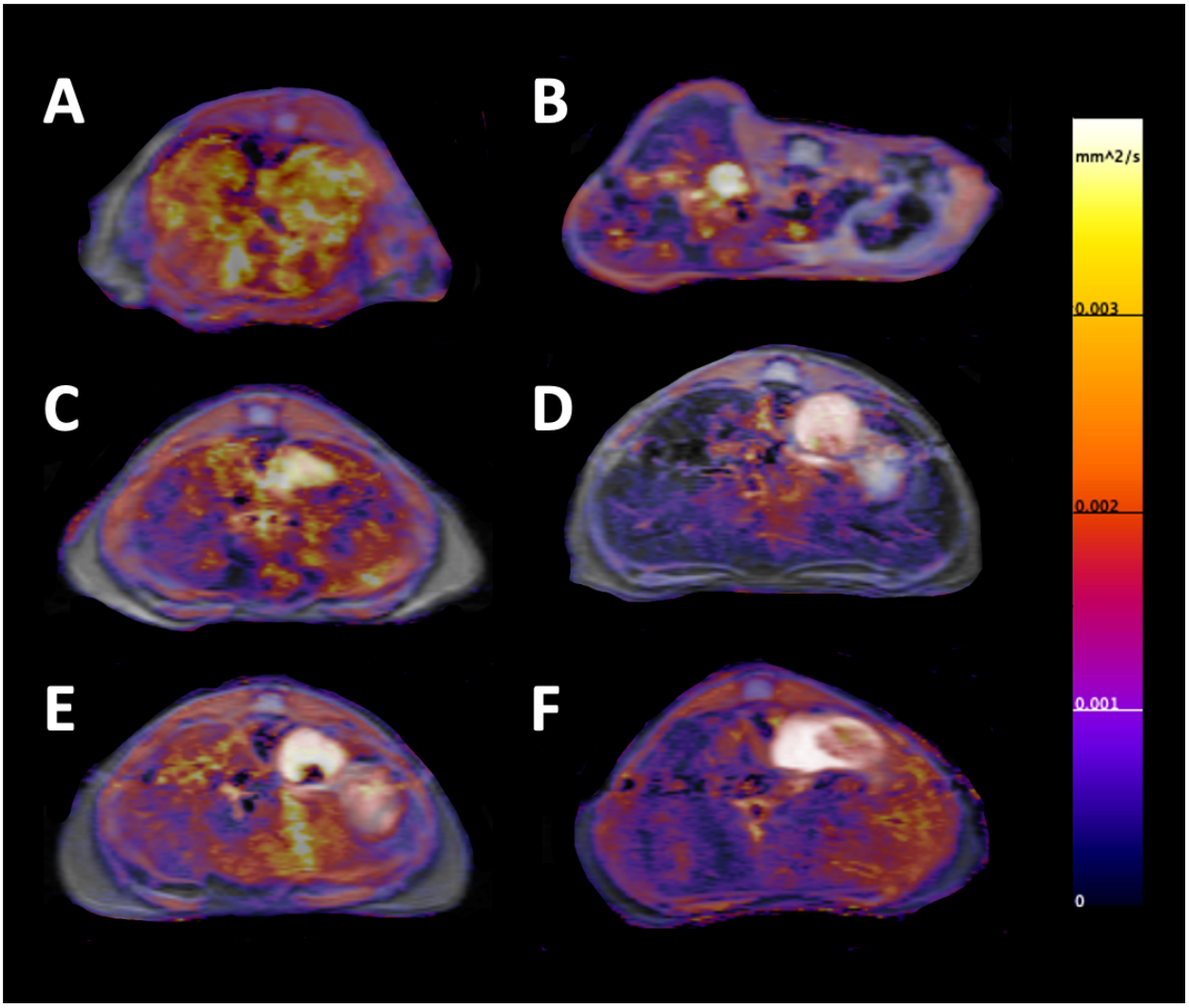

Figure 8. Color maps of a single transversal slice (out of 7) visualizing liver ADC map of a representative animal from each group in study 2 at week 4 or 12, overlaid on a grey scale anatomical scan. The color scale represents ADC values from 0 x 10^{-3} mm^2/s (purple) to 4.0 x 10^{-3} (yellow). **A.** Standard diet, 1.9 x 10^{-3} mm^2/s at week 12; **B.** MCD diet, 1.3 x 10^{-3} mm^2/s at week 4; **C.** CDAA diet, 1.0 x 10^{-3} mm^2/s at week 12; **D.** CSAA diet, 0.9 x 10^{-3} mm^2/s at week 12; **E.** WD, 1.1 x 10^{-3} mm^2/s at week 12; **F.** WD + CCl_4 regimen, 1.2 x 10^{-3} mm^2/s at week 12.

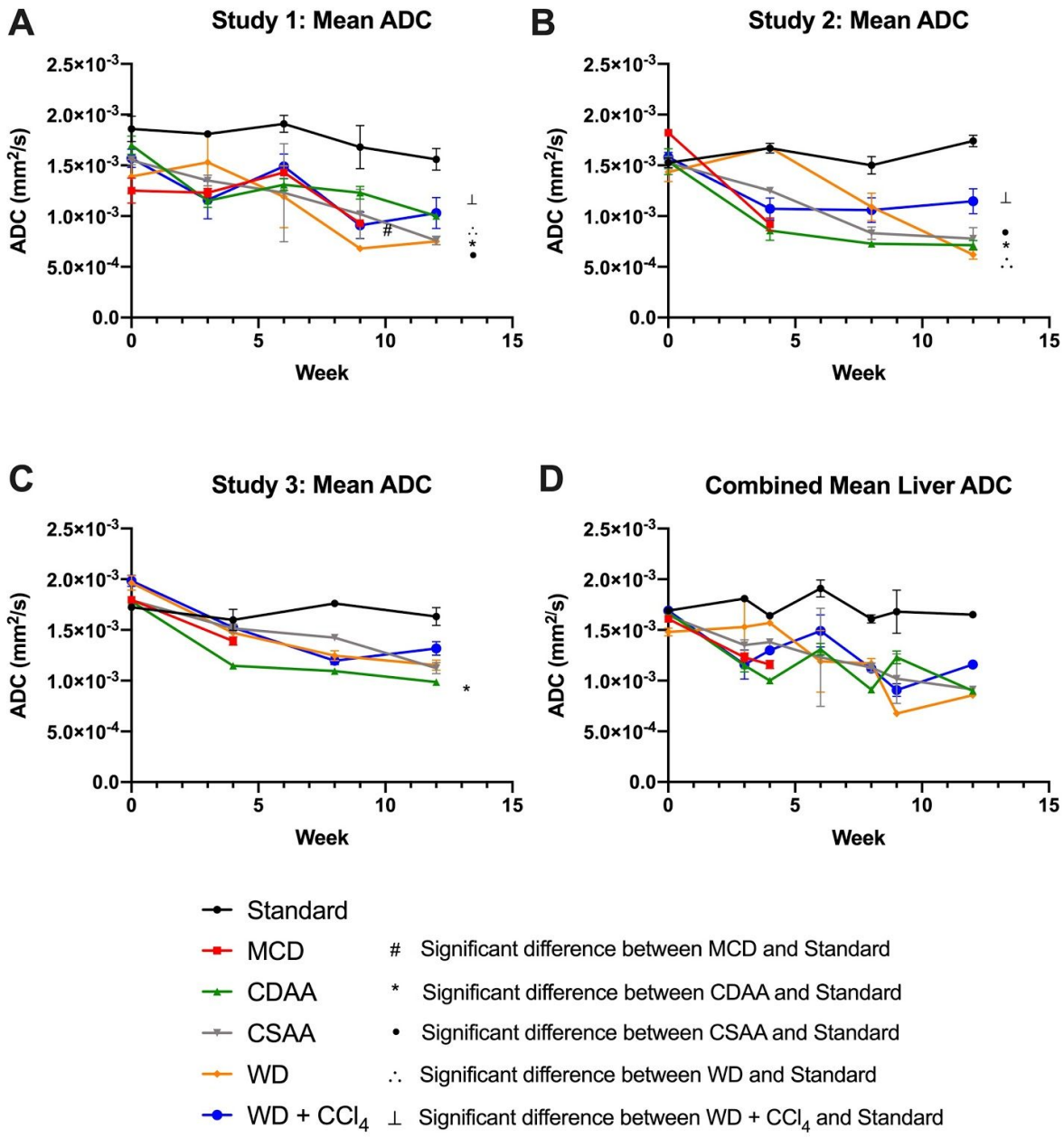

Figure 9. Graphs showing the mean liver ADC with standard error vs time by group. Standard error bars which are not shown are shorter than the symbol at each data point. **A.** Study 1: Standard (n=3), MCD (n=4), CDAA (n=4), CSAA (n=2), WD (n=3), WD + CCl_4 (n=3); **B.** Study 2: Standard (n=4), MCD (n=4), CDAA (n=4), CSAA (n=4), WD (n=4), WD + CCl_4 (n=4); **C.** Study 3: Standard (n=3), MCD (n=4), CDAA (n=4), CSAA (n=4), WD (n=4), WD + CCl_4 (n=4); **D.** Combined mean across the three studies: Standard (n=10), MCD (n=12), CDAA (n=12), CSAA (n=10), WD (n=11), WD + CCl_4 (n=11).

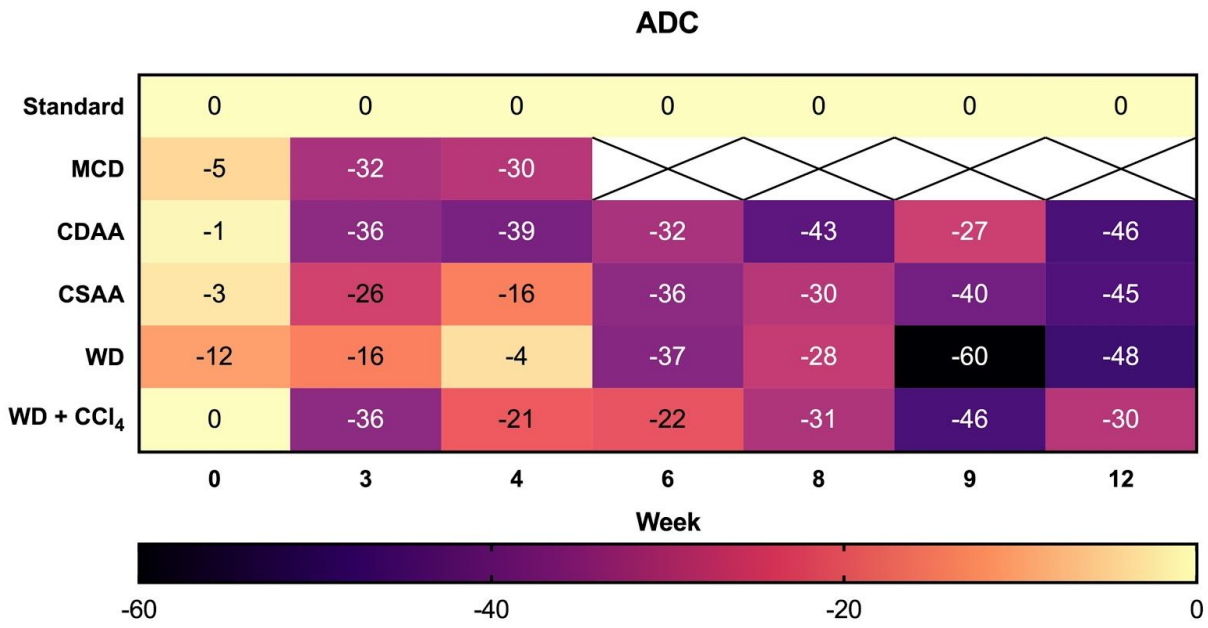

Figure 10. Heat Map representing the percent difference in combined liver ADC between experimental diet groups and mice on the standard diet at each timepoint over the three studies. Group labels are to the left of the heat map and week labels are at the bottom. Color bar indicates percent differences ranging from -60 to 0.

T_1 relaxation time

in vitro

T_1 relaxation time exhibited a strong negative correlation ($R^2 = 0.90$) with fat content in the fat phantom (Fig. 11). The reference vial containing 5% soy oil in agarose had a T_1 relaxation time of 3132 ms and the reference vial containing 50% soy oil in agarose had a T_1 relaxation time of 1327 ms suggesting an inverse relationship between the two biomarkers (Fig. 11).

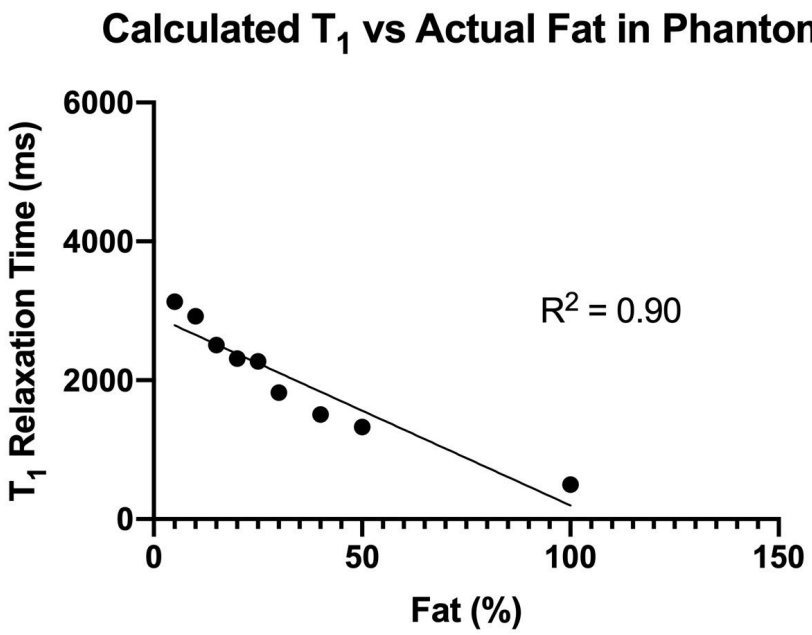

Figure 11. Graph depicting the correlation between quantified T_1 relaxation time and actual percentage of fat (by volume) in each vial of the fat phantom from 5 - 100%. The 100% vial was included in analysis in order to determine the T_1 relaxation time of fat at 11.7T.

in vivo

Liver T_1 relaxation time was quantified at each MRI timepoint in order to investigate the effects of diet and chemical based NAFLD and NASH induction on this parameter. Individual images for each TR value used were of generally high quality and the data was well fitted to the exponential recovery function. Liver T_1 relaxation time was observed to decrease in all diseased groups in each study over the 12-week time course, with relatively constant values measured in the standard diet control. T_1 findings were consistent across the three studies for the 12 week period.

In study 1, both time and diet were found to have statistically significant effects on liver T_1 relaxation time (Appendix B). When standard error is taken into account, mice on the standard diet exhibited no change in mean liver T_1 relaxation time. At baseline, mice on the standard diet

have a mean liver T_1 relaxation time of 3042 ± 183 ms compared to 3084 ± 418 ms at week 12 (Fig. 12A). All experimental groups exhibited decreases in mean liver T_1 relaxation time over the 12-week time course. Mean liver T_1 relaxation time was found to be statistically different from the mice on the standard diet for the mice on the MCD diet ($p = 0.004$), CDAA diet ($p = 0.002$), WD ($p = 0.031$) and WD + CCl_4 regimen ($p = 0.021$) (Appendix B). Mice on the WD exhibited the largest decrease by week 12 with a mean liver T_1 relaxation time of 1483 ± 73 ms (Fig. 12A). Mice on the CSAA diet exhibited the least decrease with a mean liver T_1 relaxation time of 1926 ± 152 ms at week 12 (Fig. 12A).

In study 2, both time and diet were found to have statistically significant effects on liver T_1 relaxation time (Appendix B). Mice on the standard diet exhibited a modest decrease in liver T_1 relaxation time over the course of the study with a mean liver T_1 relaxation time of 3629 ± 251 ms at baseline and 3347 ± 39 ms at week 12 (Fig. 12B). All experimental groups showed decreases in liver T_1 relaxation time that was found to be statistically different (MCD, $p = 0.017$; CDAA, $p < 0,001$; CSAA, $p < 0.001$; WD, $p = 0.008$; WD + CCl_4, $p < 0.001$) versus mice on the standard diet (Appendix B). CDAA-fed mice exhibited the greatest decrease at week 12 with a mean liver T_1 relaxation time of 1450 ± 43 ms (Fig. 12B). Mice on the WD + CCl_4 regimen had the smallest decrease by week 12 with a mean liver T_1 relaxation time of 2475 ± 320 ms (Fig. 12B).

In study 3, both time and diet were found to have statistically significant effects on liver T_1 relaxation time (Appendix B). When standard error is taken into account, mice on the standard

diet exhibited no change in mean liver T_1 relaxation time over the 12-week time course. At baseline, mice on the standard diet had a mean liver T_1 relaxation time of 3375 ± 254 ms compared with 3057 ± 23 ms at week 12 (Fig. 12C). Mice on the CDAA diet, again, exhibited the largest decrease in mean liver T_1 relaxation time at week 12 with a value of 1493 ms ± 62 while mice on the WD + CCl_4 regimen again had the smallest decrease at week 12 with a mean liver T_1 relaxation time of 2152 ms ± 69 (Fig. 12C).

Liver T_1 relaxation time was combined for each group across each of the three studies. Mice on the standard diet had a combined mean liver T_1 relaxation time of 3222 ± 68 ms at week 12 (Fig. 12D). CDAA-fed mice exhibited the largest decrease in combined mean liver T_1 relaxation time over the course of the study. At week 12, CDAA-fed mice had a combined mean liver T_1 relaxation time of 1547 ± 68 ms which represents a -52% difference versus mice on the standard diet (Fig 12D, 13). Mice on the WD exhibited a -46% difference versus mice on the standard diet with a combined mean liver T_1 relaxation time of 1678 ± 198 ms at week 12 (Fig 12D, 13). CSAA-fed mice exhibited the third largest decrease with a combined mean liver T_1 relaxation time of 1672 ± 28 ms at week 12 and a -45% difference versus mice on the standard diet at week 12 (Fig 12D, 13). Mice on the WD + CCl_4 regimen had a combined mean liver T_1 relaxation time of 2093 ± 75 ms and a -35% decrease versus mice on the standard diet at week 12 (Fig 12D, 13). Mice on the MCD diet exhibited a -45% difference versus mice on the standard diet by week 4 with a combined mean liver T_1 relaxation time of 1997 ± 100 ms (Fig 12D, 13).

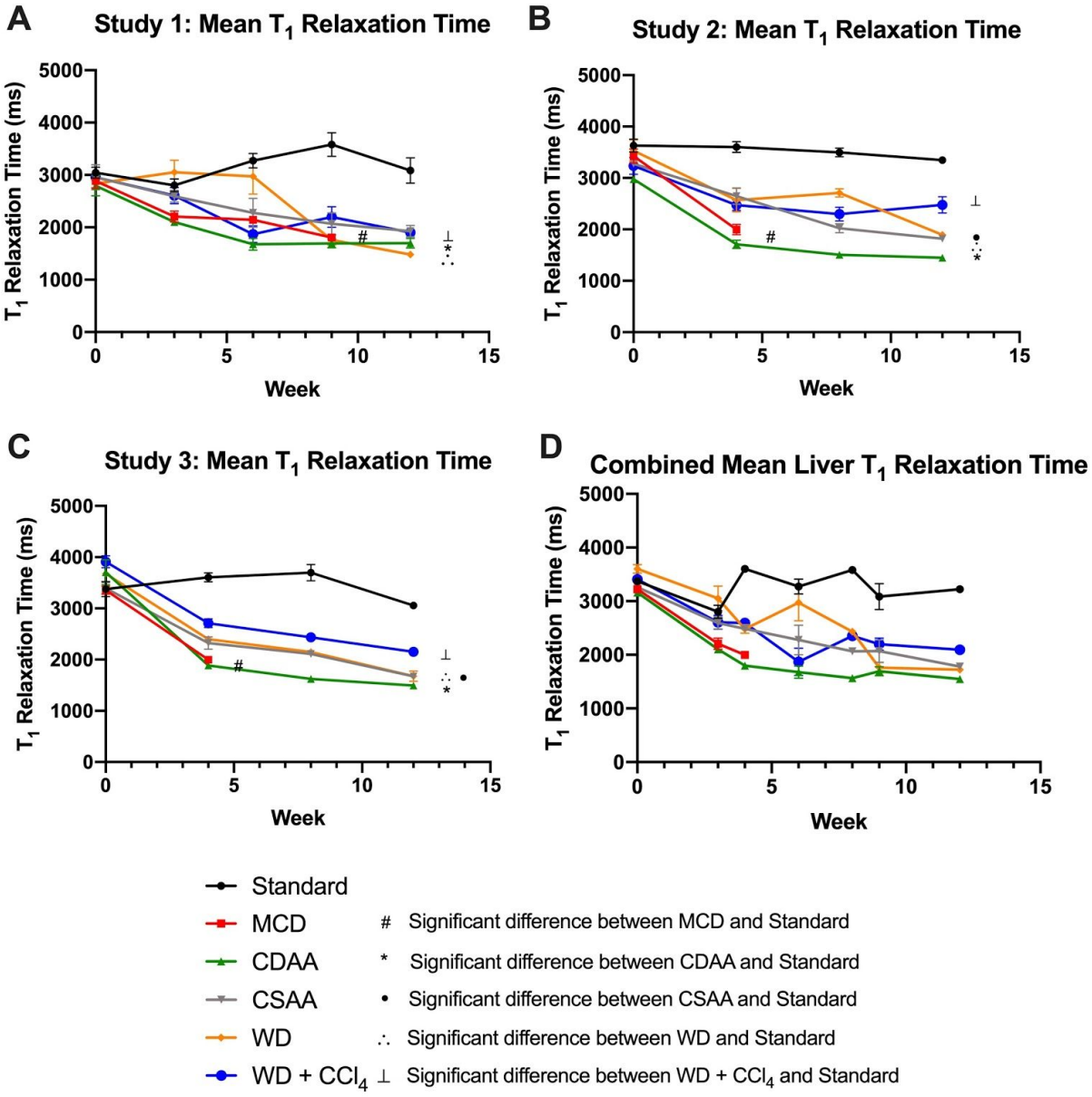

Figure 12. Graphs showing the mean liver T_1 relaxation time with standard error vs time by group. Standard error bars which are not shown are shorter than the symbol at each data point. **A.** Study 1: Standard (n=3), MCD (n=4), CDAA (n=4), CSAA (n=2), WD (n=3), WD + CCl_4 (n=3); **B.** Study 2: Standard (n=4), MCD (n=4), CDAA (n=4), CSAA (n=4), WD (n=4), WD + CCl_4 (n=4); **C.** Study 3: Standard (n=3), MCD (n=4), CDAA (n=4), CSAA (n=4), WD (n=4), WD + CCl_4 (n=4); **D.** Combined mean across the three studies: Standard (n=10), MCD (n=12), CDAA (n=12), CSAA (n=10), WD (n=11), WD + CCl_4 (n=11).

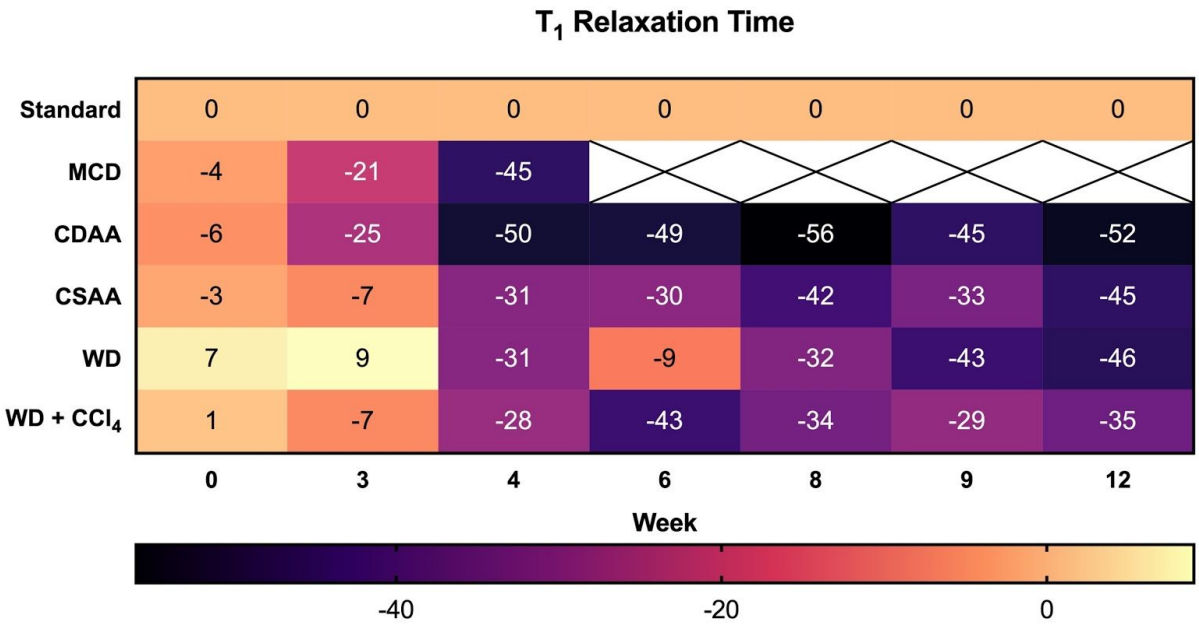

Figure 13. Heat Map representing the percent difference in combined liver T_1 relaxation time between experimental diet groups and mice on the standard diet at each timepoint over the three studies. Group labels are to the left of the heat map and week labels are at the bottom. Color bar indicates percent differences ranging from -56 to 9.

T_2 relaxation time

in vitro

A simple linear regression of liver T_2 relaxation time versus fat content in the fat phantom revealed no correlation between the two biomarkers *in vitro* (Fig. 14).

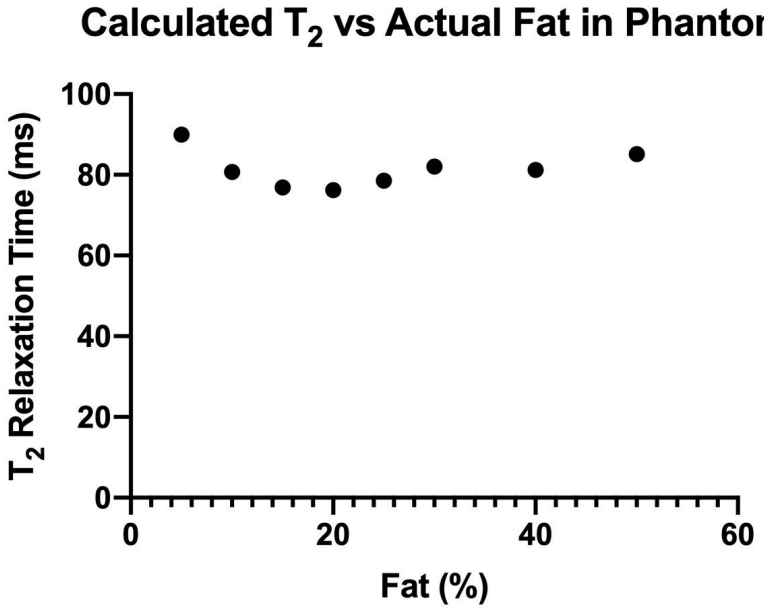

Figure 14. Graphs representing the correlation between calculated T_2 relaxation time and actual percentage of fat (by volume) in each vial of the fat phantom from 5 - 50%. The vial containing 100% fat was excluded from analysis because PDFF *in vivo* never reached that large of a percentage.

in vivo

At each MRI imaging time point, mouse liver T_2 relaxation time was quantified in order to determine the longitudinal effects of diet and chemical based NAFLD and NASH disease induction on this biomarker. Individual TE value echo images were of high quality, and the data was well fitted to a decaying exponential. While liver T_2 relaxation time remained stable in

control mice, liver T_2 relaxation time was observed to increase in all experimental groups over the course of each study.

In study 1, both time and diet were found to have statistically significant effects on liver T_2 relaxation time (Appendix B). Control mice on the standard diet showed no change in mean liver T_2 relaxation time over the 12-week time course with a baseline mean liver T_2 relaxation time of 19 ± 1 ms as compared to 19 ± 1 ms at week 12 (Fig. 15A). Mice on the MCD diet ($p < 0.001$), CDAA diet ($p < 0.001$), and WD + CCl_4 regimen ($p = 0.018$) exhibited increases in mean liver T_2 relaxation time which were found to be statistically different versus mice on the standard diet (Appendix B). Mice on the CDAA diet exhibited the largest increase with a mean liver T_2 relaxation time of 34 ± 2 ms at week 12 (Fig. 15A). Mice on the CSAA diet had the smallest increase over the 12-week time course with a mean liver T_2 relaxation time of 26 ± 1 ms at week 12 (Fig. 15A).

In study 2, both time and diet were found to have statistically significant effects on liver T_2 relaxation time (Appendix B). Mice on the standard diet showed no change in mean liver T_2 relaxation time over the course of the study. At baseline, control mice had a mean liver T_2 relaxation time of 17 ± 1 ms versus 16 ms ± 1 ms at week 12 (Fig. 15B). All experimental groups exhibited increases in liver T_2 relaxation time which were found to be significantly different (MCD, $p = 0.001$; CDAA, $p < 0.001$; CSAA, $p = 0.002$; WD, $p = 0.013$; WD + CCl_4, $p = 0.010$) from mice on the standard diet (Appendix B). Mice on the CDAA diet exhibited the largest increase with a mean liver T_2 relaxation time of 40 ± 1 ms at week 12 (Fig. 15B). Mice on the

WD + CCl_4 regimen exhibited the smallest increase at week 12 with a mean liver T_2 relaxation time of 24 ± 3 ms (Fig. 15B).

In study 3, both time and diet were found to have statistically significant effects on liver T_2 relaxation time (Appendix B). When standard error is taken into account, mice on the standard diet exhibited no change in mean liver T_2 relaxation time over the course of the study. Mice on the standard diet had a mean liver T_2 relaxation time of 19 ms ± 0 ms at baseline and 17 ms ± 1 ms at week 12 (Fig. 15C). All experimental groups exhibited increases in liver T_2 relaxation time which were found to be significantly different (MCD, $p < 0.001$; CDAA, $p < 0.001$; CSAA, $p = 0.007$; WD, $p = 0.021$; WD + CCl_4, $p = 0.016$) from mice on the standard diet (Appendix B). Mice on the MCD diet exhibited the largest increase by week 4 with a mean liver T_2 relaxation time of 32 ± 2 ms (Fig. 15C). At week 12, CDAA-fed mice had the largest mean liver T_2 relaxation time of 33 ± 1 ms (Fig. 15C). Mice on the WD + CCl_4 regimen exhibited the smallest increase at week 12 with a mean liver T_2 relaxation time of 23 ± 0 ms (Fig. 15C).

Liver T_2 relaxation time was combined in each experimental group across each of the three studies. Mice on the standard diet had a combined mean liver T_2 relaxation time of 18 ± 0 ms at week 12 (Fig. 15D). Mice on the CDAA diet exhibited the largest increase with a combined mean liver T_2 relaxation time of 35 ± 1 ms at week 12 and a +101% increase versus mice on the standard diet (Fig. 15D, 16). Mice on the CSAA diet exhibited the second largest increase with a combined mean liver T_2 relaxation time of 28 ± 1 ms at week 12 and a +60% increase versus mice on the standard diet (Fig. 15D, 16). Mice on the WD had a combined mean

liver T_2 relaxation time of 27 ± 1 ms at week 12 representing a +51% difference versus mice on the standard diet (Fig. 15D, 16). Mice on the WD + CCl_4 regimen exhibited the lowest combined mean liver T_2 relaxation time of 25 ± 1 ms at week 12 representing a +41% difference versus mice on the standard diet (Fig. 15D, 16). Mice on the MCD diet showed a steep increase with a combined mean liver T_2 relaxation time of 29 ± 1 ms at week 12 representing a +71% difference compared to control mice on the standard diet (Fig. 15D, 16).

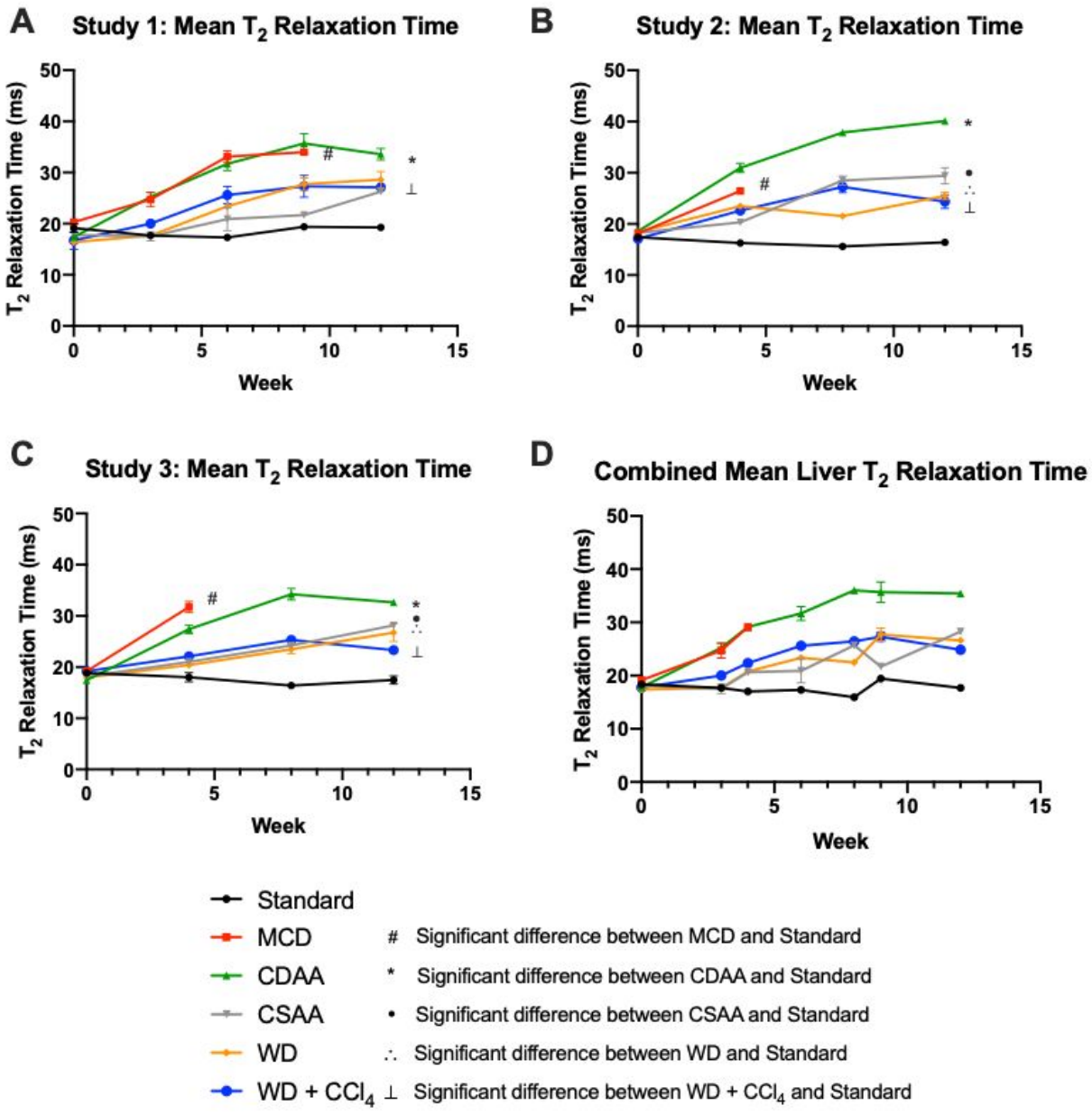

Figure 15. Graphs showing the mean liver T_2 relaxation time with standard error vs time by group. Standard error bars which are not shown are shorter than the symbol at each data point. **A.** Study 1: Standard (n=3), MCD (n=4), CDAA (n=4), CSAA (n=2), WD (n=3), WD + CCl_4 (n=3); **B.** Study 2: Standard (n=4), MCD (n=4), CDAA (n=4), CSAA (n=4), WD (n=4), WD + CCl_4 (n=4); **C.** Study 3: Standard (n=3), MCD (n=4), CDAA (n=4), CSAA (n=4), WD (n=4), WD + CCl_4 (n=4); **D.** Combined mean across the three studies: Standard (n=10), MCD (n=12), CDAA (n=12), CSAA (n=10), WD (n=11), WD + CCl_4 (n=11).

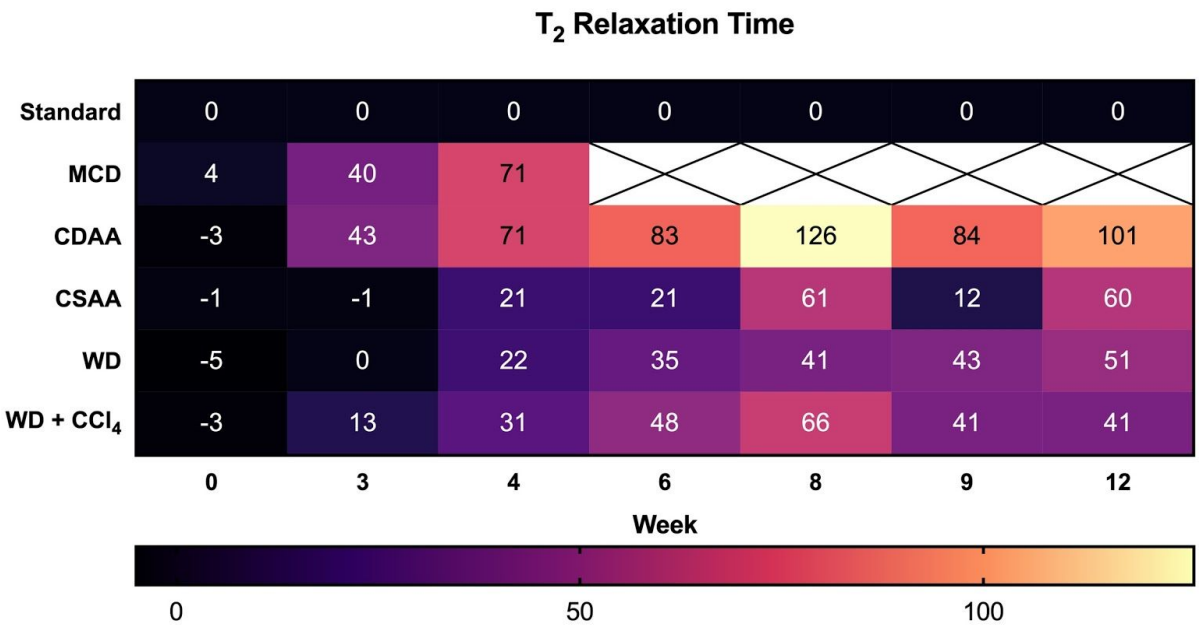

Figure 16. Heat Map representing the percent difference in combined liver T_2 relaxation time between experimental diet groups and mice on the standard diet at each timepoint over the three studies. Group labels are to the left of the heat map and week labels are at the bottom. Color bar indicates percent differences ranging from -5 to 126.

Correlations

Correlations between individual biomarkers were investigated in order to elucidate the underlying biological mechanisms for which they are a proxy for. The relationships were investigated by plotting *in vivo* data of individual mice at each time point across the three studies.

Liver T_1 relaxation time was found to decrease across all experimental groups versus control while liver PDFF was found to increase (Fig. 17A,C). A linear regression revealed a negative correlation ($R^2 = 0.55$) between T_1 and PDFF *in vivo* (Fig. 18A). Liver ADC was also found to decrease while PDFF increased in all experimental groups (Fig. 17A-B). A negative correlation ($R^2 = 0.34$) was established between ADC and PDFF (Fig. 18C). Accordingly, ADC

and T_1 exhibited a positive correlation ($R^2 = 0.38$) as both biomarkers were found to decrease over the disease time course (Fig. 17B-C; 18D). Conversely, liver T_2 relaxation time was found to increase in all experimental groups versus control alongside of PDFF with a positive correlation ($R^2 = 0.66$) (Fig. 17A,D; 18B). Both ADC and T_1 were found to have a negative correlation ($R^2 = 0.57$ and $R^2 = 0.33$, respectively) with T_2 (Fig. 18E-F).

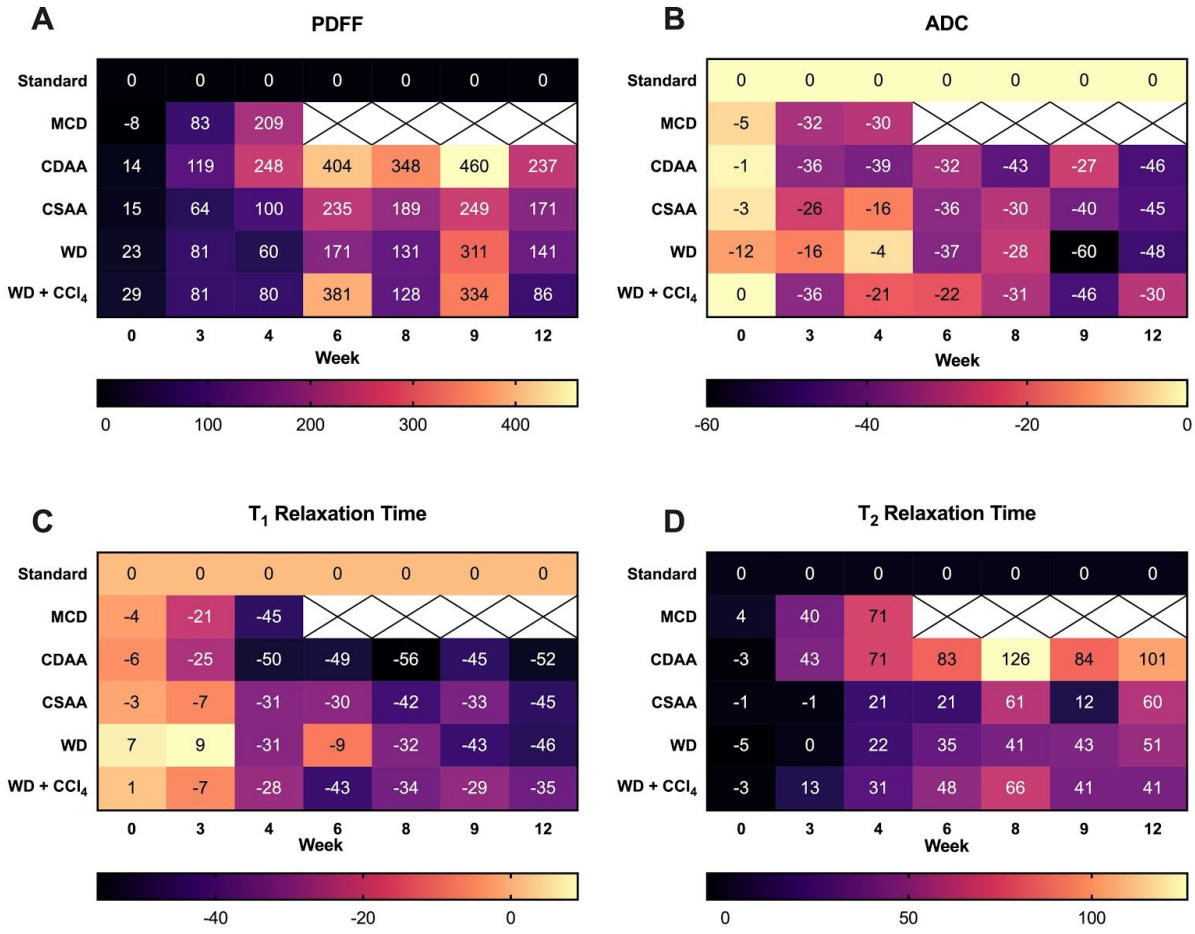

Figure 17. Heat Maps depicting the percent difference between the control group and the experimental groups for all imaging parameters across the three studies. **A**. Combined mean PDFF (Fig. 7); **B.** Combined mean ADC (Fig. 10); **C.** Combined mean T_1 (Fig. 13); **D.** Combined mean T_2 (Fig. 16).

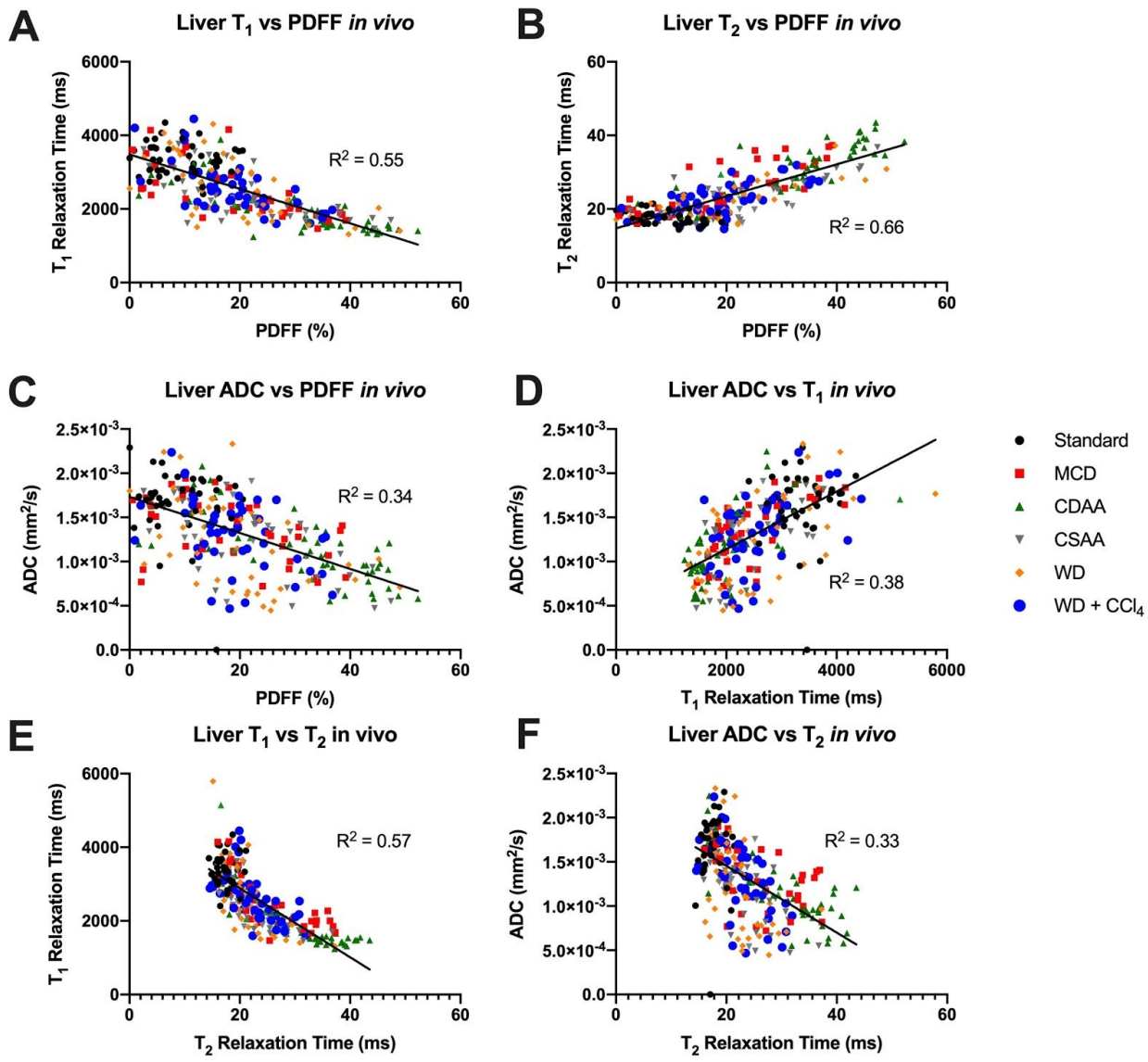

Figure 18. Correlation graphs between each of the MRI biomarkers. The correlation coefficient (R^2) was calculated based upon individual mouse data at each imaging time point across all three studies. Groups are color coded. **A.** T_1 versus PDFF; **B.** T_2 versus PDFF; **C.** ADC versus PDFF; **D.** ADC versus T_1; **E.** T_1 versus T_2; **F.** ADC versus T_2.

Dietary Intervention: Study 2

Following the 12 week diet and chemical-based disease time course in study 2, all experimental groups were placed back on a standard diet regimen identical to the mice on the standard diet. All experimental groups showed sharp regression towards basal levels in each of the measured parameters, body weight, PDFF, ADC, T_1, and T_2, following dietary intervention (Fig. 19A-E). Of note, MCD-fed mice were excluded from this experimental intervention because they were removed from study at week 4 due to diet-induced body weight loss.

Mice on the standard diet exhibited increases in body weight over this intervention time period consistent with the increases that were observed over the 12 week disease time course. At week 12, mice on the standard diet had a mean body weight of 30.9 ± 2.8 g at week 12 to 32.3 ± 2.7 g at week 16.5 (4.5 weeks post-intervention) (Fig. 19 A). Mice on the CDAA diet exhibited a -11% decrease in mean body weight (Fig. 20A) from 41.4 ± 1.3 g at week 12 to 36.8 ± 1.2 g at week 16.5 (Fig. 19 A). Similarly, CSAA-fed mice displayed a -9% decrease (Fig. 20A) in mean body weight from 39.8 ± 2.3 g at week 12 to 36.1 ± 2.1 g at week 16.5 (Fig. 19 A). WD-fed mice exhibited the most precipitous decrease in body weight of -16% (Fig. 20A) from a mean of 38.7 ± 1.6 g at week 12 to 32.7 ± 1.7 g at week 16.5 (Fig. 19 A). Of the experimental groups, mice on the WD + CCl_4 regimen displayed the least change in mean body weight over this time period with -1% decrease (Fig. 20A) and an average body weight of 35.7 ± 3.1 g at week 12 to 35.3 ± 3.3 g at week 16.5 (Fig. 19 A).

Mice on the standard diet exhibited negligible changes in mean liver PDFF over the 4.5 week intervention time course. At week 12, mice on the standard diet had a mean liver PDFF of 15 ± 1% as compared to 17 ± 2% at week 16.5 (Fig. 19B). CDAA-fed mice exhibited the largest

decrease in mean liver PDFF over this time period with a mean liver PDFF of 47 ± 2% at week 12 as compared to 11 ± 4% at week 16.5 (Fig. 19B) which represents a -76% decrease from week 12 (Fig. 20B). CSAA-fed mice exhibited a similar downward trend in body weight with a -71% decrease in liver PDFF at week 16.5 as compared to week 12 (Fig. 20B). At week 12, CSAA-fed mich had a mean liver PDFF of 40 ± 4% at week 12 as compared to 12 ± 1% at week 16.5 (Fig. 19B). WD-fed mice and mice on the WD + CCl_4 regimen also displayed similar decreases in liver PDFF with a -66% and -63% decrease, respectively, at week 16.5 as compared to week 12 (Fig. 20B). At week 12, WD-fed mice displayed a mean liver PDFF of 26 ± 6% mice on the WD + CCl_4 regimen displayed a mean liver PDFF of 25 ± 3% while at week 16.5, these groups both exhibited a mean liver PDFF of 9 ± 3% (Fig. 19B).

Mice on the standard diet again exhibited negligible changes in mean liver ADC over the intervention time course. At week 12, mice on the standard diet had a mean liver ADC of 1.7 ± x 10^{-3} ± 0.1 x 10^{-3} mm^2/s as compared to 1.7 ± x 10^{-3} ± 0.2 x 10^{-3} mm^2/s at week 16.5 (Fig. 19C). Mice on the CDAA diet exhibited at +124% increase (Fig. 20C) in liver ADC at week 16.5 as compared to week 12. At week 12 CDAA-fed mice had a mean liver ADC of 0.7 ± x 10^{-3} ± 0.1 x 10^{-3} mm^2/s as compared to 1.6 ± x 10^{-3} ± 0.1 x 10^{-3} mm^2/s at week 16.5 (Fig. 19C). CSAA-fed mice exhibited a +94 increase (Fig. 20C) over this same time period with a mean liver ADC of 0.8 ± x 10^{-3} ± 0.2 x 10^{-3} mm^2/s as compared to 1.5 ± x 10^{-3} ± 0.3 x 10^{-3} mm^2/s at week 16.5 (Fig. 19C). WD-fed mice exhibited the most precipitous increase of + 131% in mean liver ADC over this time period while mice on the WD + CCl_4 regimen displayed the least increase of +42% (Fig. 20C). At week 12, mice on the WD and WD + CCl_4 regimen, respectively, had a mean liver ADC of 0.6 ± x 10^{-3} ± 0.1 x 10^{-3} mm^2/s and 1.2 ± x 10^{-3} ± 0.2 x 10^{-3} mm^2/s (Fig. 19C). At week

16.5 these groups had a corresponding mean liver ADC of 1.4 ± x 10^{-3} ± 0.3 x 10^{-3} mm^2/s and 1.6 ± x 10^{-3} ± 0.2 x 10^{-3} mm^2/s (Fig. 19C).

Control mice on the standard diet exhibited a slight decrease in mean liver T_1 relaxation time over the intervention time course. At week 12, mice on the standard diet had a mean liver T_1 relaxation time of 3347 ± 39 ms as compared to 3907 ± 135 ms at week 16.5 (Fig. 19D). Mice on the CDAA diet exhibited a +72% increase (Fig. 20D) in mean liver T_1 relaxation time with an average of 1450 ± 43 ms as compared to 2492 ± 205 ms at week 16.5 (Fig. 19D). CSAA-fed mice displayed a +63% increase (Fig. 20D) in mean liver T_1 relaxation time with an average of 1820 ± 149 ms as compared to 2973 ± 272 ms at week 16.5 (Fig. 19D). WD-fed mice displayed the largest percent increase of +80% while mice on the WD + CCl_4 regimen exhibited the smallest increase of +45% over the intervention time course (Fig. 20D). At week 12, WD-fed mice exhibited a mean liver T_1 relaxation time of 1892 ± 143 ms while mice on the WD + CCl_4 regimen exhibited a mean liver T_1 relaxation time of 2475 ± 320 ms (Fig. 19D). At week 16.5, WD-fed mice exhibited a corresponding mean liver T_1 relaxation time of 3396 ± 120 ms while mice on the WD + CCl_4 regimen exhibited a mean liver T_1 relaxation time of 3590 ± 277 ms (Fig. 19D).

Mice on the standard diet exhibited no change in mean liver T_2 relaxation time over the intervention time course (Fig. 20E). At week 12 and 16.5, mice on the standard diet had a mean liver T_2 relaxation time of 16 ± 1 ms (Fig. 19E). CDAA-fed mice exhibited the most precipitous decrease towards basal level with a -53% decrease in mean liver T_2 relaxation time from week 12 to week 16.5 (Fig 20E). At week 12, CDAA-fed mice had a mean liver T_2 relaxation time of 40 ± 1 ms as compared to 19 ± 0 ms at week 16.5 (Fig. 19E). CSAA-fed and WD-fed mice exhibited

similar decreases in liver T_2 relaxation time over the time course with a -38% and -32% decrease, respectively (Fig. 20E). At week 12, CSAA-fed mice had a mean liver T_2 relaxation time of 29 ± 3 ms as compared to 18 ± 0 ms at week 16.5 (Fig. 19E). At week 12, WD-fed mice had a mean liver T_2 relaxation time of 25 ± 1 ms as compared to 17 ± 0 ms at week 16.5 (Fig. 19E). Mice on the WD + CCl_4 regimen exhibited the least decrease over the time course with a mean liver T_2 relaxation 24 ± 3 ms at week 12 as compared to 18 ± 1 ms at week 16.5 (Fig. 19E), representing a -24% decrease (Fig. 20E).

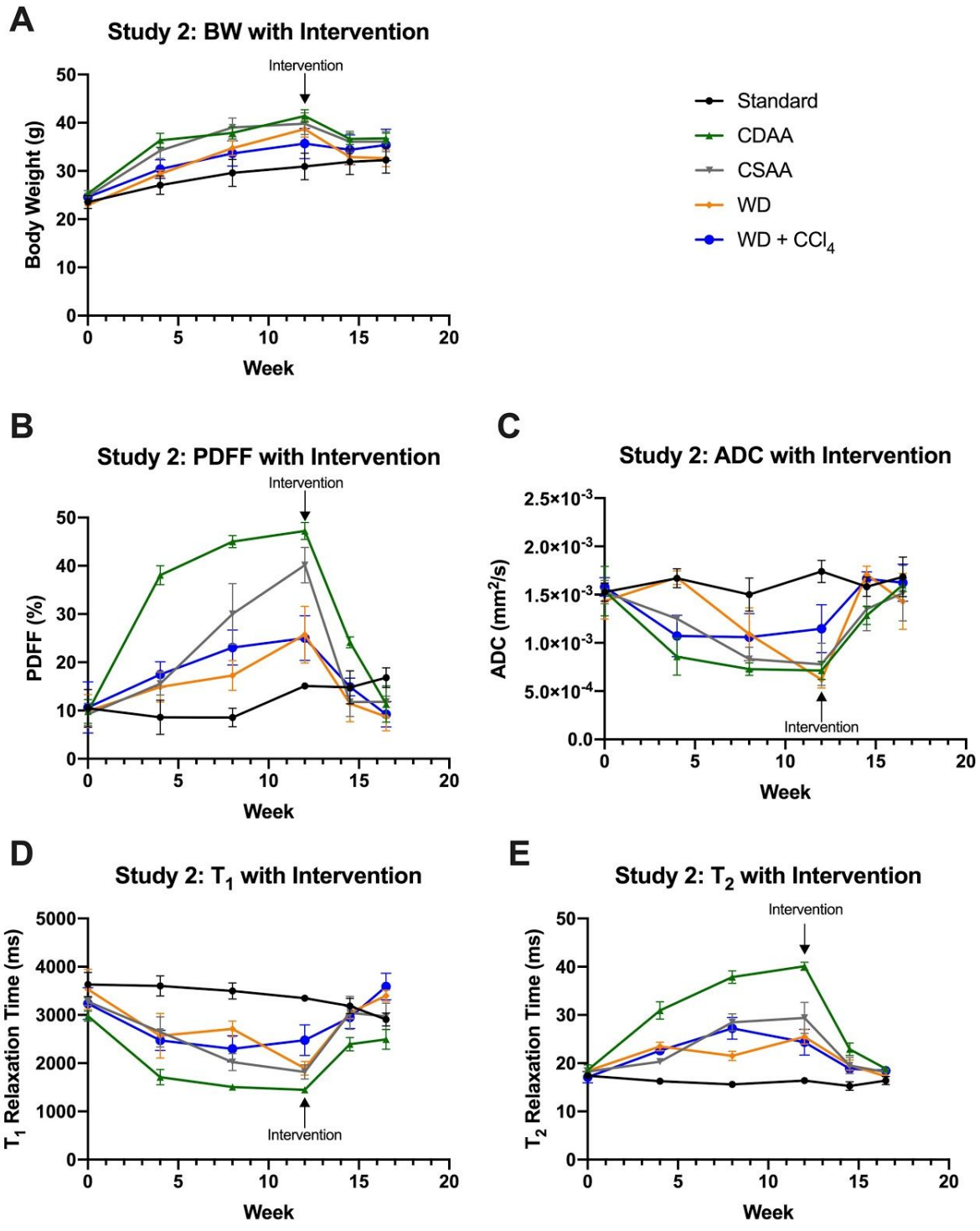

Figure 19. Graphs showing biomarker return to baseline following dietary intervention at week 12. MCD data is not included due to being removed from study at week 4. **A.** Body weight; **B.** PDFF; **C.** ADC; **D.** T_1; **E.** T_2.

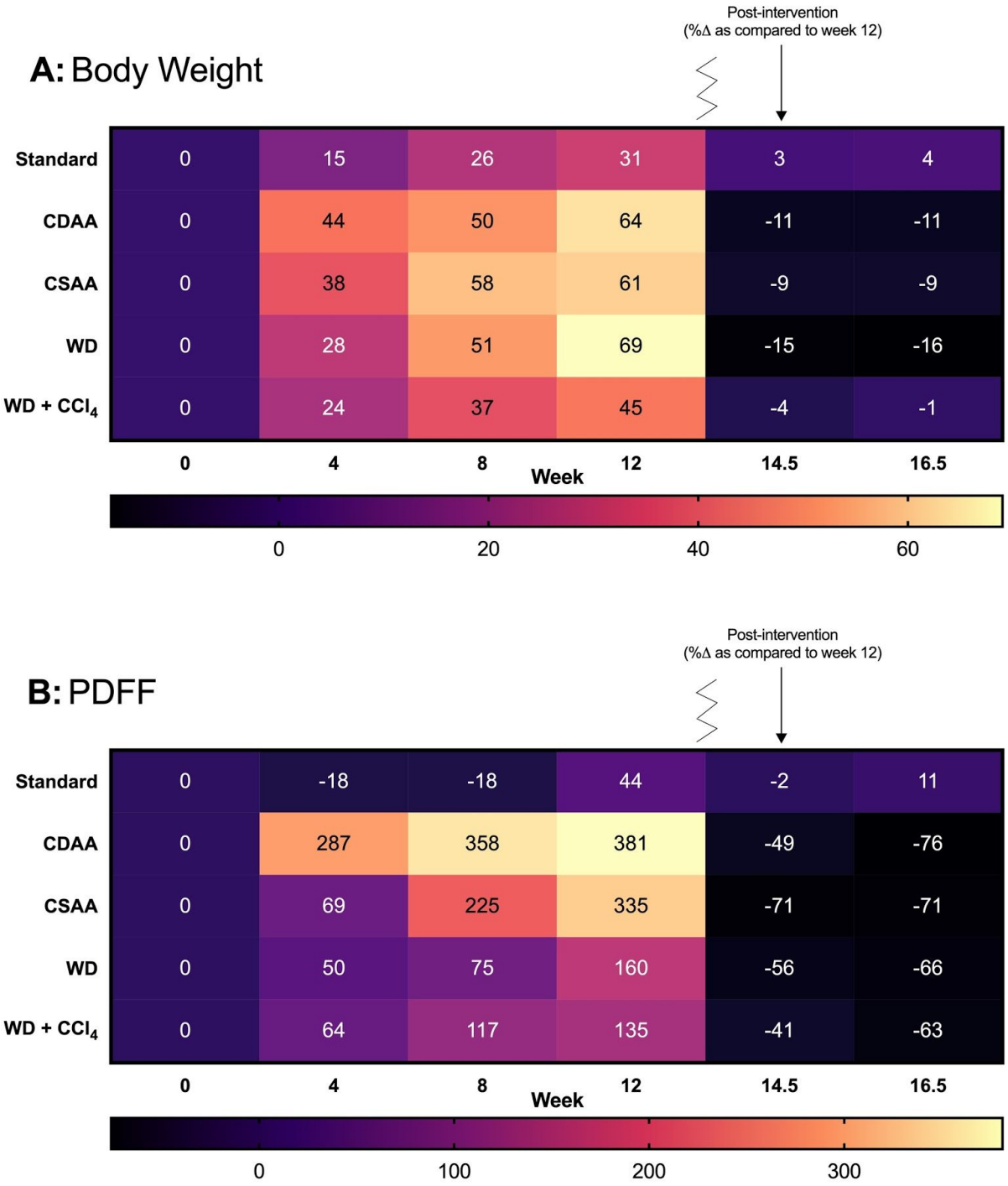

Figure 20. Heat Maps depicting the percent change in each of the parameters over the 12 week time course and then the percent change from week 12 following dietary intervention. Group labels are shown to the left of the heat map and week labels are shown underneath. **A.** mean body weight; **B.** mean liver PDFF **C.** mean liver ADC **D.** mean liver T_1 relaxation time **E.** mean liver T_1 relaxation time.

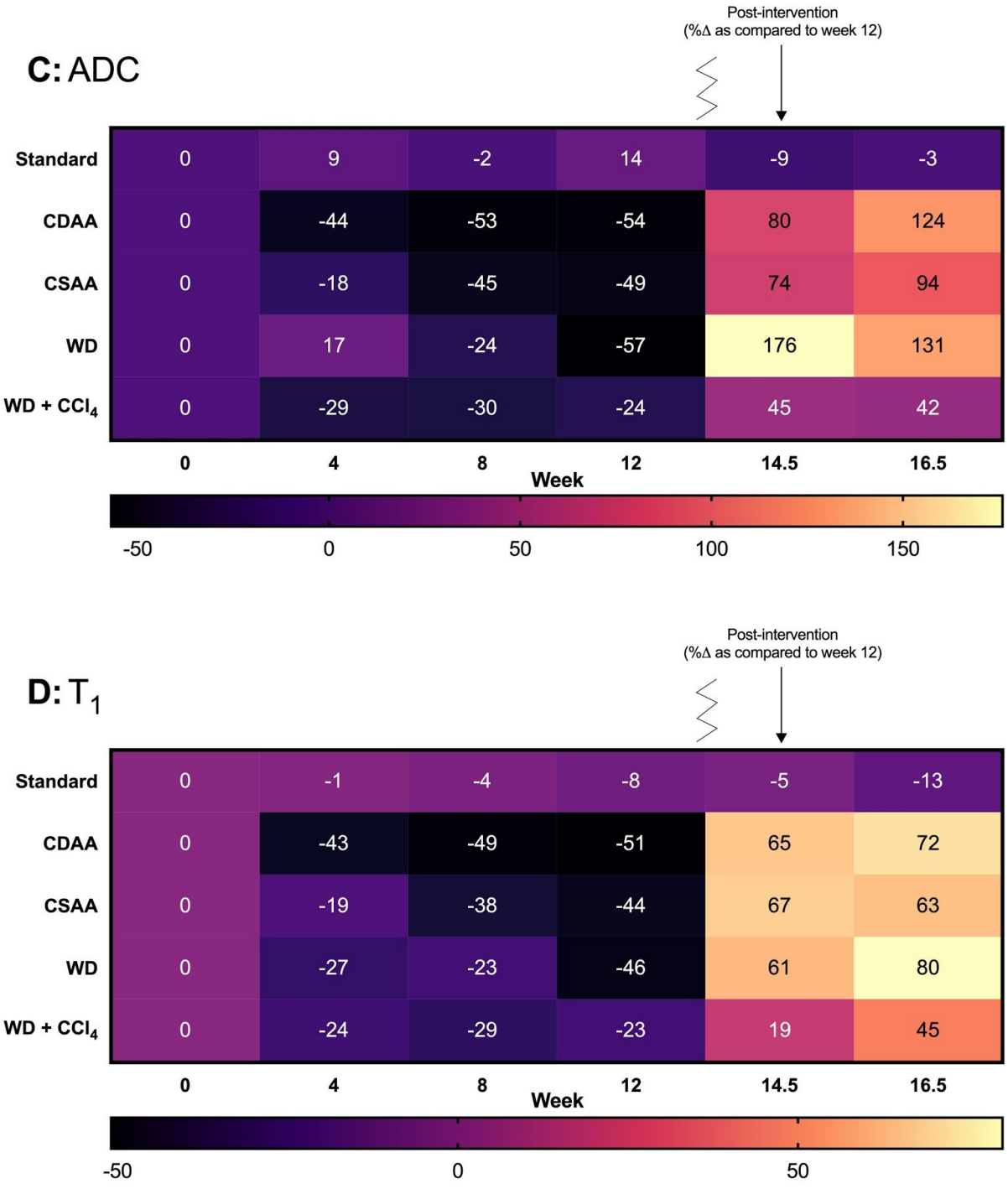

Figure 20. Heat Maps depicting the percent change in each of the parameters over the 12 week time course and then the percent change from week 12 following dietary intervention, continued.

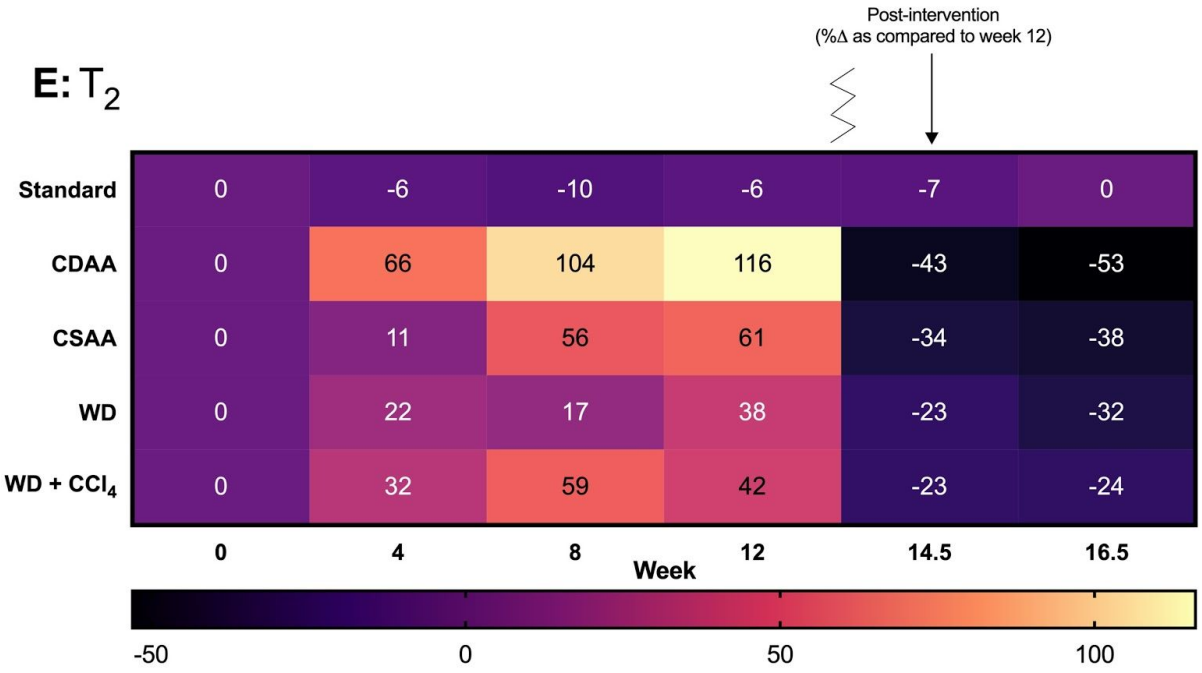

Figure 20. Heat Maps depicting the percent change in each of the parameters over the 12 week time course and then the percent change from week 12 following dietary intervention, continued.

DISCUSSION

Body Weight

Mice exhibited body weight modulation consistent with their dietary/chemical model. Mouse models of NAFLD used in this study can be broken into two major categories: (1) diets which are methionine and/or choline deficient, and (2) Western-like diets containing trans fat, saturated fat, and sugar [31]. Based upon known characteristics of these diets, we expected that CDAA-fed, CSAA-fed, and WD-fed mice would elicit relatively large increases in body weight while mice on the WD + CCl_4 regimen would display a more moderate increase in body weight. Additionally, we expected mice on the MCD diet to exhibit body weight loss.

While mice on the standard diet displayed body weight gain over the course of the study, this increase was marginal compared with CDAA-fed, CSAA-fed, WD-fed and WD + CCl_4 mice. According to the growth curve, 7-8 week male C57BL/6 mice have an average body weight between 20 and 25 ± 4 g and an average body weight between 25 and 30 ± 4 g at 14-15 weeks (which is equivalent to week 6-7 in our studies) [37]. This data is consistent with the body weight trends observed in male C57BL/6 mice on the standard diet in each of our studies in which body weight was found to be 28.5 ± 1.6 g at week 6 in study 1, 29.6 ± 2.8 g at week 8 in study 2, and 27.5 ± 1.5 g at week 8 in study 3 (Fig. 2).

Mice on the MCD diet exhibited precipitous body weight loss, as previously characterized in this model [31]. The MCD diet has been reported to cause up to 40% body weight loss in animals after 8 weeks feeding time and therefore fails to induce obesity [29, 38]. In contrast with the MCD diet, the CDAA diet has been shown to induce increases in body weight in a time dependent manner [39]. In a study by Rao *et al.* CDAA-fed male C57BL/6 mice were observed to have an average body weight between 35 and 40 ± 4 g after 12 weeks feeding

time which is on par with the observed average body weight for CDAA-fed mice in our studies at week 12 [40]. CDAA-fed mice in our studies exhibited an average body weight at week 12 of 36.2 ± 3.4 g in study 1, 41.4 ± 1.3 g in study 2, and 33.8 ± 0.8 g in study 3 (Fig. 2). A study by Mincis *et al.* which compared both CDAA-fed and CSAA-fed male C57BL/6 mice found that body weight was not significantly different between CDAA-fed and CSAA-fed mice at 12 weeks post disease induction [39]. In our studies, body weight of CDAA-fed and CSAA-fed mice followed very similar trends (Fig. 2).

The Western diet has been demonstrated to induce obesity [31]. In a study performed by Desmarchelier *et al.*, male C57BL/6 mice fed the WD exhibited an average body weight between 40 and 45 ± 1 g after 12 weeks of feeding time [41]. In our studies, WD-fed mice generally displayed some of the largest increases in body weight over time. WD-fed mice exhibited a mean body weight at week 12 of 43.0 ± 2.3 g in study 1, 38.7 ± 1.7 g in study 2, and 41.9 ± 2.1 g in study 3 (Fig. 2). In contrast, mice on the WD + CCl_4 regimen displayed smaller increases in body weight over the course of the study. A study by Tsuchida *et al.*, found that the addition of CCl_4 to a WD regimen in C57BL/6 mice attenuated body gain and also decreased food consumption [42]. Mice subjected to the WD + CCl_4 regimen in the study by Tsuchida *et al.* had an average body weight near 32 ± 2 g at 12 weeks post diet and chemical based disease induction [42]. In our study, mice on the WD + CCl_4 regimen exhibited a mean body weight at week 12 of 36.1 ± 2.0 g in study 1, 35.7 ± 3.2 g in study 2, and 33.4 ± 1.8 g in study 3 (Fig. 2). This suggests attenuation in weight gain due to the administration of CCl_4 (which has adverse side effects) and an associated decrease in food intake.

Of note, after dietary intervention (removal of experimental diets at week 12) in study 2, the body weight of all experimental groups was found to regress towards the average body weight of mice on the standard diet (Fig. 19A).

Body weight has implications in NAFLD and NASH in terms of both induction (obesity) and reduction (lifestyle modifications) [7, 8]. Our body weight data suggest that the models were highly diverse in terms of one of the most standardized noninvasive metrics which is used both preclinically and clinically in this disease. Furthermore, our body weight data suggests that these models of NAFLD and NASH are diverse in terms of their disease phenotypes, consistent with the clinical diversity of NAFLD and NASH. Based on the body weight results, we conclude that the set of models undertaken represents a diverse platform, as we sought for comprehensive testing of the imaging biomarkers and their performance in different disease settings.

Proton Density Fat Fraction

The strong correlation ($R^2 = 0.97$) which was observed between MRI quantified PDFF and actual oil percentage *in vitro* is in agreement with previously reported accuracy of MRI-PDFF and therefore permits confidence in the sensitivity and accuracy of this parameter in our experiments (Fig. 4) [12].

Hepatic steatosis is a hallmark feature of NAFLD and diet has been well-characterized as a factor contributing to the development of such [7]. Each experimental diet which was used in this study has been shown to induce steatosis and so we expected liver PDFF to exhibit monotonic increases in all experimental groups over the 12-week time course while remaining relatively stable in mice on the standard diet. Consistent with our hypothesis, mice on the

standard diet maintained a relatively constant liver PDFF over the time course in each of our studies while all experimental diets displayed large increases in liver PDFF by week 12 (Fig. 6, 7).

The MCD, CDAA, and CSAA diet used in this study all contain ~40% sucrose whereas the standard diet contains 3.18% sucrose (Appendix A). Sucrose has been indicated for its implications in lipid metabolism and ability to induce hepatic steatosis in wild-type mice [31]. Male C57BL/6 mice are prone to development of hepatic steatosis when placed on the MCD diet [30]. The MCD diet has been shown to induce hepatic steatosis as early as 4 weeks in experimental mouse models [31]. Mice on the MCD diet exhibited increases in liver PDFF by week 3 in study 1 and by week 4 in study 2 and 3 suggesting that this is a robust model for hepatic steatosis (Fig. 6). While increases in liver PDFF of this experimental group were found in all 3 studies, it was statistically significant in study 1 only, which is likely the result of shorter feeding time after having to remove mice from study, due to body weight loss in studies 2 and 3 (Appendix B). The CDAA diet is known to induce similar disease features, such as steatosis, as the MCD diet due to the shared deficiency in choline [29]. In our studies, mice on the CDAA diet exhibited a similar, while slightly more severe, trend as the MCD diet fed mice in the time course of PDFF, and presumably the development of hepatic steatosis (Fig. 6). CDAA-fed mice consistently exhibited large increases in liver PDFF which were found to be statistically significant compared to controls across all studies (Appendix B). Therefore, significant hepatic steatosis can be achieved reproducibly in CDAA-fed mice without considerable weight loss [43]. The CSAA diet contains sufficient choline and is a control for the CDAA diet. The CSAA diet (similarly high in sugar and fat versus the CDAA diet) has been reported to induce hepatic

steatosis in recent studies [40]. Consistent with recent studies, CSAA-fed mice in our studies showed a similar, but less severe, upward trend in liver PDFF over the course of 12 weeks as compared to CDAA-fed mice (Fig. 6). Of note, CSAA-fed and CDAA-fed mice exhibited similar body weight trends across each of our three studies therefore suggesting a partial decoupling of body weight and liver fat in these models (Fig. 2). This is consistent with the fact that methionine and/or choline deficient diets induce hepatic steatosis in the absence of obesity [29]. Liver PDFF of CSAA-fed mice was found to be statistically significant compared with mice on the standard diet in each of the three studies (Appendix B). Additionally, liver PDFF of CDAA-fed and CSAA-fed mice were not found to be significantly different in study 1 and 3 (Appendix B). While the CSAA diet may serve as a control for choline deficiency, it is not a model devoid of disease progression.

The Western Diet (WD) is meant to mirror the dietary components which lead to the development of NAFLD and NASH in modern day humans by including varied contents of trans fat, saturated fat, and sugar [31]. For this reason, the WD is designed to bring about hepatic and metabolic features in a way that mimics the pathophysiological changes seen clinically [31]. The induced hepatic changes are highly dependent on the components of this diet [31]. In a study performed by Schierwagen *et al*., a WD containing 19.5% casein induced hepatic steatosis after 7 weeks [31]. The WD used in this study contained 20% casein and mice on the WD exhibited steep increases in liver PDFF near this time point with a 51% increase between week 6 and 9 in study 1 and 72% increase between week 4 and 8 in study 3 (Fig. 6A,C). This observation was less pronounced in study 2 with a 16% increase between week 4 and 8 (Fig. 6B). While WD-fed mice exhibited the largest increase in body weight out of all experimental groups in study 1 and

3, WD-fed mice exhibited less precipitous increases in body weight in study 2 (Fig. 2A-C). In study 2, WD-fed mice had a lower average body weight than both CDAA-fed and CSAA-fed mice at each time point over the course of the study, consistent with natural variability (Fig. 2B). Because obesity is related to steatosis, this aberration in body weight is likely the cause of the observed less severe steatotic phenotype in study 2 and suggests a coupling of body weight with liver steatosis in our WD model (Fig. 6B). Additionally, the WD used in our studies contains 50% sucrose, which is likely contributing to the increase in liver PDFF and presumably hepatic steatosis in these mice (Appendix A). While the increases in liver PDFF of WD-fed mice were found to be statistically significant versus mice on the standard diet in study 1, and similar trends were observed in study 2 and 3, the statistical significance did not persist in study 2 and 3 (Appendix B). This lack of significant difference may be due to additional variability from the method of grouping mice. In study 1, mice were grouped at baseline based on body weight data. Whereas in study 2 and 3, mice were first imaged at baseline and then grouped to match mean liver PDFF across groups. This led to an average baseline liver PDFF varying more between groups in study 1 compared with studies 2 and 3, and may explain the statistically different PDFF for the WD versus control group being found in study 1 only (Fig. 6A-C). Overall the results for PDFF in the WD group (and corresponding lack of statistical difference versus control) suggest the steatotic phenotype of WD-fed mice is less robust as compared to CDAA and CSAA induced disease.

The observed phenotype of NAFLD in mice subjected to CCl_4 is often less severe in terms of body weight gain, and this is likely a result of the decreased food consumption in mice receiving CCl_4 due to related adverse effects such as irritation of the esophageal lining following

oral dosing [44]. Mice on the WD + CCl_4 regimen exhibited the least increase in body weight in each of the three studies compared to CDAA-fed, CSAA-fed and WD-fed mice (Fig. 2). Mice on the WD + CCl_4 regimen also consistently exhibited the lowest increases in liver PDFF of all experimental groups in each of the three studies (Fig. 6). This may be due to the decrease in consumption of the disease-inducing diet as compared to the mice on the WD only. Furthermore, body weight data and corresponding PDFF of our WD model suggested a coupling between the two and so the lower body weight of mice on the WD + CCl_4 regimen is consistent with a lower liver PDFF. Although the increase in liver PDFF of mice on the WD + CCl_4 regimen was found to be statistically significant versus control in study 1, this result may not be reliable due to lack of matching of baseline PDFF between groups as mentioned above (Appendix B) (Fig 6A). In this study, mice on the WD + CCl_4 regimen had the highest mean liver PDFF at baseline and so this initial difference versus the control group may have contributed to the observed statistical difference (Fig. 6A). Consistent with this, statistical significance for PDFF versus controls was not achieved in the WD + CCl_4 group in study 2 and 3 in which all groups were stratified to have uniform mean liver PDFF at baseline (Appendix B).

The observed increase in MRI-PDFF across all experimental groups over the course of the study is consistent with NAFLD steatosis-based progression. Furthermore, these increases transcend a wide range of preclinical models and were found to be relatively consistent and reproducible in three subsequent studies. While the above cited studies relied upon histological analysis, which requires terminal sacrifice, our studies permitted non-invasive, longitudinal quantification and detection of hepatic steatosis which was observed as early as week 3 and week 4. This suggests that MRI allows for identification and diagnosis of hepatic steatosis in the early

stages of disease progression. In clinical terms this could translate to facilitation of prompt lifestyle modifications and other interventions that may prove to be of clinical significance.

Following dietary intervention at week 12 in study 2, liver PDFF was observed to regress towards basal levels in all experimental groups. It has been found that dietary interventions which result in body weight loss between 7 and 10% is associated with improvement in liver fat in humans [45]. CDAA-fed, CSAA-fed, and WD-fed mice exhibited the largest decreases in liver PDFF following dietary intervention of -76%, -71%, and -66%, respectively (Fig. 20B). Corresponding body weight loss in these groups was -11%, -9%, and -16% at week 16.5 after 4.5 weeks back on the standard diet (Fig. 20A). Interestingly, CSAA-fed mice elicited the largest decline in liver PDFF at week 14.5, greater than CDAA-fed mice despite displaying comparable weight loss. Additionally, mice on the WD + CCl_4 regimen displayed only -1% change in body weight at week 16.5 (Fig. 20A). However, corresponding PDFF reduction in this group was -63% (Fig. 20B). This decoupling of body weight with hepatic steatosis in the choline deficient and CCl_4 models underlies the importance of more specific biomarker based assessment of NASH through a biomarker like PDFF.

Apparent Diffusion Coefficient

Elucidating a non-invasive and accurate biomarker for identifying liver fibrosis remains at the forefront of translational research in this field. The ability to objectively identify and quantify the degree of liver fibrosis in NASH patients has implications in prognosis, longitudinal surveillance, and therapeutic advance [7].

ADC has been reported to have an inverse relationship with the extent of fibrosis at 11.7 T in which decreases in liver ADC are associated with the progression of liver fibrosis [24, 46]. This relationship is consistent with fibrotic structures composed of collagen and other macromolecular deposition inhibiting the diffusional mobility of water and therefore reducing the liver water ADC as fibrosis develops [24]. Each of the models which was investigated in this study have been reported to induce varying degrees of liver fibrosis in a time-dependent manner. Additionally, C57BL/6 mice have a significantly higher tendency towards developing diet-induced hepatic fibrosis than other mouse strains [47]. Therefore, we hypothesized that liver ADC would decrease in all experimental groups while remaining relatively unchanged in mice on the standard diet.

Within the variability in the data, mice on the standard diet exhibited no noteworthy decreases in mean liver ADC in each of the studies consistent with a relative absence of fibrosis or disease in the liver tissue (Fig. 9). Additionally, this observation provides confidence that the decreases seen in all experimental models is a result of disease induction and progression. All experimental models showed decreases in liver ADC over the disease time course in each study although differentiation between groups was not as well defined versus other biomarkers such as PDFF (Fig. 9).

Nutrient-deficient diets such as the MCD and CDAA diet induce hepatic fibrosis over a shorter time period than obesogenic diets such as the WD [47]. MCD-fed mice exhibited a generally downward trend in average liver ADC over the 9-week time course in study 1 (Fig. 9A). This decrease was observed to be statistically significant versus mice on the standard diet (Appendix B). In study 2 and 3, MCD-mice exhibited steep declines in average liver ADC

between 0 and 4 weeks post disease induction (Fig. 9B-C). These decreases, however, were not statistically significant versus mice on the standard diet, and this is likely at least partly due to the limited feeding time of this model based on adverse effects including excessive body weight loss (Appendix B). Furthermore, in each study mice were grouped by either body weight or liver PDFF and so baseline liver ADC was not explicitly matched, potentially leading to some additional variability than otherwise (Fig. 9). Even so, the observed decreases in liver ADC across this model are likely attributable to the development of liver fibrosis. A study by Simon *et al.,* showed that mice developed fibrosis in as short as 2 weeks on the MCD diet [31]. A study conducted by Wei *et al.* utilizing histopathology as a terminal endpoint identified two-fold increases in collagen content in the liver of MCD-fed C57BL/6 mice at 8 weeks consistent with the development of liver fibrosis [48]. The findings of Simon *et al.* and Wei *et al.* provide confidence in the development of fibrosis in MCD-fed mice in our studies, and therefore in attributing the observed decreases in liver ADC to disease induction. CDAA-fed mice also exhibited steep decreases in liver ADC following relatively short feeding times (Fig. 9). Regardless of baseline stratification, CDAA-fed mice consistently exhibited the earliest and largest decrease in average liver ADC at week 3 in study 1 and week 4 in study 2 and 3 (Fig. 9). These decreases were found to be statistically significant in each study (Appendix B). Consistent with these results, in the same study conducted by Wei *et al*., CDAA feeding in C57BL/6 mice induced fibrosis by week 4 [48]. CSAA-fed mice also exhibited a downward trend in mean liver ADC, though to a lesser degree than CDAA-fed mice as was observed for PDFF (Fig. 9).

Consistent with the longer feeding time for fibrosis induction in obesogenic diets, WD-fed mice exhibited a mean liver ADC value within range of mice on the standard diet at

week 3 in study 1 and week 4 in study 2 and 3 (Fig. 9A-C) [47]. From week 3 and 4 in each respective study however, WD-fed mice elicited nearly-monotonic decreases in average liver ADC through week 12 (Fig 9A-C). In study 2, WD-fed mice exhibited the largest decrease in mean liver ADC across all experimental groups by week 12 (Fig. 9B). Fibrosis is likely to be playing a role in this observation. As reported in a study by Dorn *et al.,* a diet containing high fat and sucrose, similar to the WD used in our study, induced NASH with fibrosis in mice [31]. Furthermore, variations of the WD diet which incorporate sucrose most closely reflects the human phenotype by inducing aspects of metabolic syndrome which are thought to stimulate the development of fibrosis [31]. Conversely, in each of the three subsequent studies, mice on the WD + CCl_4 regimen exhibited the least decrease in average liver ADC by week 12 as compared to all other experimental groups (Fig. 9). CCl_4 has shown strain-dependent and route-dependent effects [49]. The C57BL/6 strain of mice has shown intermediate susceptibility to developing liver fibrosis following administration of CCl_4 intraperitoneally (IP) [49]. Fibrosis can be observed 2-4 weeks post CCl_4 treatment when this route of administration is utilized [49]. Exposure via oral gavage, however, is known to elicit intestinal inflammation rather than have hepatic effects [49]. Because mice were dosed via oral gavage in our experiments, this may account for the marginal decreases in mean liver ADC. Additionally, the possibility of lower feeding rates in these mice due to esophageal irritation has implications in fibrosis as well. Mice on the WD + CCl_4 regimen exhibited the smallest increases in mean liver PDFF as well as the smallest decreases in mean liver ADC in each of the three studies (Fig. 6, 9). Further studies which adjust the administration route of WD + CCl_4 to IP and monitor food intake may provide a better overview of this experimental model.

Notably, ADC regressed towards basal levels in all experimental groups following dietary intervention in study 2 (Fig. 19C). Importantly, it has been demonstrated that body weight loss of ≥10% corresponds with improvement in histologic grade of fibrosis [7]. Mice on the WD exhibited the sharpest return to baseline following 2.5 weeks of post intervention consistent with a sharp decrease of -15% in body weight during this time period as well (Fig. 20C). As lifestyle modifications are currently the first line of treatment for NAFLD, this suggests that the obesity seen in this model may be closely associated with or the driver of fibrosis induction/progression.

T_1 relaxation time

T_1 relaxation time represents one of the more exploratory biomarkers in our studies. T_1 is an inherent MRI parameter which draws from the rotational mobility of molecules within a tissue, in our case that of water molecules and labile groups in fat molecules [25]. T_1 is therefore sensitive to biologic and structural properties of tissues such as water content and macromolecular structure including fat [25]. Since the measured T_1 in our studies is an effective T_1 based almost entirely on water and fat components, as the relative concentrations of water and fat change, so too will the effective (or measured) T_1. Therefore, we hypothesized that tissue structure and water content (inversely related to fat content) changes in the liver following diet- and chemical-based disease induction would cause modulation in this parameter.

Liver T_1 relaxation time was found to decrease in a time-dependent manner across all experimental groups in our studies while mice on the standard diet maintained a relatively constant mean liver T_1 relaxation time between 2800 and 3700 ms (Fig. 12). We hypothesize that the observed decrease in all experimental groups is due to a significant extent to increasing liver fat content.

At 3T, a clinical study of NAFLD patients found the average T_1 relaxation time of NAFLD livers to be 1134 ± 97 ms [50]. Preclinical MRI is usually performed at higher field strengths in order to increase sensitivity in the typically smaller tissue volumes being studied. At 7T, C57BL/6 mice were found to have a mean healthy liver T_1 relaxation time of 995 ± 58 ms [28]. T_1 relaxation time is known to increase with increasing field strength [51]. Therefore, baseline liver T_1 relaxation time should be > 995 ms at 11.7T. In our studies at 11.7T, mean liver T_1 relaxation at baseline was 3332 ± 76 ms (Fig. 12).

T_1 has been reported both to increase and to decrease in the presence of the NAFLD spectrum across different studies, preclinically and clinically, which is likely at least partly due to magnetic field strength dependence of T_1. In a preclinical study of CCl_4-induced disease in mice, mean liver T_1 relaxation time was found to be significantly shorter in mice treated with 12 IP injections of CCl_4 as compared to mice treated with 6 IP injections of CCl_4 at 9.4T [52]. Conversely, clinical evaluation of patients with confirmed diagnosis of NAFLD revealed significantly *longer* liver T_1 relaxation times in patients with steatosis as compared to a control non-diseased cohort at 1.5T [53].

At 1.5T, fat has been reported to have a T_1 relaxation time of ~200 ms while non-fatty tissues such as healthy human liver have a T_1 relaxation time of ~570 ms [54]. Likewise, fat is known to have a shorter T_1 relaxation time than water at 11.7T [27]. In our fat phantom, T_1 relaxation time was found to be 3130 ms at 5% oil content and 500 ms at 100% oil content at 11.7T (Fig. 11). The difference in T_1 of fat and non-fatty tissues at lower field strengths is therefore less (~200 ms versus ~570 ms, respectively, or a less than 3 fold difference) while the difference which was observed in our phantom at 11.7T is much greater (~500 ms versus ~>3100 ms, or a greater than 6 fold difference). Therefore, the presence of fat at higher field strengths would conceivably exert a greater shortening effect on the effective liver T_1 relaxation time, even in the presence of other possibly influential covariates such as inflammation, while this effect would be less pronounced and even possibly secondary to other disease-based drivers at lower field strengths. More specifically, with higher percentages of fat, the measured T_1 is expected to decrease due to the much lower T_1 of fat compared with that of water at 11.7T.

Consistent with this, a strong negative correlation ($R^2 = 0.90$) between T_1 relaxation time and oil content in our fat phantom was observed (Fig. 11). Furthermore, the quantified T_1 relaxation time across the various fat concentrations *in vitro* also coincides with the liver T_1 relaxation times and their corresponding liver PDFF values *in vivo*. For example, in the 5% oil vial, T_1 relaxation time was found to be 3130 ms *in vitro*. In the 30% vial, T_1 relaxation time was 1823 ms and in the 40% vial, 1508 ms. In study 1, mice on the standard diet exhibited a mean liver PDFF of 6 ± 1% and a corresponding T_1 relaxation time of 3274 ± 237 ms at 6 weeks (Fig. 6A, 12A). In study 2, MCD mice exhibited a mean liver PDFF of 29 ± 2% with a corresponding T_1 relaxation time of 1997 ± 201 ms at 4 weeks (Fig. 6B, 12B). In study 3, CDAA mice had a

mean liver PDFF of 39 ± 3% with a corresponding T_1 relaxation time of 1625 ± 136 ms at 8 weeks (Fig. 6C, 12C). Therefore, a negative correlation ($R^2 = 0.52$) between T_1 and PDFF was established *in vivo*, permitting confidence in the translation of our hypothesis from the fat phantom to our models of NAFLD and NASH (Fig. 18A). Furthermore, we can conclude that at 11.7T, effective liver T_1 is a sensitive biomarker for steatosis.

T_2 relaxation time

Similar to T_1, T_2 relaxation time is an inherent MRI parameter which is driven by the rotational mobility of water and labile group fat protons [25]. Compared with T_1, T_2 is more sensitive to lower frequency rotational motion and therefore presents a distinct biomarker, but one that is also dependent on tissue structure and water content. We hypothesized that T_2 relaxation time would change longitudinally following diet- and chemical-based NASH disease induction based on the expected structural and compositional differences between healthy and NASH-based diseased livers.

In our studies, liver T_2 relaxation time was found to increase in all experimental groups over the 12-week time course while remaining stable in mice on the standard diet (Fig. 15). Based on results from the fat phantom, T_2 relaxation time showed no correlation with oil percentages between 5 and 50% (Fig. 14). Therefore, the universal and monotonic disease-dependent increase in T_2 relaxation time we found *in vivo* must be driven by something other than the increasing fat content in the liver. A likely candidate for this effect is inflammation. Inflammation is a hallmark feature of NASH and is associated with edema which

is known to cause a prolonged water T_2 relaxation time [26]. Therefore, we postulate that liver inflammation is driving the observed increases in liver T_2 relaxation time.

Investigation of the T_2 parameter in relation to NAFLD and NASH has produced similar trends in the literature. A study performed by Chow *et al.* examined the effects of CCl_4-induced disease on T_2 relaxation time in C57BL/6 mice [28]. At 7T, T_2 relaxation time was found to increase up to 4 weeks post disease induction at which point it remained relatively stable throughout the duration of the 8-week study [28]. Hepatic inflammation and edema were confirmed by histology [28]. A study by Guimaraes *et al.* examined the correlation of T_2 with hepatic fibrosis both clinically and preclinically [55]. On the clinical side, Guimaraes *et al.* conducted a retrospective study of patients who had previously undergone both liver MRI and biopsy within a 6-month period and found that T_2 relaxation time increased with increasing fibrosis at 1.5T [55]. While there was a significant difference in T_2 values between patients with histologically confirmed mild versus severe fibrosis, this finding became insignificant when inflammation was used as a covariate [55]. Preclinically, T_2 relaxation time was found to increase with the degree of diethylnitrosamine (DEN) induced fibrosis in rats at 4.7T [55]. DEN is a carcinogen known to cause hepatic fibrosis as well as inflammation [29, 55, 56]. Additionally, rat liver T_2 relaxation time in this study exhibits strong agreement with the liver T_2 relaxation time observed in our studies (Fig. 15). Control rats had a mean liver T_2 relaxation time of 25.2 ± 0.8 ms while rats subjected to DEN exhibited a mean liver T_2 relaxation time of 31.1 ± 1.5 ms at week 5 and 49.4 ± 0.4 ms at week 9 [55].

Each of the experimental mouse models used in our studies have been shown to induce inflammation, albeit on different time frames and to different extents. In our studies, mice on the

MCD diet consistently exhibited steep, monotonic increases in liver T_2 relaxation time by week 3 and week 4 which were found to be statistically significant in each of the three subsequent studies (Fig. 15, Appendix B). A study by Wang *et al.* and a study by Matsunaga *et al.*, demonstrated that C57BL/6 mice fed an MCD diet developed liver inflammation at 2 and 8 weeks, respectively [31]. Additionally, a study conducted by Tosello-Trampont *et al.*, found that wild-type mice on the MCD diet exhibited elevated expression of tumor necrosis factor-α (TNF-α), which is a serum biomarker of inflammation, as early as 10 days post-disease induction [31]. This suggests that MCD feeding can lead to early development of NASH [31]. CDAA-fed mice also displayed large increases in liver T_2 relaxation time early in the time course (Fig. 15). The CDAA-diet is known to induce a similar, while more severe NASH phenotype as compared to the MCD diet [29]. In a study by Mincis *et al.*, CDAA feeding was found to significantly activate the expression of genes associated with liver inflammation, including TNF-α, as early as 4 weeks post disease induction [39]. TNF-α levels were found to decrease slightly by 12 weeks, consistent with the plateau and slight downward trend observed in this group from week 8 and 9 to week 12 in our studies (Fig. 15, 16) [39]. Both MCD and CDAA-fed mice elicited the largest and earliest increases in mean liver T_2 relaxation time over the disease time course in each of our studies. The CSAA diet displayed modest increases in liver T_2 relaxation time in each of our studies (Fig. 15). Consistent with this observation, in the study by Mincis *et al.*, CSAA-fed mice exhibited significantly less upregulation of inflammatory markers at week 4 and 12 as compared to CDAA-fed mice [39].

The presence of sugar, or sucrose, in the WD is suggested to be a trigger for the inflammatory process in the liver [31]. While increases in liver T_2 relaxation time in WD-fed

mice had a slower onset as compared to MCD-fed and CDAA-fed mice, WD-fed mice exhibited large increases by week 12 which were found to be statistically significant in study 2 and 3 (Fig. 15, Appendix B). While significance was not achieved in study 1, this could be attributable to a slightly more delayed onset of inflammation between 0 and 3 weeks as compared to study 2 and 3 (Fig. 15, Appendix B). The study performed by Dorn *et al.* showed that mice fed a WD containing 30% sucrose developed liver inflammation after 12 weeks [31]. Another study by Machado *et al.* showed that the WD induced hepatic inflammation in mice after 16 weeks, however, the degree of inflammation was significantly less pronounced as compared to MCD-fed mice in this study [31]. This is consistent with both the time course as well as severity of increases in liver T_2 relaxation time in mice on the WD in our studies. Mice on the WD + CCl_4 regimen exhibited a similar trend in liver T_2 relaxation time over the 12-week time course as mice on the WD (Fig. 15). Although CCl_4 has been reported to contribute to the development of hepatic inflammation, it induces a more acute form which is reduced 48 hours post-dose [52]. In our studies, mice were not imaged within 48 hours of CCl_4 dosing, and so the trend in liver T_2 relaxation time in this group is consistent with the WD component being the major driver for T_2 based detection of inflammation (Fig. 15). However, mice on the WD + CCl_4 regimen exhibited slightly lower mean liver T_2 relaxation time at week 12 as compared to mice on the WD (Fig. 15). This may be due to the above mentioned possible decrease in food intake due to adverse events related to CCl_4 oral dosing, and subsequently attenuated diet based liver inflammation.

Although liver T_2 relaxation time exhibited a positive correlation ($R^2 = 0.66$) with PDFF *in vivo* in our studies, hepatic steatosis is a prerequisite to inflammation in the NAFLD to NASH spectrum (Fig. 18B) [1]. In fact, inflammation is a distinguishing factor between NAFLD and NASH [31]. Therefore, it is expected that steatosis would approximately parallel the presence of inflammation *in vivo*, given that the onset of steatosis occurred within a few weeks of the start of the diets.

Furthermore, the accumulation of fat in the liver is suggested to trigger secretion of inflammatory markers such as TNF-α [57]. Upon closer investigation of the relationship between liver T_2 and PDFF, it was revealed that there is no correlation ($R^2 = 0.07$) at PDFF values < 20% while at PDFF values > 20%, a positive correlation ($R^2 = 0.54$) is observed (Fig. 21A,B). Likewise, at T_1 relaxation times > 2300 ms (the T_1 relaxation times correlating with ≤ 20% fat in the phantom), again almost no correlation ($R^2 = 0.16$) is observed with T_2 (Fig. 21D). At T_1 relaxation times < 2300 ms (the T_1 relaxation times correlating with > 20% fat in the phantom), a moderate negative correlation ($R^2 = 0.42$) is established (Fig. 21C). This further reflects the progression of NAFLD, or simple fatty liver, to NASH in which fatty liver becomes accompanied by inflammation, consistent with T_1 and T_2 correlating at this point.

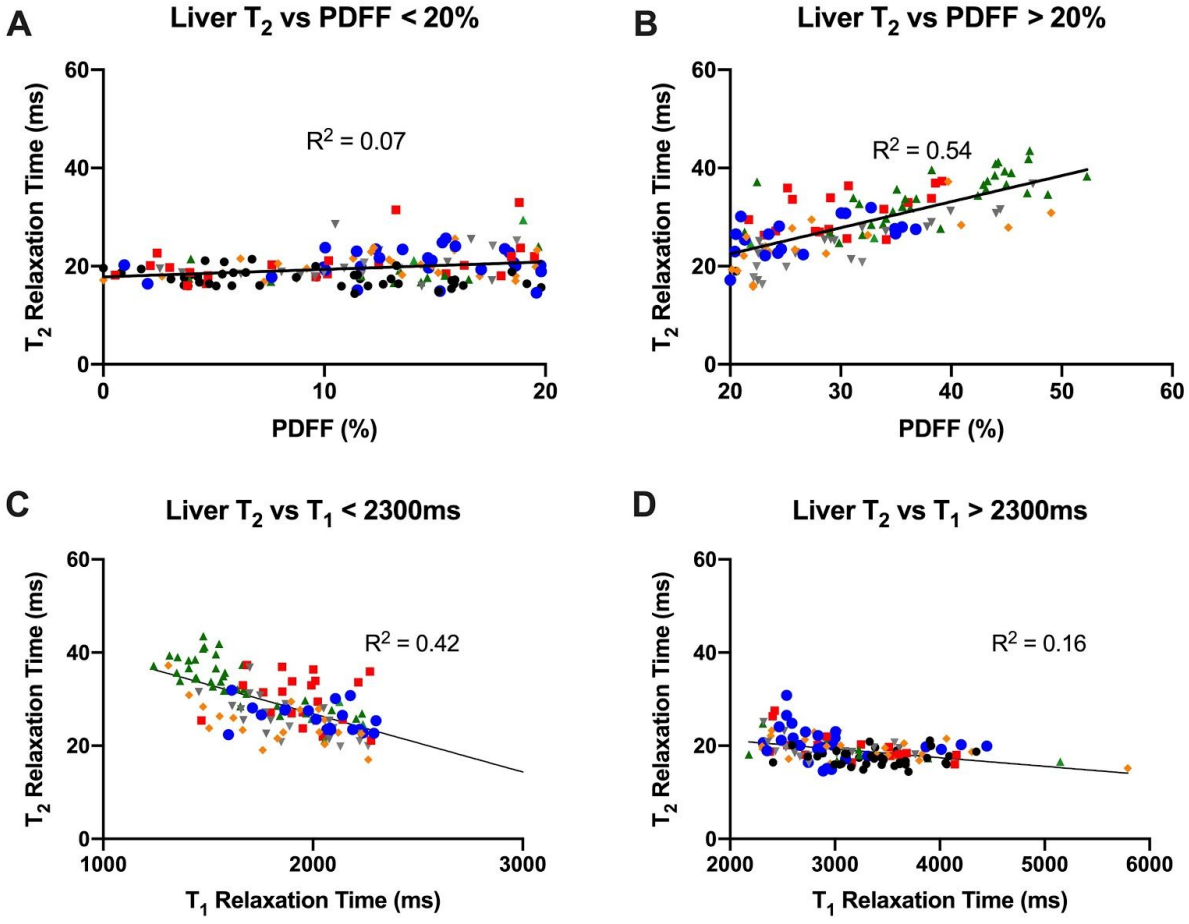

Figure 21. Graphs depicting the correlation of T_2 with PDFF and T_1 with high and low values excluded. **A.** PDFF values < 20%; **B.** PDFF values > 20%; **C.** T1 values < 2300 ms; **D.** T1 values > 2300 ms.

Biomarker Comparisons

Hepatic steatosis is a fundamental aspect of the NAFLD spectrum. MRI-based PDFF was found to be consistent and reproducible across our three studies suggesting that it is viable as a biomarker for more broad diagnosis and longitudinal evaluation of hepatic steatosis (Fig. 6). The use of MRI for PDFF is appropriate in both preclinical and clinical trials in which the intervention being examined is likely to have an anti-steatotic effect [16]. Additionally, because

steatosis has been observed to correlate with body weight, interventions which are targeted at weight loss would also be appropriate in an MRI-PDFF-based study [16]. Limitations of this biomarker include its inability to detect other features of NASH including inflammation and fibrosis [16]. Also, PDFF is often associated with quality control challenges caused by patient size, positioning and motion [16]. Ultimately, while PDFF provides a largely viable surrogate to liver biopsy for diagnosis of hepatic steatosis, it is best used in combination with the evaluation of other biomarkers presented here such as ADC, T_1, and T_2 in the evaluation of NAFLD and NASH.

We postulate that ADC changes were driven by the presence of collagen deposition and hydrophobic macromolecular structures associated with fibrosis in the liver [24]. Therefore, ADC may serve as a biomarker for the detection of NASH based liver fibrosis. Quantification of ADC using MRI could help overcome current limitations in diagnosis of fibrosis which are associated with observer subjectivity as well as geographic sampling limitation. Parametric ADC colormaps over the MR liver images illustrate heterogeneity which would likely lead to sampling error if liver histopathology was used as a terminal endpoint (Fig. 8). Of note, steatosis is known to have confounding effects on the ADC parameter; increases in steatosis correlate with decreases in ADC [24, 46]. Fat accumulation in the liver diminishes interstitial space thus interfering with the diffusion of water molecules [46]. In our studies, liver ADC was found to have a moderate negative correlation ($R^2 = 0.34$) with liver PDFF *in vivo* which may be indicative of the non-fibrosis specific effect of hepatic fat on this biomarker (Fig. 18C). Further work is needed to fully elucidate liver ADC as a biomarker in NASH.

Liver T_1 relaxation time was found to have a moderate positive correlation ($R^2 = 0.38$) with liver ADC *in vivo* (Fig. 18D). It is possible that the presence of liver fibrosis may be a contributor to the measured disease-dependent shortening effect on liver T_1 relaxation time as was reported in the study by Mueller *et al* [52]. However, considering the variability of data in other studies on the relationship between liver fibrosis and T_1 relaxation time as well as the stronger correlation between fat and T_1 *in vitro* and *in vivo* in our studies, it remains likely that the shortening effect on liver T_1 relaxation time was primarily associated with increasing liver fat and its corresponding shorter T_1 relaxation time. Additionally, inflammation could have a lengthening effect on T_1. We conclude that liver T_1 is a sensitive and disease-specific biomarker across a broad range of NAFLD/NASH disease severities and subtypes. Further work should further interrogate the drivers for liver T_1 changes in these disease settings and the roles of fat concentration, fibrosis and inflammation in determining effective T_1. Upon further standardization, T_1 could have positive implications in the diagnosis and quantification of the comprehensive NAFLD spectrum including steatosis, inflammation, and fibrosis. Notably, T_1 is a much more universally and broadly measured parameter than PDFF, and is based on simpler acquisition and modeling methods. T_1 is therefore attractive for broad use in preclinical and clinical MRI labs. A potential limitation however is apparent from our results which suggest T_1 may be a different biomarker at higher magnetic field strength and therefore is not a purely *translational* biomarker. Despite this it presents unique opportunities for higher field strength labs in terms of investigation of NASH disease biology and discovery and translation of novel NASH therapeutics in preclinical work, that may not be as feasible at lower field strength.

Liver T_2 relaxation time was elucidated as a biomarker that is likely inflammation driven in our studies, as also evidenced by its lack of correlation with oil concentration *in vitro* (Fig. 14). Although studies have concluded correlation between liver T_2 relaxation time and degree of fibrosis, T_2 was only marginally correlated ($R^2 = 0.33$) with liver ADC in our studies (Fig. 18F). It is important to note that fibrosis occurs in the presence of inflammation in NASH [5]. Therefore, the changes which are seen in T_2 in the presence of fibrosis are likely still a result of the underlying inflammation. As inflammation is the defining factor between NAFLD and NASH, quantification of liver T_2 may serve as a useful and complementary biomarker in NASH. For T_2, the literature suggests that the biomarker correlates similarly with NASH based disease across magnetic field strengths. However, as for T_1, field strength dependencies should be further considered and examined.

Summary

NAFLD is a spectrum disease which encompasses the progression of hepatic steatosis (NAFLD) to NASH in which the liver becomes additionally inflamed, with or without fibrosis. Our studies have shown modulation which was found to be reproducible in each of the parameters of our experimental multiparametric MRI protocol (PDFF, ADC, T_1, and T_2) following diet- and chemical-based NAFLD and NASH disease induction. Our results indicate that our MRI multiplexed biomarker protocol covers the breadth of the major hallmark features which are associated with these diseases. All four biomarkers were robustly able to detect the

presence of disease versus control, disease progression in most of the models and studies that were run, and intervention-based normalization (after diet cessation). At the same time the four biomarkers proved to be complementary and (albeit in the absence of planned IHC) our results are consistent with differential disease based drivers across these MRI biomarkers.

Our multiparametric MRI protocol holds implications in diagnosis, prognosis, and treatment response. While further work is required to correlate our findings with IHC and to further elucidate the biomarkers, the results indicate potential for a biomarker package like this be used to noninvasively and objectively classify NASH subtypes in preclinical testing. While the acquisition was relatively efficient in our protocol, we believe there will be ways to streamline MRI data collection, and importantly also the analysis pipelines, which will make our multiparametric MRI protocol even more viable for routine use by academic labs or pharmaceutical companies that are leading efforts to treat NASH.

Such implementation and use may lead to better and more disease target-specific prediction of therapies with true clinical potential, and more impactful translation of such therapies. These findings lay the groundwork for testing of novel therapeutics using our paradigm which is an important next step in the near future. Furthermore, the ability to quantify a wide range of MRI parameters efficiently in one imaging session will allow for proper staging and stratification of clinical trials. Additionally, this MRI protocol may help to avoid over-reliance upon liver sampling as an endpoint, both preclinically and clinically. Our work

therefore presents comprehensive ground work with significant implications in propelling NAFLD and NASH research and related therapeutic strategies forward.

APPENDIX A: Diet Composition

PicoLab® Rodent Diet 20 5053*

DESCRIPTION

PicoLab® Rodent Diet 20 is a 20% protein diet formulated for rat, hamster and mouse breeding colonies. This diet is formulated using the unique and innovative concept of Constant Nutrition®, paired with the selection of highest quality ingredients to assure minimal inherent biological variation in long-term studies. Irradiation gives reliable microbial control and eliminates the need for autoclaving. Irradiation treatment and special 3-ply packaging provide virtually bacteria-free dietary control.

Features and Benefits

- Constant Nutrition® formula helps minimize nutritional variables
- Formulated with 20% protein
- High quality animal protein added to create a superior balance of amino acids for optimum performance
- Recommended for rat breeding colonies and mice not requiring a higher energy diet
- Precision processing and selection of highest quality ingredients assures Constant Nutrition® quality
- Irradiation gives reliable microbial control and eliminates the need for autoclaving

Product Forms Available

- Oval pellet, 10 mm x 16 mm x 25 mm length (3/8"x5/8"x1")
- Meal (ground pellets), special order

Other Versions Available

- 5061 Pico-Vac® Lab Rodent Diet

GUARANTEED ANALYSIS

Crude protein not less than	20.0%
Crude fat not less than	4.5%
Crude fiber not more than	6.0%
Ash not more than	7.0%

INGREDIENTS

Ground corn, dehulled soybean meal, wheat middlings, ground wheat, fish meal, cane molasses, wheat germ, dried beet pulp, brewers dried yeast, dehydrated alfalfa meal, ground oats, soybean oil, dried whey, calcium carbonate, salt, DL-methionine, menadione dimethylpyrimidinol bisulfite (vitamin K), choline chloride, pyridoxine hydrochloride, cholecalciferol, vitamin A acetate, dl-alpha tocopheryl acetate, biotin, thiamin mononitrate, folic acid, vitamin B_{12} supplement, nicotinic acid, riboflavin, calcium pantothenate, manganous oxide, zinc oxide, ferrous carbonate, copper sulfate, zinc sulfate, calcium iodate, cobalt carbonate, sodium selenite.

FEEDING DIRECTIONS

Feed ad libitum to rodents. Plenty of fresh, clean water should be available to the animals at all times.

Rats- All rats will eat varying amounts of feed depending on their genetic origin. Larger strains will eat up to 30 grams per day. Smaller strains will eat up to 15 grams per day. Feeders in rat cages should be designed to hold two to three days supply of feed at one time.

Mice-Adult mice will eat up to 5 grams of pelleted ration daily. Some of the larger strains may eat as much as 8 grams per day per animal. Feed should be available on a free choice basis in wire feeders above the floor of the cage.

Hamsters-Adults will eat up to 14 grams per day.

12/11/09

CHEMICAL COMPOSITION[1]

Nutrients[2]	
Protein, %	**20.0**
Arginine, %	1.22
Cystine, %	0.28
Glycine, %	0.96
Histidine, %	0.50
Isoleucine, %	0.97
Leucine, %	1.56
Lysine, %	1.16
Methionine, %	0.70
Phenylalanine, %	0.90
Tyrosine, %	0.59
Threonine, %	0.77
Tryptophan, %	0.26
Valine, %	1.00
Serine, %	1.03
Aspartic Acid, %	2.19
Glutamic Acid, %	4.34
Alanine, %	1.15
Proline, %	1.47
Taurine, %	0.02
Fat (ether extract), %	**5.0**
Fat (acid hydrolysis), %	**5.6**
Cholesterol, ppm	141
Linoleic Acid, %	2.19
Linolenic Acid, %	0.26
Arachidonic Acid, %	<0.01
Omega-3 Fatty Acids, %	0.33
Total Saturated Fatty Acids, %	0.93
Total Monounsaturated Fatty Acids, %	0.99
Fiber (Crude), %	**4.7**
Neutral Detergent Fiber[3], %	16.4
Acid Detergent Fiber[4], %	6.0
Nitrogen-Free Extract (by difference), %	**52.9**
Starch, %	33.9
Glucose, %	0.19
Fructose, %	0.23
Sucrose, %	3.18
Lactose, %	1.34
Total Digestible Nutrients,%	**76.2**
Gross Energy, kcal/gm	**4.07**
Physiological Fuel Value[5], kcal/gm	**3.41**
Metabolizable Energy, kcal/gm	**3.07**

Minerals	
Ash, %	**6.1**
Calcium, %	0.81
Phosphorus, %	0.63
Phosphorus (non-phytate), %	0.33
Potassium, %	1.07
Magnesium, %	0.22
Sulfur, %	0.34
Sodium, %	0.30
Chlorine, %	0.51
Fluorine, ppm	10
Iron, ppm	220
Zinc, ppm	87
Manganese, ppm	85
Copper, ppm	13
Cobalt, ppm	0.71
Iodine, ppm	0.97
Chromium, ppm	0.81
Selenium, ppm	0.30

Vitamins	
Carotene, ppm	1.5
Vitamin K (as menadione),ppm	3.3
Thiamin Hydrochloride, ppm	17
Riboflavin, ppm	8.0
Niacin, ppm	90
Pantothenic Acid, ppm	17
Choline Chloride, ppm	2000
Folic Acid, ppm	3.0
Pyridoxine, ppm	9.6
Biotin, ppm	0.30
B_{12}, mcg/kg	51
Vitamin A, IU/gm	15
Vitamin D_3 (added), IU/gm	2.2
Vitamin E, IU/kg	99
Ascorbic Acid, mg/gm	—

Calories provided by:	
Protein, %	24.651
Fat (ether extract), %	13.205
Carbohydrates, %	62.144

*Product Code

1. Formulation based on calculated values from the latest ingredient analysis information. Since nutrient composition of natural ingredients varies and some nutrient loss will occur due to manufacturing processes, analysis will differ accordingly.
2. Nutrients expressed as percent of ration except where otherwise indicated. Moisture content is assumed to be 10.0% for the purpose of calculations.
3. NDF = approximately cellulose, hemi-cellulose and lignin.
4. ADF = approximately cellulose and lignin.
5. Physiological Fuel Value (kcal/gm) = Sum of decimal fractions of protein, fat and carbohydrate (use Nitrogen Free Extract) x 4,9,4 kcal/gm respectively.

LabDiet
www.labdiet.com

MCD Diet

Dyets Inc.

2508 Easton Ave., Bethlehem, Pennsylvania 18017
Within 610 Area Code: 868-7701, FAX -868-5170
Outside 610 Area Code: 800-275-3938
FAX: 800-329-3938
E-Mail Address: Sales@dyets.com

DYET# 518810

Choline Deficient and Iron Supplemented L-Amino Acid Defined Rat Diet without L-Methionine (as per fax of 10-16-01)

L-Arginine			12.7	
L-Histidine			3.4	
L-Lysine HCl			9.1	
L-Tyrosine			5.7	
L-Tryptophan			1.8	
L-Phenylalanine			7.3	
L-Methionine			**0**	
L-Cystine			3.7	
L-Threonine			4.6	
L-Leucine			10.5	
L-Isoleucine			6.1	
L-Valine			6.3	
Glycine			6.2	
L-Proline			7.6	
L-Glutamic Acid			28.9	
L-Alanine			5.1	
L-Aspartic Acid			15.8	
L-Serine			7.2	
Kcal/gm	4	total L-AA*.....	142.00	568
Ingredient			gm/Kg	kcal/gm
Cornstarch	3.6		100	360
Dextrin	3.63		100	363
Sucrose	4		408.58	1634.32
Cellulose (401855)	0		50	0
Corn Oil	9		50	450
Salt Mix #200000	0.47		35	16.45
Sodium Bicarbonate	0		4.3	0
Vitamin Mix #30005	3.92		10	39.2
Primex	9		100	900
Ferric Citrate, U.S.P	0		0.12	0
		total.....	1000	
			Kcal/Kg	4330.97

*This includes the 2 g/kg of Cystine added to #118753.
Dr. D. Nakae, Nara Medical College, 5/10/89
Modified on October 16, 2001
Key words: MCD diet,

CDAA and CSAA Diet

Dyets Inc.

2508 Easton Ave. Bethlehem, Pennsylvania 18017
Within 610 Area Code: 868-7701, FAX -868-5170
Outside 610 Area Code: 800-275-3938
FAX: 800-329-3938
E-Mail Address: sales@dyets.com

Diet # 518753 & 518754

Choline Deficient and Sufficient Iron Supplemented L-AA Defined Rodent Diet

	518753 **518754**
L-Alanine	5.1
L-Arginine	12.7
L-Aspartic Acid	15.8
L-Cystine	3.7
L-Glutamic Acid	28.9
Glycine	6.2
L-Histidine	3.4
L-Isoleucine	6.1
L-Leucine	10.5
L-Lysine-HCl	9.1
L-Methionine	1.7
L-Phenylalanine	7.3
L-Proline	7.6
L-Serine	7.2
L-Threonine	4.6
L-Tryptophan	1.8
L-Tyrosine	5.7
L-Valine	6.3
kcal/gm 4 total L-AA*…….	**143.7** **574.8**

			518753		**518754**	
Ingredient	kcal/gm		**gm/Kg**	**kcal/gm**	**gm/Kg**	**kcal/gm**
Cornstarch	3.6		100	360	100	360
Dextrin	3.63		100	363	100	363
Sucrose	4		406.67	1626.68	392.19	1568.76
Cellulose, Microcrystalline	0		50	0	50	0
Corn Oil	9		50	450	50	450
Primex	9		100	900	100	900
Salt Mix #215001 (no Fe Added)	0.47		35	16.45	35	16.45
Sodium Bicarbonate	0		4.3	0	4.3	0
Vitamin Mix #300050	3.87		10	38.7	10	38.7
Choline Bitartrate	0		0	0	14.48	0
Ferric Citrate, U.S.P.	0		0.33	0	0.33	0
		other total	856.30	3754.83	856.30	3696.91
		grand total	**1000.00**	**4329.63**	**1000.00**	**4271.71**

Dr. D. Nakae, Nara Medical College, May 10, 1989

Western Diet

Dyets Inc.

2508 Easton A Bethlehem, Pennsylvania 18017
Within 610 Area Code: 868-7701, FAX -868-5170
Outside 610 Area Code: 800-275-3938
FAX: 800-329-3938
E-Mail Address: dyets@enter.net

DYET#100000

AIN-76A Purified Rodent Diet

Ingredient	kcal./gm	grams/kg	kcal./kg
Casein	3.58	200	716
Sucrose	4	500	2000
Cornstarch	3.6	150	540
DL-Methionine	4	3	12
Cellulose	0	50	0
Corn Oil	9	50	450
Mineral Mix #200000	0.47	35	16.45
Vitamin Mix # 300050	3.92	10	39.2
Choline Bitartrate	0	2	0
		1000.00	**3773.65**

Journal of Nutrition v107, 1341(1977)
Journal of Nutrition v110, 1726(1980)

APPENDIX B: SPSS Statistics

Table 3. Results of the mixed ANOVA conducted with a 95% confidence interval showing the effect of both time and diet on **A.** PDFF; **B.** ADC **C.** T_1; **D.** T_2. P values < 0.050 represent effects which are statistically significant. Greyed out boxes indicate effects that are not statistically significant. *P values calculated in a secondary mixed ANOVA which included the MCD group and all data up to week 9. **P values calculated in a secondary mixed ANOVA which included the MCD group and all data up to week 4.

		Time	**Diet**
Fat Fraction	Study 1	F(1, 36) = 7.36, p = 0.024	F(4,9) = 19.96, p < 0.001
	Study 2	F(1, 45) = 42.32, p < 0.001	F(4, 15) = 15.23, p < 0.001
	Study 3	F(1, 39) = 13.42, p = 0.003	F(4, 13) = 9.03, p = 0.001
	Study 1*	F(1, 36) = 9.93, p = 0.008	F(5, 12) = 13.78, p < 0.001
	Study 2**	F(1, 18) = 54.99, p < 0.001	F(5, 18) = 4.07, p = 0.012
	Study 3**	F(1, 17) = 35.74, p < 0.001	F(5, 17) = 2.98, p = 0.041
ADC	Study 1	F(1, 36) = 8.48, p = 0.017	F(4,9) = 6.81, p = 0.008
	Study 2	F(1, 45) = 9.42, p = 0.008	F(4, 15) = 10.38, p < 0.001
	Study 3	F(1, 39) = 12.71, p = 0.003	F(4, 13) = 4.52, p = 0.017
	Study 1*	F(1, 36) = 7.21, p = 0.020	F(5, 12) = 6.62, p = 0.004
	Study 2**	F(1, 18) = 3.81, p = 0.067	F(5, 18) = 2.20, p = 0.100
	Study 3**	F(1, 17) = 20.64, p < 0.001	F(5, 17) = 1.53, p = 0.233
T_1	Study 1	F(1, 36) = 10.22, p = 0.011	F(4,9) = 8.77, p < 0.004
	Study 2	F(1, 45) = 25.40, p < 0.001	F(4, 15) = 23.37, p < 0.001
	Study 3	F(1, 39) = 48.40, p < 0.001	F(4, 13) = 39.89, p < 0.001
	Study 1*	F(1, 36) = 10.59, p = 0.007	F(5, 12) = 7.83, p = 0.002
	Study 2**	F(1, 18) = 20.96, p < 0.001	F(5, 18) = 6.88, p = 0.001
	Study 3**	F(1, 17) = 57.70, p < 0.001	F(5, 17) = 4.81, p = 0.006
T_2	Study 1	F(1, 36) = 19.88, p = 0.002	F(4,9) = 24.47, p < 0.001
	Study 2	F(1, 45) = 57.44, p < 0.001	F(4, 15) = 34.79, p < 0.001

Table 3. Results of the mixed ANOVA conducted with a 95% confidence interval showing the effect of both time and diet on **A.** PDFF; **B.** ADC **C.** T_1; **D.** T_2, continued.

		Time	**Diet**
T_2	Study 3	$F(1, 39) = 29.65$, $p < 0.001$	$F(4, 13) = 18.13$, $p < 0.001$
	Study 1*	$F(1, 36) = 24.40$, $p < 0.001$	$F(5, 12) = 20.15$, $p < 0.001$
	Study 2**	$F(1, 18) = 144.30$, $p < 0.001$	$F(5, 18) = 14.27$, $p < 0.001$
	Study 3**	$F(1, 17) = 52.73$, $p < 0.001$	$F(5, 17) = 12.39$, $p < 0.001$

Table 4. Results of the post-hoc Tukey HSD test using a 95% confidence interval showing statistical significance of each of the experimental diet groups versus all other groups is shown for each MRI biomarker: **A.** PDFF; **B.** ADC; **C.** T_1; **D.** T_2. P values < 0.050 represent differences between the control group and each of the experimental groups which are statistically significant and are highlighted yellow. *P values calculated in a secondary mixed ANOVA which included the MCD group and all data up to week 9. **P values calculated in a secondary mixed ANOVA which included the MCD group and all data up to week 4.

A: PDFF		Standard	MCD	CDAA	CSAA	WD	WD + CCl_4
Study 1	Standard		p < 0.001*	p < 0.001	p = 0.007	p = 0.002	p = 0.001
	MCD			p = 0.835*	p = 0.630*	p = 0.791*	p = 1.00*
	CDAA				p = 0.155	p = 0.523	p = 0.348
	CSAA					p = 0.913	p = 0.925
	WD						p = 1.000
	WD + CCl_4						
Study 2	Standard		p = 0.121**	p < 0.001	p = 0.009	p = 0.361	p = 0.134
	MCD			p = 0.884**	p = 0.400**	p = 0.397**	p = 0.654**
	CDAA				p = 0.026	p < 0.001	p = 0.002
	CSAA					p = 0.284	p = 0.624
	WD						p = 0.966
	WD + CCl_4						
Study 3	Standard		p = 0.060**	p = 0.001	p = 0.038	p = 0.068	p = 0.530
	MCD			p = 0.999**	p = 0.830**	p = 0.225**	p = 0.312**
	CDAA				p = 0.128	p = 0.070	p = 0.011
	CSAA					p = 0.996	p = 0.515
	WD						p = 0.707
	WD + CCl_4						

Table 4. Results of the post-hoc Tukey HSD test using a 95% confidence interval showing statistical significance of each of the experimental diet groups versus all other groups is shown for each MRI biomarker: **A.** PDFF; **B.** ADC; **C.** T_1; **D.** T_2, continued.

B: ADC		Standard	MCD	CDAA	CSAA	WD	WD + CCl_4
Study 1	Standard		p = 0.005*	p = 0.040	p = 0.039	p = 0.007	p = 0.035
	MCD			p = 0.850*	p = 0.995*	p = 0.845*	p = 0.992*
	CDAA				p = 0.967	p = 0.383	p = 0.997
	CSAA					p = 0.802	p = 0.997
	WD						p = 0.575
	WD + CCl_4						
Study 2	Standard		p = 0.165**	p < 0.001	p = 0.002	p = 0.013	p = 0.010
	MCD			p = 1.000**	p = 0.754**	p = 0.245**	p = 0.975**
	CDAA				p < 0.001	p = 0.194	p = 0.246
	CSAA					p = 0.846	p = 0.907
	WD						p = 1.000
	WD + CCl_4						
Study 3	Standard		p = 0.785**	p = 0.024	p = 0.852	p = 0.239	p = 0.998
	MCD			p = 0.940**	p = 0.998**	p = 0.997**	p = 0.861**
	CDAA				p = 0.095	p = 0.592	p = 0.041
	CSAA					p = 0.697	p = 0.956
	WD						p = 0.371
	WD + CCl_4						

Table 4. Results of the post-hoc Tukey HSD test using a 95% confidence interval showing statistical significance of each of the experimental diet groups versus all other groups is shown for each MRI biomarker: **A.** PDFF; **B.** ADC; **C.** T_1; **D.** T_2, continued.

C: T_1		Standard	MCD	CDAA	CSAA	WD	WD + CCl_4
Study 1	Standard		p < 0.004*	p = 0.002	p = 0.056	p = 0.032	p = 0.021
	MCD			p = 0.864*	p = 0.905*	p = 0.922*	p = 0.963*
	CDAA				p = 0.522	p = 0.756	p = 0.559
	CSAA					p = 0.995	p = 0.999
	WD						p = 1.000
	WD + CCl_4						
Study 2	Standard		p = 0.017**	p < 0.001	p < 0.001	p = 0.008	p < 0.001
	MCD			p = 0.659**	p = 0.903**	p = 0.159**	p = 0.991**
	CDAA				p = 0.050	p = 0.001	p = 0.015
	CSAA					p = 0.234	p = 0.970
	WD						p = 0.532
	WD + CCl_4						
Study 3	Standard		p = 0.012**	p < 0.001	p < 0.001	p < 0.001	p = 0.001
	MCD			p = 0.988**	p = 0.929**	p = 0.451**	p = 0.041**
	CDAA				p = 0.325	p = 0.066	p = 0.001
	CSAA					p = 0.848	p = 0.017
	WD						p = 0.086
	WD + CCl_4						

Table 4. Results of the post-hoc Tukey HSD test using a 95% confidence interval showing statistical significance of each of the experimental diet groups versus all other groups is shown for each MRI biomarker: **A.** PDFF; **B.** ADC; **C.** T_1; **D.** T_2, continued.

D: T_2		Standard	MCD	CDAA	CSAA	WD	WD + CCl_4
Study 1	Standard		p < 0.001*	p < 0.001	p = 0.470	p = 0.054	p = 0.018
	MCD			p = 1.000*	p = 0.001*	p = 0.007*	p = 0.008*
	CDAA				p < 0.001	p = 0.007	p = 0.005
	CSAA					p = 0.610	p = 0.367
	WD						p = 0.997
	WD + CCl_4						
Study 2	Standard		p = 0.001**	p < 0.001	p = 0.001	p = 0.015	p = 0.002
	MCD			p = 0.217**	p = 0.080**	p = 0.092**	p = 0.213**
	CDAA				p < 0.001	p < 0.001	p < 0.001
	CSAA					p = 0.430	p = 0.950
	WD						p = 0.830
	WD + CCl_4						
Study 3	Standard		p < 0.001**	p < 0.001	p = 0.007	p = 0.021	p = 0.016
	MCD			p = 0.073**	p < 0.001**	p < 0.001**	p = 0.002**
	CDAA				p = 0.005	p = 0.001	p = 0.006
	CSAA					p = 0.964	p = 1.000
	WD						p = 0.992
	WD + CCl_4						

REFERENCES

1. Bertot L, Adams L. The Natural Course of Non-Alcoholic Fatty Liver Disease. *Int. J. Mol. Sci.* 2016;17:774-786.

2. Perumpail BJ, Khan MA, Yoo ER, Cholankeril G, Kim D, Ahmed A. Clinical Epidemiology and Disease Burden of Nonalcoholic Fatty Liver Disease. *World J Gastroenterol.* 2017;23:8263-8276.

3. Bellentani S, Marino M. Epidemiology and natural history of non-alcoholic fatty liver disease (NAFLD). *Annals of Hepatol*. 2009;8:S4-S8

4. Oligschlaeger Y. Mouse Models for NASH: Are we there yet? *J.Genet. DNA Res.* 2017;1:102

5. Wynn TA, Ramalingam TR. Mechanisms of fibrosis: therapeutic translation for fibrotic disease. *Nat Med*. 2013;18:1028-1040.

6. DeWeerdt S. Disease progression: Divergent paths. *Nat Outlook.* 2017;551:S92-S93.

7. Wong T, Wong RJ, Gish RG. Diagnostic and Treatment Implications of Nonalcoholic Fatty Liver Disease and Nonalcoholic Steatohepatitis. *Gastroenterol. & Hepatol.* 2019;15:83-89.

8. Younossi ZM. The Epidemiology of Nonalcoholic Steatohepatitis. *Clinical Liver Disease.* 2018;11:92-94.

9. Nalbantoglu I, Brunt EM. Role of liver biopsy in nonalcoholic fatty liver disease. *World J Gastroenterol* 2014;20:9026-9037.

10. Szanto KB, Li J, Cordero P, Oben JA. Ethnic differences and heterogeneity in genetic and metabolic makeup contributing to nonalcoholic fatty liver disease. *Diabetes, Metabolic Syndrome and Obesity: Targets and Therapy.* 2019;12:357-367.

11. Hallsworth K, Adams L. Lifestyle modification in NAFLD/NASH: Facts and figures. *J. Hep. Reports* 2019;1:468-479.

12. Tanaka N, Kimura T, Fujimori N, Nagrckaya T, Komatsu M, Tanaka E. Current status, problems, and perspectives of non-alcoholic fatty liver disease research. *World J. Gastroenterol.* 2019;25:163-177.

13. Dufour J-F, Caussy C, Loomba R. Combination for therapy non-alcoholic steatohepatitis: rationale, opportunities and challenges. *Gut.* 2020;0:1-8.

14. Reimer KC, Wree A, Roderburg C, Tacke F. New drugs for NAFLD: lessons from basic models to the clinic. *Hepatol. Int.* 2020;14:8-23.

15. Rockey DC, Caldwell SH, Goodman ZD, Nelson RC, Smith AD. Liver Biopsy. *Hepatol.* 2009;1017-1044.

16. Caussy C, Reeder SB, Sirlin CB, Loomba R. Non-invasive, quantitative assessment of liver fat by MRI-PDFF as an endpoint in NASH trials. *Hepatol.* 2018;68:763-772.

17. Ooi GJ, Clouston A, Johari Y, Kemp WW, Roberts SK, Brown WA, Burton PR. Evaluation of the histological variability of core and wedge biopsies in nonalcoholic fatty liver disease in bariatric surgical patients. *Surgical Endoscopy.* 2020.

18. Jensen VS, Tveden-Nyborg P, Zacho-Rasmussen C, Quaade ML, Ipsen DH, Hvid H, Fledelius C, Wulff EM, Lykkesfeldt J. Variation in diagnostic NAFLD/NASH read-outs in paired liver samples from rodent models. *Journal of Pharmacological and Toxicological Methods.* 2020;101:1-9.

19. Dyson JK, Anstee QM, McPherson S. Non-alcoholic fatty liver disease: a practical approach to diagnosis and staging. *Front. Gastroentrol.* 2014;5:211-218.

20. Lee SS, Park SH. Radiologic evaluation of nonalcoholic fatty liver disease. *World J Gastroenterol.* 2014;20:7392-7402.

21. Castera L, Friedrich-Rust M, Loomba, R. Noninvasive Assessment of Liver Disease in Patients With Nonalcoholic Fatty Liver Disease. *Gastroenterol.* 2019;156:1264-1281.

22. Dulai PS, Sirlin CB, Loomba R. MRI and MRE for non-invasive quantitative assessment of hepatic steatosis and fibrosis in NAFLD and NASH: Clinical trials to clinical practice *J Hepatol.* 2016;65:1006–1016.

23. Sumida Y, Nakajima A, Itoh Y. Limitations of liver biopsy and non-invasive diagnostic tests for the diagnosis of nonalcoholic fatty liver disease/nonalcoholic steatohepatitis. *World J Gastroenterol.* 2014;20:475-485.

24. Saito K, Tajima Y, Harada T. Diffusion-weighted imaging of the liver: Current applications. *World J. Radiol.* 2016;8:857-867.

25. Shah B, Anderson SW, Scalera J, Jara H, Soto JA. Quantitative MR Imaging: Physical Principles and Sequence Design in Abdominal Imaging. *RadioGraphics.* 2011;31:867-880.

26. Bartolozzi C, Lencioni R, Donati F, Cioni D. Abdominal MR: liver and pancreas. *European Radiol.* 1999;9:1496-1512

27. Marzola P, Boschi F, Moneta F, Sbarbati A, Zancanaro C. Preclinical In vivo Imaging for Fat Tissue Identification, Quantification, and Functional Characterization. *Front. Pharmacol.* 2016;7:336.

28. Chow AM, Gao DS, Fan SJ, Qiao Z, Lee FY, Yang J, Man K, Wu EX. Measurement of Liver T1 and T2 Relaxation Times in an Experimental Mouse Model of Liver Fibrosis. *J. Magn. Reson. Imaging.* 2012;36:152-158.

29. Herck MAV, Vonghia L, Francque SM. Animal Models of Nonalcoholic Fatty Liver Disease--A Starter's Guide. *Nutrients.* 2017;9:1072-1085.

30. Zhong F, Zhou X, Xu J, Gao L. Rodent Models of Nonalcoholic Fatty Liver Disease. *Digestion.* 2019;10:1-14.

31. Stephenson K, Kennedy L, Hangrove L, Demieville J, Thomson J, Alpini G, Francis H. Updates on Dietary Models of Nonalcoholic Fatty Liver Disease: Current Studies and Insights. *Gene Expression.* 2018;18:5-17.

32. Chachay VS, Macdonald GA, Martin JH, Whitehead JP, O'Moore-Sullivan TM, Lee P, Franklin M, Klein K, Taylor PJ, Ferguson M, Coombes JS, Thomas GP, Cowin GJ, Kirkpatrick CMJ, Prins JB, Hickman IJ. Resveratrol Does Not Benefit Patients With Nonalcoholic Fatty Liver Disease. *Clinical Gastroenterol. Hepatol.* 2014;12:2092-2103.

33. Nakade Y, Murotani K, Inoue T, Kobayashi Y, Yamamoto T, Ishii N, Ohashi T, Ito K, Fukuzawa Y, Yoneda M. Ezetimibe for the treatment of non-alcoholic fatty liver disease: A meta-analysis. *Hepatol. Res.* 2017;47:1417-1428.

34. Rinella M, Tacke F, Sanyal A, Anstee Q. Report on the AASLD/EASL joint workshop on clinical trial endpoints in NAFLD. *J. of Hepatol.* 2019;71:823-833.

35. Stejskal EO, Tanner JE. Spin diffusion measurements: spin echoes in the presence of a time-dependent field gradient. *J. Chem. Physics.*1965;42:288-292.

36. Mills R. Self-diffusion in normal and heavy water in the range 1– 45 deg. *J. Phys. Chem.* 1973;77:685–688.

37. Envigo. C57BL/6NHsd www.envigo.com/products-services/research-models-services/models/research-models/mice/inbred/c57bl-6-inbred-mice/c57bl-6nhsd/. Accessed 20 May 2020.

38. Bertola A. Rodent models of fatty liver diseases. *Liver Res*. 2018;2:3-13.

39. Minicis S, Agostinelli L, Rychlicki C, Sorice GP, Saccomanno S, Candelaresi C, Giaccari A, Trozzi L, Pierantonelli I, Mingarelli E, Marzioni M, Muscogiuri G, Gaggini M, Nenedetti A, Gastaldelli A, Guido M, Svegliati-BAroni G. HCC Development Is Associated to Peripheral Insulin Resistance in a Mouse Model of NASH. *PLoS ONE* 2014;9:e97136.

40. Rao A, can de Peppel IP, Gumber S, Karpen SJ, Dawson P. Attenuation of the Hepatoprotective Effects of Ileal Apical Sodium Dependent Bile Acid Transporter (ASBT) Inhibition in Choline-Deficient L-Amino Acid-Defined (CDAA) Diet-Fed Mice. *Front. Med.* 2020;7:1-13.

41. Desmarchelier C, Dahlfoff C, Keller S, Sailer M, Jahreis G, Daniel H. C57BL/6 N mice on a western diet display reduced intestinal and hepatic cholesterol levels despite a plasma hypercholesterolemia. *BMC Genomics*. 2012;13:84-100.

42. Tsuchida T, Lee YA, Fujiwara N, Ybanez M, Allen B, Martins S, Fiel MI, Goossens N, Chou H, Hoshida Y, Friedman S. A Simple Diet- and Chemical-Induced Murine NASH Model with Rapid Progression of Steatohepatitis, Fibrosis, and Liver Cancer. *J Hepatol.* 2018;69:385–395.

43. Willebrords J, Pereira I, Maes M, Yanguas S, Colle I, Bossche B, Da Silva T, Marques C, Oliveria S, Andraus W, Alves V, Cogliati B, Vinken M. Strategies, models and biomarkers in experimental non-alcoholic fatty liver disease research. *Prog. in Lipid. Res.* 2015;59:106-125.

44. Castro R, Diehl A. Towards a definite mouse model of NAFLD. *J. of Hepatol.* 2018;69:272-274.

45. Brunner K, Henneberg C, Wilechansky R, Long M. Nonalcoholic Fatty Liver Disease and Obesity Treatment. *Curr. Obes. Rep.* 2019;8:220-228.

46. Anderson SW, Jara H, Ozonoff A, O'Brien M, Hamilton JA, Soto JA. Effect of Disease Progression on Liver Apparent Diffusion Coefficient and T2 Values in a Murine Model of Hepatic Fibrosis at 11.7 Tesla MRI. *J Magn. Reason. Imaging.* 2012;35:140-146.

47. Hansen H, Feigh M, Veidal S, Rigbolt K, Vrang N, Fosgerau K. Mouse models of nonalcoholic steatohepatitis in preclinical drug development. *Drug Discovery Today.* 2017;22:1707-1718.

48. Wei G, An P, Vaid K, Nasser I, Huang P, Tan L, Zhao S, Schuppan D, Popov Y. Comparison of murine steatohepatitis models identifies a dietary intervention with robust fibrosis, ductular reaction, and rapid progression to cirrhosis and cancer. *Am J. Physiol. Gastrointest. Liver Physiol.* 2020;318:G174–G188.

49. Scholten D, Trebicka J, Liedtke C, Weiskirchen R. The carbon tetrachloride model in mice. *Laboratory Animals.* 2015;49:4-11.

50. Kim J, Lee Y, Park Y, Kim B, Lee S, Yeon J, Lee C. Multiparametric MRI Index for the Diagnosis of Non-Alcoholic Steatohepatitis in Patients with Non-Alcoholic Fatty Liver Disease. *Scientific Reports.* 2020;10:2671-2680.

51. Graaf R, Brown P, McIntyre S, Nixon T, Behar K, Rothman D. High Magnetic Field Water and Metabolite Proton T_1 and T_2 relaxation in Rat Brain In Vivo. *Magn. Res. Med.* 2006;56:386-394.

52. Müller A, hochrath K, Stroeder J, Hittatiya K, Schneider G, Lammert F, Buecker A, Fries P. Effects of Liver Fibrosis on Tissue Relaxation Times in Different Mouse Models Assessed by Ultrahigh Field Magnetic Resonance Imaging. *BioMed Res. Int.* 2017;2017:1-10.

53. Kuru öz D, Kul P, Erden A, Erden I, Ankara/TR. Diagnostic value of hepatic T1 mapping (using MOLLI sequences), T2 mapping and MR elastography in nonalcoholic fatty liver disease. ECR 2019 / C-2046.

54. Cassidy F, Yokoo T, Aganovic L, Hanna R, Bydder M, Middleton M, Hamilton G, Chavez A, Schwimmer J, Sirlin C. MR Imaging Techniques for the Detection and Quantification of Liver Steatosis. *Radiographics.* 2009;29:231-260.

55. Guimaraes A, Siqueira L, Uppal R, Alford J, Fuchs B, Yamada S, Tanabe K, Chung R, Lauwers G, Chew M, Boland G, Sahani D, Vangel M, Hahn P, Caravan P. T2 relaxation time is related to liver fibrosis severity. *Quant Imaging Med Surg.* 2016;6:103-114.

56. Kessler S, Hoppstadter J, Hosseini K, Laggai S, Haybaeck J. Lack of Kupffer cell depletion in diethylnitrosamine-induced hepatic inflammation. *J. Hepatol.* 2019;70:813-815.

57. Ferolla S, Silva L, Ferrari M, Cunha A, Martins F, Couto C, Ferrari T. Dietary approach in the treatment of nonalcoholic fatty liver disease. *World J. Hepatol.* 2015;7:2522-2534.

58. *Lab Diets.* https://www.labsupplytx.com/labdiet/picolab-rodent-diet-20/. Accessed 20 May 2020.

59. *Dyets, Inc.* https://dyets.com. Accessed 20 May 2020.